

© 2021 by Zoë Richter. All rights reserved.

—

BY

ZOË RICHTER

THESIS

Submitted in partial fulfillment of the requirements
for the degree of Master of Science in Nuclear, Plasma, Radiological Engineering
in the Graduate College of the
University of Illinois at Urbana-Champaign, 2021

Urbana, Illinois

Master's Committee:

Professor Kathryn D. Huff
Dr. Madicken Munk

Abstract

Pebble-bed HTGR designs present a unique modeling challenge. Pebble-beds can have a variety of pebble compositions due to varying levels of burnup, and the pebbles are mobile in the core- entering from the top and exiting through the bottom - and may fall in a haphazard arrangement. This work introduces a simple 20 MWth pebble-bed HTGR reactor design (named Sangamon20) and investigates not only the neutronics of the base model, but the changes to core neutronics after making changes to the simulation: heterogenizing versus homogenizing the pebble center, imposing a symmetry assumption, and changing the arrangement of pebble fuel compositions, all using Serpent 2 and Python. In contrast to previous works using a uniform lattice and single pebble composition, Sangamon20 uses a random dispersal of seven different pebble compositions, each corresponding to a different level of burnup. The heterogenization tests compare k_{eff} , thermal and fast flux profiles, and the neutron lethargy-adjusted energy spectra in the whole-core, reflector, coolant, and a randomly chosen fresh and discharge-burnup pebble. Shuffling and symmetry tests monitor changes to k_{eff} and the outward neutron current at the outer reflector boundary. These two tests caused a minor (less than 0.65%) difference in either. However, for the heterogenization tests, k_{eff} differed by over 4.0%, and the pebble spectra at certain higher energies disagreed by a factor of 2-4. A complete fuel isotopic composition is accessible at ***ref comps zenodo***, and this thesis discusses select isotopic inventories.

Acknowledgments

I'd like to thank my advisor, Dr. Kathryn Huff, for offering her knowledge and support through these trying times and uncertainties. I would also like to thank Dr. Madicken Munk, whose insight and experience was invaluable. To Nathan Ryan, my tireless reviewer: thank you for all of your hard work. I would like to thank everyone in the Advanced Reactors and Fuel Cycles group, past and present, for giving me their time, aid, and experience: Amanda Bachmann, Dr. Andrei Rykhlevskii, Ansh Chaube, Greg Westphal, Gwendolyn Chee, Mehmet Turkmen, Roberto Fairhurst, Sam Dotson, and Sun Myung Park.

Thank you to my family, for always believing in me; Trinket, for loving hugs; and Sara, without whom nothing in this project would have a good name.

This work is supported by the Nuclear Regulatory Commission Fellowship Program. Acks.

Table of Contents

List of Tables	vi
List of Figures	vii
Chapter 1 Introduction	1
1.1 Motivation	1
1.2 Objectives	2
1.3 Background	2
1.3.1 The High Temperature Gas Cooled Reactor: Beginnings and Concepts	2
1.3.2 Earliest Operational HTGRs	4
1.3.3 Serpent 2	6
Chapter 2 Literature Review	8
2.1 Computational Models	8
2.1.1 Serpent 2	8
2.1.2 Work in Other Software	8
2.1.3 Fuel Modeling	9
2.2 Modern HTGRs	10
2.2.1 PBMR	10
2.2.2 Next Generation Nuclear Plant (NGNP)	13
2.2.3 X-energy	14
2.2.4 HTR-10	14
Chapter 3 Methodology	15
3.1 Sangamon200	16
3.2 Sangamon20	18
3.2.1 Inner Core Volume Determination	18
3.2.2 Graphite Reflector Thickness Determination	20
3.3 Fuel Composition	21
3.4 Heterogenization Tests	21
3.5 Reactor Sensitivity to Pebble Locations and Symmetry	22
Chapter 4 Results	24
4.1 Fuel Isotopic Compositions	24
4.2 Full-Core Control Model	31
4.3 Effect of Homogenizing	41
4.4 Sensitivity Tests	54
4.4.1 Effects of Symmetry Assumption	54
4.4.2 Effects of Pebble Shuffling	56

Chapter 5 Conclusion	58
5.1 Summary and Discussion	58
5.2 Future Work	59
5.3 Appendix A: Symmetry Test	60
5.4 Appendix B: Shuffle Test	71
References	85

List of Tables

1.1	Helium Coolant Specific Activities, reproduced from Table 2 in [4]	6
1.2	Pebble Dust Specific Activities, reproduced from Table 3 in [4]	6
3.1	Reactor Parameters	15
4.1	Sensitivity Run Summary	54
4.2	Shuffling Run Summary	57

List of Figures

1.1 Side-View of the 1955 Daniels' Concept, [2]	3
1.2 Diagram of Coolant Flow in the 1955 Daniel's Concept, [2]	3
2.1 PBMR Schematic: Vertical Cross-section [12]	11
2.2 Diagram of Fuel Regions, from [14]	12
3.2 Detector Placement Inside Reflector	17
3.3 Curve of Possible Height and Radii by Packing Fraction	20
3.4 Geometry of the Single-Pebble Burnup Calculation for Sangamon20	21
3.5 Symmetry Test Run Layouts	22
3.6 Shuffle Test Run 1 Example	23
4.1 Mesh Figures For Single Pebble Burnup	24
4.1 Mesh Figures For Single Pebble Burnup(cont.)	25
4.2 Evolution of Certain Isotopic Concentrations in Pebbles over Six Six-Month Passes (cont.)	27
4.2 Evolution of Certain Isotopic Concentrations in Pebbles over Six Six-Month Passes (cont.)	28
4.2 Evolution of Certain Isotopic Concentrations in Pebbles over Six Six-Month Passes (cont.)	29
4.2 Evolution of Certain Isotopic Concentrations in Pebbles over Six Six-Month Passes (cont.)	30
4.3 Legend for Geometry Figures	31
4.4 Full Core	32
4.5 Radial Thermal and Fast Flux Profiles	33
4.5 Radial Thermal and Fast Flux Profiles (cont.)	34
4.6 Axial Thermal and Fast Flux Profiles	34
4.6 Axial Thermal and Fast Flux Profiles (cont.)	35
4.7 Thermal and Fast Flux Profiles	36
4.7 Thermal and Fast Flux Profiles (cont.)	37
4.8 Lethargy Adjusted Neutron Flux Energy Spectra	38
4.8 Lethargy Adjusted Neutron Flux Energy Spectra (cont.)	39
4.8 Lethargy Adjusted Neutron Flux Energy Spectra (cont.)	40
4.9 Full Core Using Heterogenized Pebbles	41
4.10 Radial Thermal and Fast Flux Profiles: Heterogenized Pebbles	42
4.10 Radial Thermal and Fast Flux Profiles: Heterogenized Pebbles (cont.)	43
4.11 Axial Thermal and Fast Flux Profiles: Heterogenized Pebbles	44
4.11 Axial Thermal and Fast Flux Profiles: Heterogenized Pebbles	44
4.12 Thermal and Fast Flux Profiles	45
4.13 Lethargy Adjusted Neutron Flux Energy Spectra: Core Using Heterogenized Pebbles	46
4.13 Lethargy Adjusted Neutron Flux Energy Spectra: Core Using Heterogenized Pebbles (cont.)	47
4.13 Lethargy Adjusted Neutron Flux Energy Spectra: Core Using Heterogenized Pebbles (cont.)	48
4.14 Relative Difference in Radial Thermal and Fast Flux Profiles Between Cores Using Homogenized and Heterogenized Pebbles	49
4.14 Relative Difference in Radial Thermal and Fast Flux Profiles Between Cores Using Homogenized and Heterogenized Pebbles (cont.)	50

4.15 Relative Difference in Lethargy Adjusted Neutron Flux Energy Spectra Between Cores using Homogenized and Heterogenized Pebbles	51
4.15 Relative Difference in Lethargy Adjusted Neutron Flux Energy Spectra Between Cores using Homogenized and Heterogenized Pebbles (cont.)	52
4.15 Relative Difference in Lethargy Adjusted Neutron Flux Energy Spectra Between Cores using Homogenized and Heterogenized Pebbles (cont.)	53
4.16 Sensitivity Analysis: 0° - 60°	55
4.17 An Image Generated by Subtracting 4.16b from 4.4b.	56
 5.1 Sensitivity Analysis: 60° - 120°	61
5.2 An Image Generated by Subtracting 5.1b from 4.4b.	62
5.3 Sensitivity Analysis: 120° - 180°	63
5.4 An Image Generated by Subtracting 5.3b from 4.4b.	64
5.5 Sensitivity Analysis: 180° - 240°	65
5.6 An Image Generated by Subtracting 5.5b from 4.4b.	66
5.7 Sensitivity Analysis: 240° - 300°	67
5.8 An Image Generated by Subtracting 5.7b from 4.4b.	68
5.9 Sensitivity Analysis: 300° - 360°	69
5.10 An Image Generated by Subtracting 5.9b from 4.4b.	70
5.11 An example of RGB values. If the value for red and blue are held constant, shifting the value for green up or down shifts the resulting color along the color gradient to the left of the green value, which ranges from red to yellow. The arrows on the green gradient indicate what the current color is. As one can see, moving the slider to the the right - increasing the value of green - will make the color more yellow, while moving it to the left, or decreasing the green level, will shift it towards orange and red.	71
5.12 Shuffle Analysis: Run 1	72
5.13 An Image Generated by Subtracting ?? from 4.4b.	73
5.14 Shuffle Analysis: Run 2	74
5.15 An Image Generated by Subtracting ?? from 4.4b.	75
5.16 Shuffle Analysis: Run 3	76
5.17 An Image Generated by Subtracting ?? from 4.4b.	77
5.18 Shuffle Analysis: Run 4	78
5.19 An Image Generated by Subtracting ?? from 4.4b.	79
5.20 Shuffle Analysis: Run 5	80
5.21 An Image Generated by Subtracting ?? from 4.4b.	81
5.22 Shuffle Analysis: Run 6	82
5.23 An Image Generated by Subtracting ?? from 4.4b.	83

Chapter 1

Introduction

1.1 Motivation

The effects of climate change increase in severity every year. From 1980 to present, the global temperature anomaly - defined as the difference between the current average global temperature and the average temperature from 1951-1980 - has steadily increased to 1.02 °C. With a growing interest in reducing the global carbon footprint, comes a bevy of new research into sustainable energy, and the next generation of nuclear reactors.

One such class of reactors are the high temperature gas-cooled reactors, or HTGRs. While HTGRs can have a variety of fuel forms, this work concerns itself with pebble-bed reactors. Pebble-type fuels consist of a sphere of graphite, approximately the size of a billiard ball, embedded with tri-structural isotropic (TRISO) particles. In addition, plant operators can refuel online, reducing the need for planned shutdowns.

The next generation of nuclear reactors also include designs smaller than the conventional Light Water Reactor (LWR) seen in the USA today. So-called Small Modular Reactors, or SMRs, are small enough to be shipped, reactor pressure vessel and all, in a standard shipping truck or train. Owing to their small size, they are also easier and cheaper to manufacture. One can deploy an SMR in a variety of new settings, such as isolated towns or work sites, or station them together in one plant to fill the role of a single larger reactor.

This work used a pebble-bed HTG-SMR as a starting point, and modeled a generic 200MWth reactor based on existing designs - the Sangamon200. Then it scaled down to a target size - a 20MWth pebble bed HTGR. Reactors with a capacity of 70 MWth or less are microreactors - often deployed in areas only needing a small amount of power, used for research and testing, or used to supply heat for other industrial processes, such as producing hydrogen.

Down-sized modular reactors, such as SMRs or microreactors, have a few inherent safety benefits over their larger cousins, which also prompts their development. The smaller scale of the reactor pressure vessel (RPV) makes the large active cooling loops of contemporary commercial nuclear reactors unnecessary. For smaller reactors, passive systems relying on natural convection and surface heat transfer remove decay heat after something such as a station black-out (SBO). Under normal operation, with station power, supplementary fans and surface coolers can aid heat removal [1].

The 20MWth model, hereafter referred to as Sangamon20, is of a highly simplified design, for use in future testing and analysis.

1.2 Objectives

This work briefly describes a 200 MWth pebble-bed HTGR SMR, inspired by concepts from the PBMR and X-energy reactors, henceforth named Sangamon200. After establishing the larger reactor as a baseline, a scaled-down 20 MWth model, Sangamon20, uses it in its design, and is the focus of this work.

A series of tests modify the original Sangamon20 design, and analyses their effect on k_{eff} , fast and thermal flux, and neutron energy spectrum. These modifications include heterogenizing versus homogenizing the pebble centers, applying a 6-point symmetry to the core (using one-sixth to approximate the entire core), and re-assigning pebble fuel compositions to test randomness and pebble mixing. Additionally, Chapter 4 discusses the isotopic compositions for all pebble burnups and their trends over increasing burnup.

1.3 Background

While HTGRs and pebble beds have had a recent resurgence in interest and research, they are, in fact, an older concept.

1.3.1 The High Temperature Gas Cooled Reactor: Beginnings and Concepts

High temperature gas cooled reactors, or HTGRs, are a prominent Generation IV reactor design which often uses helium as a coolant, and graphite as a moderator in thermal designs. Their fuel form uses TRISO particles, which consists of a small kernel of fuel, less than half a millimeter across, surrounded by layers of carbon and silicon carbide to protect the fuel kernel and prevent the leakage of radioisotopes. Fuel elements are made by embedding these TRISO particles in graphite. In prismatic HTGRs, the graphite is in the shape of hexagonal columns. In pebble-bed reactors, the graphite is in the shape of spheres - around the size of a billiard ball. Many of these pebbles enter the core through the top, and slowly move down in a manner similar to grain in silos.

Preliminary concepts for a gas-cooled reactor existed as early as 1942. Farrington Daniels - more commonly known for his work in chemistry and solar power technology - is attributed with establishing the first theoretical designs. A professor from the University of Wisconsin, Professor Daniel's work with Oak Ridge National Laboratory (ORNL) nailed-down the most basic characteristics of the HTGR. The choice of helium for coolant, graphite for moderator, the direct gas turbine cycle, and the use of uranium or thorium carbides for fuel all came from his work [2].

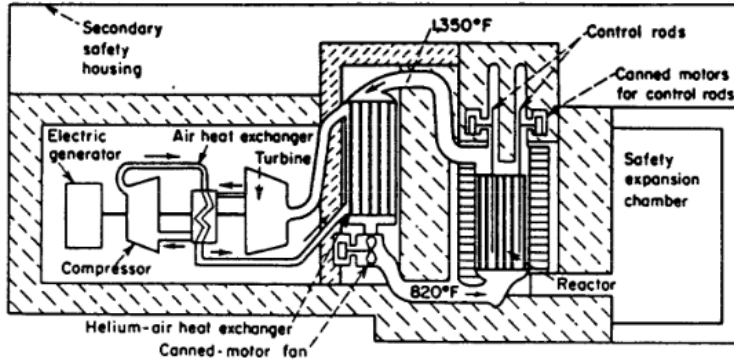


Figure 1.1: Side-View of the 1955 Daniels' Concept, [2]

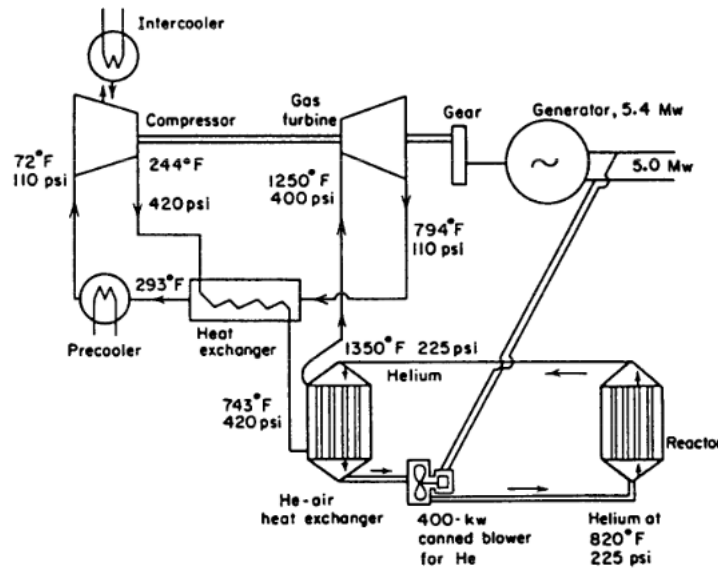


Figure 1.2: Diagram of Coolant Flow in the 1955 Daniel's Concept, [2]

Figures 1.1 and 1.2 show the 1955 design proposed by Professor Daniels. Like many modern modular reactor plant designs, Professor Daniels suggested that the reactor be mostly underground. A key difference between the Farrington Daniels designs and modern HTGRs is the fuel form. While modern designs use TRISO particles embedded in graphite, the Daniels' design uses solid graphite blocks, with channels for both coolant and fuel. Within the fuel channels, fuel loaded in either a pellet or cartridge form, both a mixture of 10% uranium dicarbide and graphite powder. In addition to these fuel channels, the design included an outer ring of graphite reflector in which used thorium to breed ^{233}U . Control rods are of a boron-containing molybdenum. Steel wires that would melt in the case of an accident held more of the same above the core, dropping the safety rods in case of an accident [2].

1.3.2 Earliest Operational HTGRs

The earliest operational HTGRs: the AVR, from Germany; Dragon, operating in the UK; and Peach Bottom 1, which operated in the US came online in the 1960s [3].

Dragon

The Dragon prismatic HTGR was a test reactor operated in Winfrith, UK, from 1964 to 1975, making it the oldest of the reactors discussed in this chapter. It operated at inlet and outlet temperatures of 350 °C and 750 °C and 20MWt [3]. Dragon's main purpose was to test reactor materials, with an emphasis on fuels. It originally used uranium and thorium as fuel, but switched to a purely uranium-based fuel with a lower enrichment later in life. The fuel elements themselves were similar in shape to the Daniels' design - hexagonal prisms with fuel rod channels.

Contrary to the fuel philosophy seen today, Dragon originally allowed fission products released from fuel elements into the circulating helium coolant. The fission products are then purged from the helium. However, Dragon later switched to a coated-particle fuel when it became clear that having such fission product releases would be difficult to manage [2].

Peach Bottom 1

Peach Bottom 1 operated from 1966 to 1974, by the Philadelphia Electric Company. It was the first operational HTGR in the US, and the first to produce electric power. It was slightly larger than Dragon, at a nameplate capacity of 115 MWt/40MWe and a slightly lower operating temperature range at 327°C to 700°C inlet to outlet [3]. Like Dragon, Peach Bottom 1 was a prismatic reactor; however, Peach Bottom used coated uranium and thorium carbide particles from the beginning. The original fuel used a single coating of pyrolytic carbon. However, after multiple fuel failures, Peach Bottom upgraded to bistructural isotropic, or BISO, fuels by adding an additional layer. Peach Bottom would later upgrade the fuel once again by adding a silicon carbide layer, forming TRISO particles [3]. One operational benefit of upgrading to TRISO particles from BISO particles was that the superior fission product retention meant that Peach Bottom 1 could remove the helium purging systems. In addition to the inner fuel region, Peach Bottom, like the Daniels' design, bred ^{233}U in an outer region using thorium.

Beyond changing the number and materials for fuel coatings, the experiences in Peach Bottom 1 helped to develop HTGR fuel elements. Operators saw that they could dilute the fuel with graphite moderating material more so than other diluents. This has the advantage of saving fuel material, improving heat transfer, and reducing radiation damage. Additionally, operational experience showed that, in order to prevent the creation and buildup of ^{236}U and ^{237}Np , which are neutron poisons, the ^{235}U and ^{233}U should be kept separate [2].

In the end, Peach Bottom 1 closed after operators determined it to be uneconomical.

AVR

The Arbeitsgemeinschaft Versuchsreaktor (AVR) was an experimental pebble-bed reactor operated in the Jülich Research Center from 1967 to 1988. It had a capacity of 46 MWt/15MWe, with inlet and outlet temperatures of 275°C and 950°C [3]. In fact, the AVR reached the highest operating temperatures of any commercial nuclear plant. Like the others in this early time period, the AVR used a combination of uranium and thorium fuels, though it began with bi-structural isotropic (BISO) particles. The core held around 100,000 graphite pebbles, almost a third of which had fuel in them.

Despite not being built for experimental purposes, the AVR still housed many experiments that improved our body of knowledge on HTGR technology. During the first few years of its life, the goal of the AVR was to demonstrate that it was a reliable technology. After this initial period, the AVR shifted focus to allow various experiments.

In the initial phase they needed to show that the reactor could operate safely, could control the core power and temperatures, safely shutdown, and remain sub-critical for long periods of time. This proved to be quite the undertaking, as the AVR shifted from highly enriched to low enriched fuel over time, which caused a variation in fuel pebble compositions, on top of the range of compositions inherent to a multi-pass pebble cycle due to varying burnup.

The AVR also provided data to validate simulations of pebble-bed reactors, and conducted an experiment to better characterize the radial distribution of temperatures in the core. Operators loaded a number of marked pebbles into the core, each housing a series of wires that would melt at a certain temperature, the lowest being 655°C, the highest 1280°C. Those conducting the test tracked pebble location using flow data, and examined them after they were ejected to determine what temperatures the pebbles experienced. Despite the outlet temperature being 950°C, multiple pebbles experienced a temperature greater than or equal to the 1280°C maximum temperature in the melt wires. The results noted that these pebbles went through a zone with a spike in local power density, which could account for the temperature spike [4].

The AVR also demonstrated the inherent safety of HTGR reactors in accident scenarios by purposefully causing failures of the active cooling system. In the first, the coolant blowers were shutoff, and no shutdown rods inserted, while operating at full power. The operators additionally shut the main circuit valves to prevent natural circulation to regions outside the active core. Overall, the changes to core temperatures were unremarkable. The hottest regions cooled, while the coldest regions warmed up. Additionally, due to negative temperature feedback coefficients, the reactor power immediately declined in response to the "accident". The temperature slowly rose to 2 MW again over 24 hours, only to level out around 300 kW. A further test provided data on loss of coolant and depressurization accidents. As before, the core temperature changes were unremarkable. The upper core region cooled, while the lower, originally cooler core region slowly rose in temperature. The experiment's data helped validate HTGR

computer models, which allowed the results to aid in the analysis of other HTGRs [4].

Beyond accident safety, the AVR allowed for testing and demonstration of the safety qualities of TRISO and BISO fuel elements; especially relating to high temperature tolerance, and fission product retention. Initial tests used BISO based pebbles, then later transitioned to TRISO, then to low-enriched-uranium (LEU) TRISO pebbles. The TRISO-LEU pebbles had good fission product retention compared with their BISO-based predecessors, based on the activity of samples taken from the circulating helium. Beyond radioisotopes being directly released into the coolant gas, the AVR also showed that in order to accurately characterize the source term of an HTGR pebble bed reactor, one must take the dust from the pebbles into account. Dust from the pebbles bumping and scraping against each other deposited on reactor surfaces in the primary loop. Sixty kg of dust had accumulated by the end of the reactor's life, which averages to 3 kg of dust each year. Measurements of specific activity in the dust showed that the activities of ^{137}Cs , ^{134}Cs , ^{131}I , ^{90}Sr , and ^{60}Co were on the order of $\frac{Bq}{g}$. Even though relatively little dust accumulates, the activity of this dust is fairly high, especially compared to the activity of the coolant gas [4].

Isotope	Specific Activity in Primary Coolant Gas [$\frac{Bq}{m^3}$]
Σ Fission noble gas	4.6×10^{08}
3H	3.7×10^{07}
^{14}C	1.9×10^{07}
^{137}Cs	3.0×10^{02}
^{131}I	5.2×10^{02}
^{110m}Ag	4.9×10^{01}
^{90}Sr	2.0×10^{02}
^{60}Co	1.0×10^{01}

Table 1.1: Helium Coolant Specific Activities, reproduced from Table 2 in [4]

Isotope	Specific Activity in Dust [$\frac{Bq}{g}$]
^{137}Cs	2 - 96
^{134}Cs	0.7 - 27
^{131}I	0 - 3
^{110m}Ag	0.1 - 43
^{89}Sr	0.6 - 42
^{90}Sr	19 - 363
^{60}Co	0.2 - 8

Table 1.2: Pebble Dust Specific Activities, reproduced from Table 3 in [4]

1.3.3 Serpent 2

Serpent 2 is: "a multi-purpose three-dimensional continuous-energy Monte Carlo particle transport code" [5] from the VTT Technical Research Center of Finland. The first iteration, Serpent 1, began development in 2004. The development of Serpent 2 is presently on-going. Serpent 2 has three main applications: traditional reactor physics,

coupled multi-physics, and neutron and photon transport.

Chapter 2

Literature Review

2.1 Computational Models

While this thesis only used Serpent 2 [6] for modeling, work to improve HTGR modeling in one program can inform efforts in another. Therefore, this chapter includes discussion of software beyond Serpent 2.

2.1.1 Serpent 2

In order to create and model complex geometries, Serpent 2 uses constructive solid geometry (CSG), which defines homogeneous material cells using user-defined universes, cells, lattices, and specially-defined nested objects to define particle and pebble geometries. Using these special objects, and the particle dispersal routine in Serpent 2, we can create TRISO particles and pebble bed reactors. Previous work has tested with up to 60 million individual particles [5].

Physics use a combination of classical kinematics, ENDF reaction laws, and random sampling. For particle transport, Serpent 2 uses surface tracking and Woodcock-delta tracking. For material data, it uses ACE format libraries for microscopic cross sections, and pre-generates macroscopic cross sections before beginning transport. To further speed-up calculations, Serpent 2 uses a unionized energy grid. Serpent 2 validation studies compare against MCNP, and validation is ongoing for radiation shielding and criticality safety analysis [5]. While the differences between Serpent 2 and other Monte Carlo programs are usually marginal, Serpent 2 experiences the same issues validating its results as other Monte Carlo programs (related to small differences in data libraries [5]).

2.1.2 Work in Other Software

A 1996 effort to improve MCNP developed a new sampling method for Monte Carlo. Its creators dubbed the version of MCNP that used the sampling algorithm as MCNP-BALL. After testing by performing isotopic inventory and criticality calculations the MCNP-BALL code results were accurate to 0.2%. The work developing MCNP-BALL also answered a weakness in core simulation due related to difficulties in modeling reactors with a so-called "double-heterogeneity" - having two or more types of pebble in a single reactor [7].

An additional look into MCNP HTGR simulations examined the ability to create what would normally be a stochastic geometry with a uniform design. Specifically, it used a body-centered-tetragonal (BCT) and hexagonal close pack (HCP) lattice for the TRISO particles. For low packing fractions, such as ones seen in TRISO-in-pebble packing, the particles are far enough apart that the differences between two crystal lattice structures are insignificant. In smaller cores, with adequate reflectors, the differences between the pebble packing lattices were more significant, but manageable. Additionally, the effect of completely homogenizing the coating of the TRISO particles - blending them with the graphite matrix - lowered k_{eff} . For methods using less dramatic homogenization methods, such as blending the four TRISO coatings into one uniform layer, the computational load decreased, and the results were marginally different from the 4-coating TRISO particle [8].

BEAU, or Burnup Equilibrium Analysis Utility [9], models depletion and multiple burnup states for a continuously refueled pebble bed reactor. It uses the multiple burnup state method (MBSM) to do so, which improves on most full-core pebble bed computational methods by including all burnup states for a pebble rather than homogenizing them into a representative average pebble.

BEAU is a Python-based coupling software that combines either MCNP5 or Serpent with ORIGEN2, using new interface inspired by the MOCUP software named mocup.py. Mocup.py takes the output files from an MCNP5 or Serpent simulation, and turns them into an object for aiding in depletion simulations. BEAU is for fuel cycle analysis and finding the maximum burnup equilibrium. It was bench-marked against results for a pebble-bed HTGR in INL's PEBBED and VSOP [9].

2.1.3 Fuel Modeling

BEAU aided in the design of a pebble bed fluoride high temperature reactor (PB-FHR) named the Mark-1 PB-FHR [9]. The Mark-1 PB-FHR handles pebble locations using a face-centered cubic (FCC) lattice in which all burnup states seen in the reactor are present. Assuming a uniformly mixed core, the closeness of the different burnup compositions in the lattice provide a fairly good estimation of the true core.

A more general study examined the effects of pebble packing on the core neutronics in an HTGR [10]. Rather than model a full core, the study created a unit cell as a reference. The study considers body centered cubic (BCC) and hexagonal close-packed (HCP) lattice unit cells. Instead of using a variety of compositions to represent an equilibrium, middle-of-life (MOL) core, the study used an enrichment of 9.6% - lower than the standard 15% for fresh HTGR pebble-fuel - for all pebbles. For each lattice configuration, tests varied the fuel/moderator (F/M) ratio, and examined the effects on core neutronics and isotopic compositions. The analysis shows no significant difference between BCC and HCP cells. The study determined it would be difficult to select a truly 'optimal' energy spectrum vis-à-vis minimizing the accumulation of particularly harmful fission products. The author concluded

that F/M ratios less than 1/1 favor reducing actinide inventories, while ratios greater than 1/1 can reduce the generation of fission products that would corrode the layers of the TRISO fuel.

Earlier work on HTGRs by General Atomic determined the composition of discharged thorium/uranium prismatic fuel elements. The study assumed fuel recycling to complement the proposed breed/burn fuel cycle. Additionally, the fuel cycle assumes the reactor can start with an initial feed material of 93% U-235, which is currently infeasible (at least in commercial reactors in the United States) [11].

2.2 Modern HTGRs

The following discusses more recent HTGR designs, which are the inspiration for Sangamon200 and Sangamon20.

2.2.1 PBMR

The PBMR is a South African pebble bed HTGR design. While it did not ultimately make it to construction, its design has offered invaluable insight to later HTGR pebble bed designs. The PBMR is heavily based on the German High Temperature Reactor (HTR) design, and has a nameplate thermal power of 400 MW, with inlet-outlet temperatures of 500 °C to 900 °C. It is a modular design, with each unit containing a graphite moderated, helium-cooled-core housed in a steel pressure vessel. In accident scenarios, the PBMR would rely on passive safety features using conduction and convection to provide cooling.

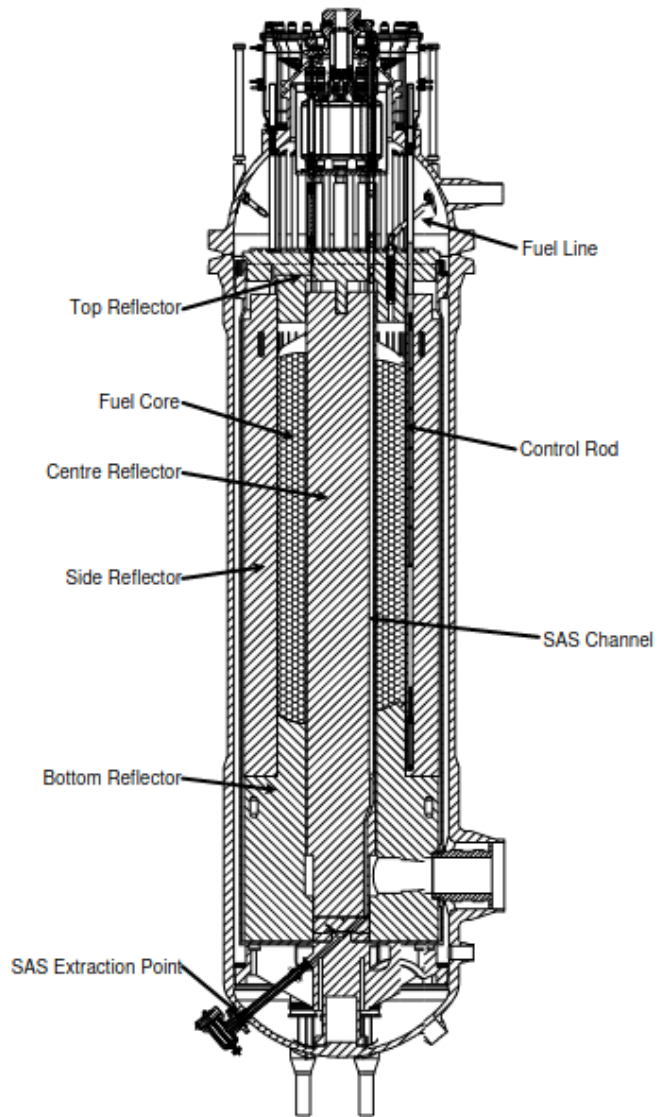


Figure 2.1: PBMR Schematic: Vertical Cross-section [12]

Each core unit would hold around half a million pebbles, which used LEU based TRISO particles as the fuel form. These TRISO particles are pressed into a 2.5 [cm] radius graphite sphere, which then has an additional 0.5 [cm] thick layer of graphite pressed around it, to form a 3.0 [cm] radius pebble - around the size of a billiard ball. The pebbles would undergo a six-pass cycle to reach a target end burnup of $92,000 \left[\frac{MWd}{tU} \right]$ [12].

As part of the design process, multiple 400 MWth PBMR benchmarks underwent development and testing. An early benchmark using MCNP5 simplified the fuel by assuming an equilibrium pebble enrichment of 9.6 wt%, a common tactic. It also uses a BCC lattice for pebble positions. Its calculated k_{eff} differed from previous MCNP4b results by as much as 1,315 pcm [13].

An improved benchmark modeled the original VSOP benchmark more closely. A full-core model used a cubic array to map TRISO particles inside the pebbles, while an HCP lattice defines pebble locations [14]. As an improvement on previous benchmarks, it adds back in the fuel regions from the VSOP model, which tracks pebbles in channels and axial layers to simulate their movement through the core. However, it does simplify these layers, see Figure 2.2, below:

Figure 2: Sketch showing the numbering of flow channels and fuel regions (layers) in the VSOP (left) and MCNP (right) equilibrium core models.

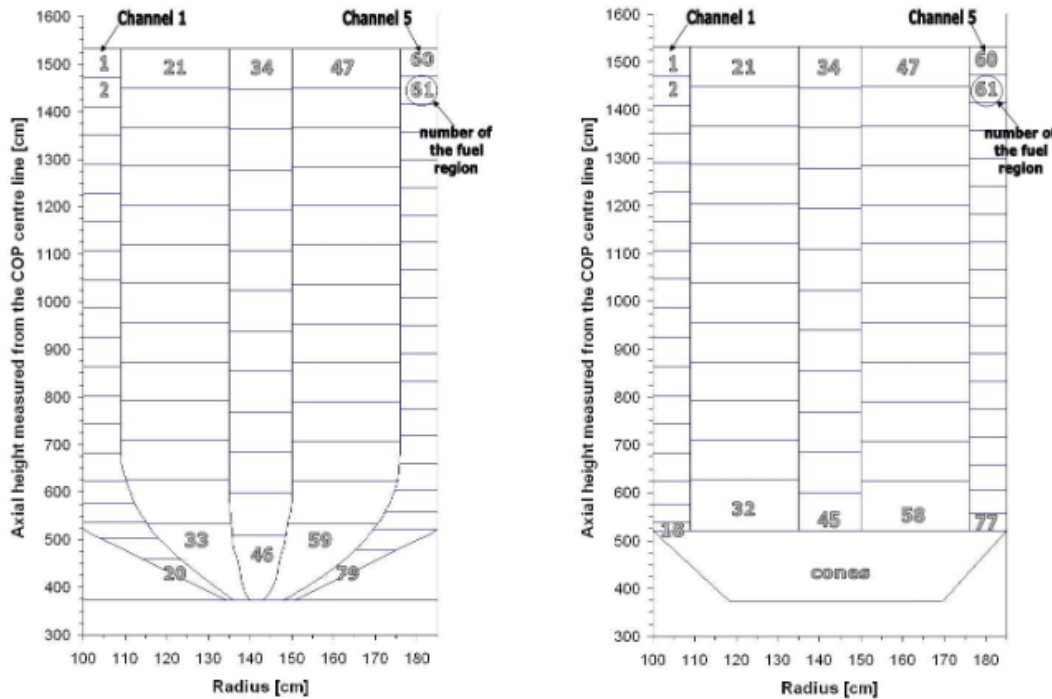


Figure 2.2: Diagram of Fuel Regions, from [14]

To simplify, the different pebble burnups in each region are averaged. This study also investigated the effects of different pebble packing arrangements, but rather than use a full-core, a representative one-meter cube of pebbles

defines a reference model. The study tested random, HCP, BCC, and FCC at packing fractions of 0.542 and 0.61. It found that across identical packing fractions, differences in reactivity were small, though k_{eff} values differed by several standard deviations [14].

An additional work performed criticality and burnup calculations using MCNP5 and MONTEBURNS 2.0. It, like many other pebble-bed models, uses an averaged 9.6% enriched fuel to simulate an equilibrium core [15]. It tested three pebble arrangements: a BCC lattice with a packing fraction of 0.68, a random arrangement with a packing fraction of 0.61, and a simple cubic (SC) lattice with a packing fraction of 0.52. The initial k_{eff} were similar: 1.2395, 1.2357, and 1.2223, respectively. However, the effective full power days (EFPDs) and end of life burnup required to reach an end k_{eff} of 1.02 differed considerably. BCC required 1200 EFPDs and ended on 99,000 $\frac{MWD}{T}$, random ended on 1000 EFPDs and a burnup of 92,000 $\frac{MWD}{T}$, and the SC lattice required 800 EFPDs and achieved a final burnup of 86,000 $\frac{MWD}{T}$ [15]. However, for the random pebble arrangement, which was used to validate the model, the disagreement in excess reactivity was approximately 14%.

A study using VSOP focused on possible power peaking and the formation of hot spots. To test hot spots forming, a mass of fresh pebbles were purposefully introduced in the fuel region corresponding to the peak power. Even for a very large cluster of fresh pebbles, maximum fuel power only increased by 16%. However, the volumetric power density increased to 18.66 from 11.32 $\frac{MW}{m^3}$ [16]. Of note, this scenario is highly unlikely - the region of highest power is three meters into the core, by which point fresh pebbles would have been burned slightly. This is in addition to the already accidental loading of over one thousand fresh pebbles at once.

2.2.2 Next Generation Nuclear Plant (NGNP)

Like the PBMR, the NGNP did not make it to construction. However, work in analyzing reactor designs and materials still applies to other work. The NGNP project downselected its design choices to two reactors - a prismatic HTGR and a pebble-bed HTGR. While the NGNP project eventually opted for the Areva prismatic HTGR design [17] due to reasons related to pebble costs, studies noted that, technologically speaking, there was no inherent advantage or disadvantage between the two technologies [18].

Even though the reactor didn't make it to construction or operation, a plethora of research conducted in support of the NGNP project is applicable to similar reactors. One such study is a whole-core depletion study of the proposed prismatic HTGR design. It uses a once through fuel cycle, and assumed an average burnup of 100-150 $\left[\frac{GWd}{t} \right]$ after an 18 to 24 month stint in the core. Much of the work from this study is applicable only to prismatic designs, namely the effects of the number of batches cycling, and fuel shuffling on core neutronics [19].

2.2.3 X-energy

Based on experience from the PBMR project, the X-energy Xe-100 is a 200 MWt HTGR pebble-bed SMR. It is similar in design to all of its predecessors, featuring LEU TRISO particle fuel in 3.0 [cm] radius pebbles. While the Xe-100, or similar design, is not in operation as of this publication, the project is still ongoing. It is this reactor, and by extension the PBMR, that the micro-reactor described in this thesis is most heavily influenced by.

The Xe-100 uses approximately 220,000 pebbles in a six-pass cycle, and fuel pebbles identical to the ones intended for the PBMR [20]. However, while the number of passes is unchanged, the target end burnup for the pebbles is higher, at $160,000 \left[\frac{MWD}{tU} \right] + [21]$. Another key difference from the PBMR beyond size is the lack of central reflector.

While the Xe-100 is not built, there have been studies conducted by ORNL providing data on the production and material properties of the PBMR-type fuel pebble.

2.2.4 HTR-10

The HTR-10 is a 10 MW, HTGR model. Multiple studies exist examining the effects of pebble and TRISO arrangement on the HTR model. These studies primarily work with the Reactor Monte Carlo (RMC) or MCNP5 programs. A base benchmark study created the HTR-10 in MCNP. Pebbles contained 8335 TRISO particles on average, dispersed in a cubic lattice. Pebbles, meanwhile, are in a BCC arrangement, such that F/M ratios and void fractions stay constant [22].

A later study used RMC to study the explicit modeling of the random nature of both the pebbles and particles in the core, a 'double heterogeneity' [23]. The Random Sequential Addition (RSA) method was used to distribute the TRISO particles within the pebbles (the packing fraction was less than 30%, the maximum RSA can achieve). The Discrete Element Method (DEM) dispersed pebbles. To simplify the model, it assumed that all pebbles have identical TRISO dispersal patterns. Testing showed this caused little (σ less than 0.00014) error between this simplification and a model using different TRISO arrangements in each pebble. The RMC model had good agreement with VSOP HTR-10 simulations [23].

Other work with the HTR-10 introduces a new method of explicit random particle dispersion for use in RMC, called the Random Universe Geometry method (RUG). RUG improves on RSA by allowing a higher particle packing fraction, and on the DEM by being faster and simpler to implement [24]. Whenever a particle enters a cell that is stochastic, the algorithm randomly samples from a list of possible materials, and determines the contents of the cell mid-transport. The RUG method has good agreement with preliminary testing using HTR-10 benchmarks [24].

Chapter 3

Methodology

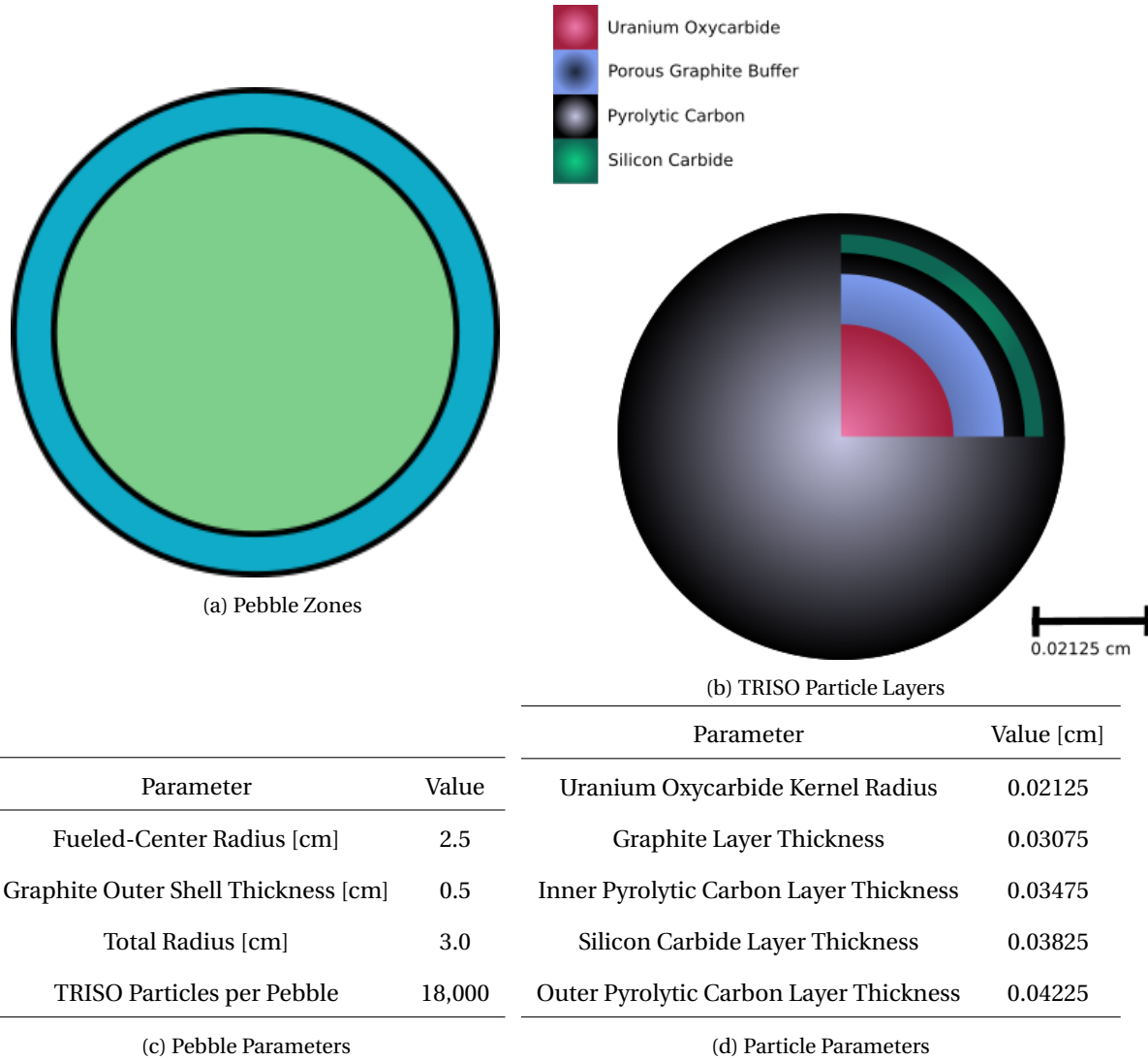
This chapter introduces Sangamon20, a scale-down of Sangamon200, a 200MWth design inspired by the PBMR and Xe-100. Both Sangamon200 and Sangamon20 are uranium oxycarbide(UCO)-pebble fueled, helium cooled microreactors.

Parameter	Sangamon200	Sangamon20
Thermal Power [MW]	200	20
Average Core Temperature [K]	800	800
Enrichment	15.5%	19.75%
Average Core Pressure [MPa]	5.9	5.9
Core Diameter [cm]	248	180
Core Height [cm]	1150	180
Reflector Thickness [cm]	90	75
Number of Pebbles	220,000	23,000

Table 3.1: Reactor Parameters

All simulations used Serpent 2 [6], and supplementary calculations using Python [25], [26] and PyNE [27]. The Serpent 2 particle dispersal routine determined pebble and TRISO locations. It takes the number of particles, defined by the user, or η_{pf} , the packing fraction (the total volume of particles divided by the volume of that space). The dispersal routine has the user define the particle radius, and the size and shape of the volume housing the particles. The routine first randomly determines a single point for each particle contained in the volume. Then, the routine uses the 'growth factor' and 'shake factor' - both described as fractions of the particle radius, and iterates. During each iteration, the size of the point's radius increases by the growth factor. Additionally, the center will move in a random direction a distance equal to the shake factor. If the particle growth causes the particle to overlap with another particle or leave the volume, it doesn't grow that cycle. Similarly, if the center's movement causes overlap or the particle to leave the containing volume, it doesn't move. The dispersal routine iterates until all particles are to their full size, contained in the volume, and not overlapping with any other particles. The routine generates an output file, in which each line gives the location of the particle center (in x,y,z coordinates), the particle radius, and the name of the particle type, to associate it with the "pbed" card (see [6]) later.

In order to determine isotopic compositions in the pebbles, a Serpent 2 burnup simulation of a single pebble ran in burnup steps of 180, 360, 540, 720, 900, and 1080 days - to represent six, six-month passes. The single pebbles are the only simulations that utilize individually defined TRISO particles by default. Each pebble has an inner region containing the TRISO particles embedded in graphite, and an outer region consisting only of graphite, see 3.1a. Each region homogenized by volume fraction using the "mix" card (see [6]) in Serpent 2.



3.1 Sangamon200

Sangamon200 is a 200 MW_{th} helium cooled reactor, with parameters as defined in Table 3.1. Though the model does use some parameters from pre-established designs, it is a simplification. The top and bottom of the reactor

core are a flat surface, to create a cylindrical shape. The graphite reflector surrounds it with no barriers between the reflector and active core region. These are the only simulated parts of the reactor - there are no control rods included. In addition, the graphite reflector is a solid cylindrical shell, a container for the pebbles.

While Sangamon200 is not the focus of this assessment, some parameters determined aided in Sangamon20's design. A surface detector placed in the reflector, just inside the outer bound of the reflector, shown in 3.2, tracks the outward neutron current.

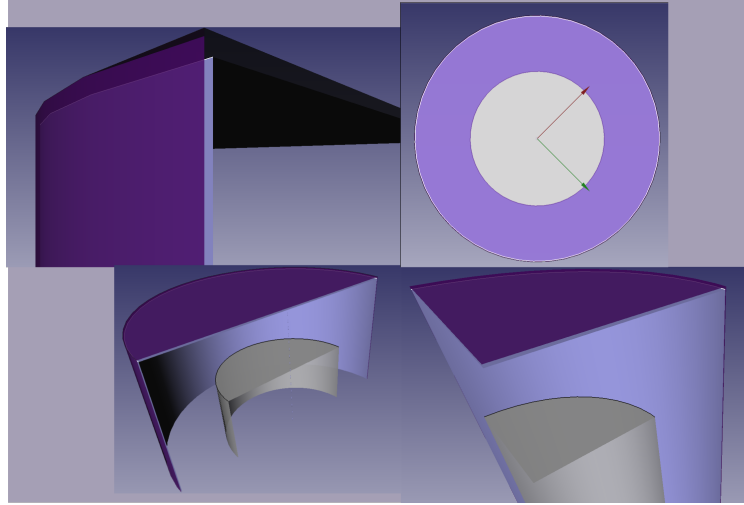


Figure 3.2: Detector Placement Inside Reflector

This detector measures the outward neutron current (** serpent outputs units of [number/s], is current still the best word? ***) in $\left[\frac{\#}{s}\right]$. To arrive at the unit of $\left[\frac{\#}{cm^2 s}\right]$ most are familiar with, we divide by the detector's surface area thusly:

$$J^+ = \frac{J_s^+}{S_d} \quad (3.1)$$

where

$$\begin{aligned} J^+ &= \text{outward neutron current } \left[\frac{\#}{cm^2 s}\right] \\ J_s^+ &= \text{surface unadjusted outward neutron current } \left[\frac{\#}{s}\right] \\ S_d &= \text{detector surface area } [cm^2] \end{aligned} \quad (3.2)$$

After accounting for the surface area, the outward current at the detector is $7.351 \times 10^{11} \left[\frac{n}{cm^2 s}\right]$.

3.2 Sangamon20

Sangamon20 is a 20 MWth helium-cooled pebble bed reactor, fueled with 19.75% enriched uranium oxycarbide. While the capacity of Sangamon20 is 10% that of Sangamon200, it isn't sufficient to simply scale Sangamon200's dimensions down to 10% of their original values, as that wouldn't have the correct volume for the required pebbles, and the neutronics would be inconsistent.

3.2.1 Inner Core Volume Determination

The first assumption made in the scale-down is that Sangamon200 and Sangamon20 have the same power density, or $\left[\frac{\text{kW}}{\text{g UCO}} \right]$.

To calculate the mass of fuel in Sangamon200:

$$M_{f,200} = \frac{4}{3}\pi r_u^3 \rho_u n_T n_{p,200} \quad (3.3)$$

where

$M_{f,200}$ = mass of fuel in Sangamon200 [g]

r_u = the radius of the UCO kernel inside a TRISO particle [cm]

ρ_u = the density of UCO in [$\frac{\text{g}}{\text{cc}}$]

n_T = number of TRISO particles in one pebble

n_p = number of pebbles in Sangamon200 (3.4)

Using the parameters in 3.1, the power density of Sangamon200 and Sangamon20 is $0.11 \left[\frac{\text{kW}}{\text{g}} \right]$. With a power capacity of 20 MWth, one can calculate the total mass of UCO in Sangamon20 as

$$M_{f,20} = \frac{P}{\rho_p} = 181818.18 \text{ [g]} \quad (3.5)$$

where

$$M_{f,20} = \text{total mass of UCO in Sangamon20 [g]}$$

$$P = \text{Thermal power of Sangamon20 [kW]}$$

$$\rho_p = \text{Sangamon20's power density } [\frac{kW}{g}] \quad (3.6)$$

The above calculates the mass of a single pebble using the density of UCO and the total volume of UCO kernels in a single pebble. The total mass of fuel in the reactor divided by the mass of fuel in a single pebble gives the number of pebbles in the reactor, as follows:

$$n_{p,20} = \frac{M_{f,20}}{\frac{4}{3} r_u^3 n_T \rho_u} \quad (3.7)$$

where

$$n_{p,20} = \text{number of pebbles in Sangamon20 [-]}$$

$$M_{f,20} = \text{total mass of UCO in Sangamon20 [g]}$$

$$r_u = \text{radius of a UCO kernel [cm]}$$

$$n_T = \text{number of TRISO particles in a single pebble [-]}$$

$$\rho_u = \text{density of UCO } [\frac{g}{cm^3}] \quad (3.8)$$

Rounding up - there can only be complete pebbles - we arrive at the number of pebbles in 3.1.

Knowing the number of pebbles is insufficient - the exact dimensions of the active core region are still undefined. To determine the volume of this space, the formula uses concept of the packing fraction. The packing of even uniform objects in a 3-dimensional space is a complicated problem [28]. Assuming the pebble behavior is random loose packing [28] - the pebbles have unsystematically fallen into the core and the core is unshaken - the packing fraction in the range of 0.56 to 0.60 [28]. Using the definitions above, the active core volume is

$$V_{c,20} = \frac{n_{p,20} \frac{4}{3} \pi r_p^3}{\eta_{pf}} \quad (3.9)$$

where

$$\begin{aligned}
 V_{c,20} &= \text{volume of the active core in Sangamon20 [cm}^2\text{]} \\
 n_{p,20} &= \text{number of pebbles in Sangamon20 [-]} \\
 r_p &= \text{radius of a pebble [cm]} \\
 \eta_{pf} &= \text{packing fraction [-]}
 \end{aligned} \tag{3.10}$$

Using the formula for the volume of a cylinder, one can plot possible sets of $r_{c,20}$ and $h_{c,20}$ that satisfy the volume requirement.

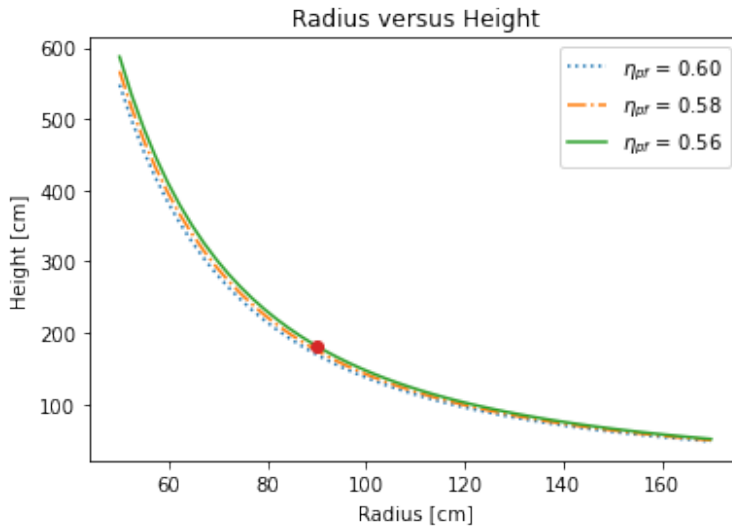


Figure 3.3: Curve of Possible Height and Radii by Packing Fraction

The most critical configurations for a cylinder are either a *square* shape, in which the height is equal to the diameter, or a *flat* shape in which diameter is significantly greater than height. As a flat shape is disadvantageous for a reactor, Sangamon20 is the former. The point indicated in 3.3 shows the radius and height selected for Sangamon20 - a radius of 90 [cm], and a height of 180 [cm].

3.2.2 Graphite Reflector Thickness Determination

The reflector must be sufficiently thick to keep the reactor critical, and protect the pressure vessel. To ensure this, the outward current in Sangamon20 must be less than or equal to the outward current in Sangamon200 at the outer reflector boundary. The detector layout in Sangamon20 is identical to 3.2.

3.3 Fuel Composition

The number of passes the pebble has theoretically experienced determines its isotopic composition. Seven possible pebble compositions exist, one for each of the six 6-month passes, plus an additional composition for fresh pebbles. The seven pebble compositions are equally and randomly distributed in the core.

The design approximates the exact isotopic composition by running a burnup calculation using Serpent 2 for a single pebble in a cube. It uses a reflective boundary condition to simulate the presence of other pebbles or the reflector. Just as with the location of the pebbles in the full core, the Serpent 2 particle dispersal routine generated the TRISO particle locations.

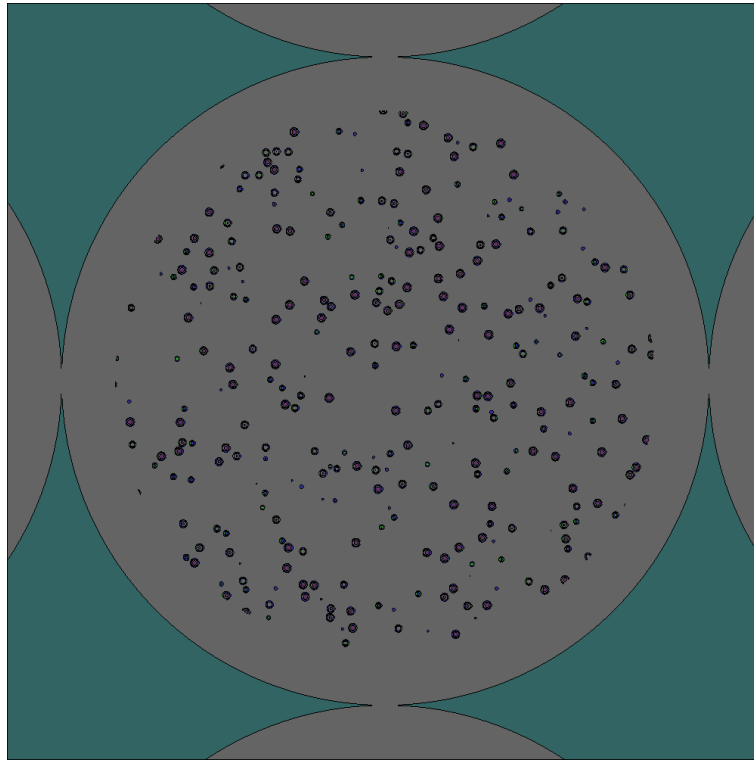


Figure 3.4: Geometry of the Single-Pebble Burnup Calculation for Sangamon20

Once the depletion simulation determines the isotopic compositions, the model homogenizes the pebbles by volume, to improve performance. The volume of a TRISO particle, and more specifically, a UCO kernel, is constant.

3.4 Heterogenization Tests

As described above, the pebbles use the approximation of a homogenized 'fueled-center', to reduce computational load. However, a few tests performed undid this change, explicitly defining all TRISO particles in the pebbles, as

they are in the single-pebble (infinite lattice) depletion models which generated the equilibrium fuel composition.

3.5 Reactor Sensitivity to Pebble Locations and Symmetry

Due to the random nature of pebble locations, it is entirely possible to have bands in the reactor such that multiple pebbles of same (or similar) burnup form lines or pockets. In the interest of better characterizing the neutronics of the reactor, a sensitivity analysis tested various pebble composition locations. The *shuffling* test maintained the pebble locations, but changed what composition the individual pebbles were. A second test completely changed the location of the pebbles in the core by randomly dispersing them again. The third analyzed the effects of utilizing a symmetry simplification, in order to improve computational speed. The core used a $\frac{1}{6}$ slice approximation. The slice used to simplify changed in each test, shown in 3.6. In each test, all other parameters remain the same.

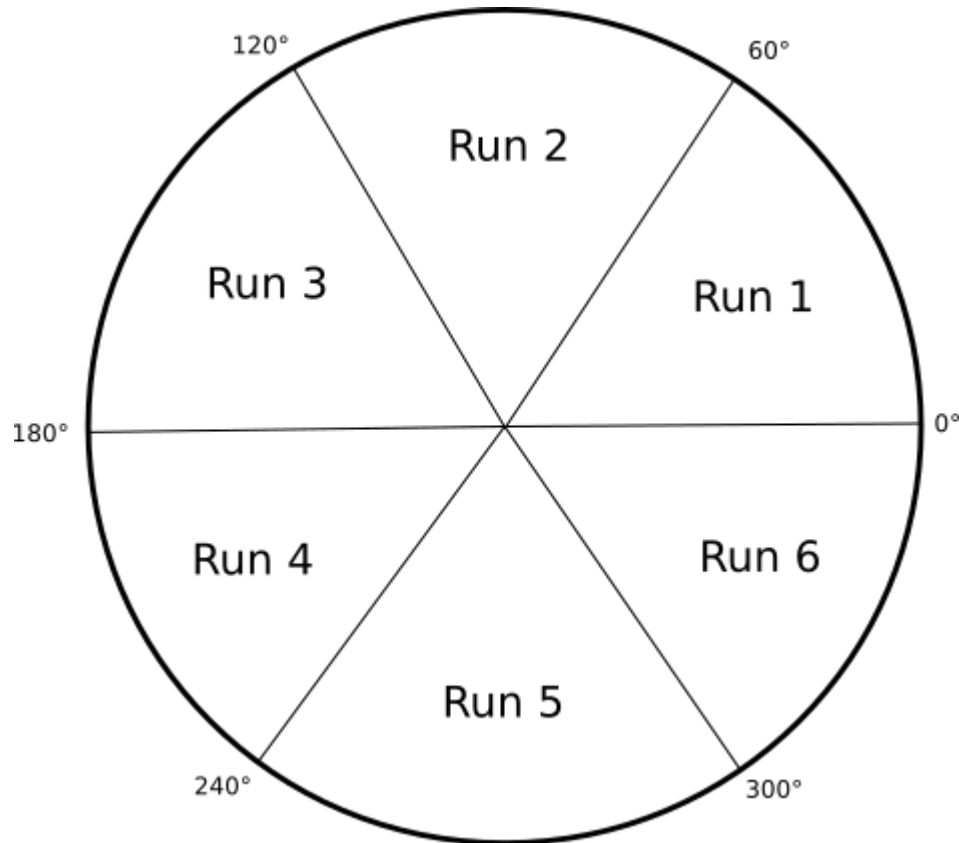


Figure 3.5: Symmetry Test Run Layouts

The shuffle tests change which fuel composition is in which pebble. As an example, Run 1 in the shuffle test makes all fresh, or "zero-pass" pebbles of the first-pass composition, first-pass pebbles of the second-pass, and so on, as follows:

$$\begin{array}{rcl} 0 & \longrightarrow & 1 \\ 1 & \longrightarrow & 2 \\ 2 & \longrightarrow & 3 \\ 3 & \longrightarrow & 4 \\ 4 & \longrightarrow & 5 \\ 5 & \longrightarrow & 6 \\ 6 & \longrightarrow & 0 \end{array}$$

Figure 3.6: Shuffle Test Run 1 Example

Run 2 makes the originally fresh (zero-pass) pebbles the second pass composition, the first-pass pebbles the third-pass composition, and so on. The other four tests follow in this same pattern.

Chapter 4

Results

*** messages surrounded by three * are notes to the reviewer, if you'd like to ctrl-f for them ***

This chapter first presents the atomic fraction of particular isotopes, the reports the results of the three model variation tests.

4.1 Fuel Isotopic Compositions

The isotopic compositions in the Sangamon20 full-core models use those generated from an infinite cubic lattice of pebbles, which use explicitly modeled TRISO particles. The fuel is fresh at the first depletion time step, and goes through six burnup cycles, each lasting six months.

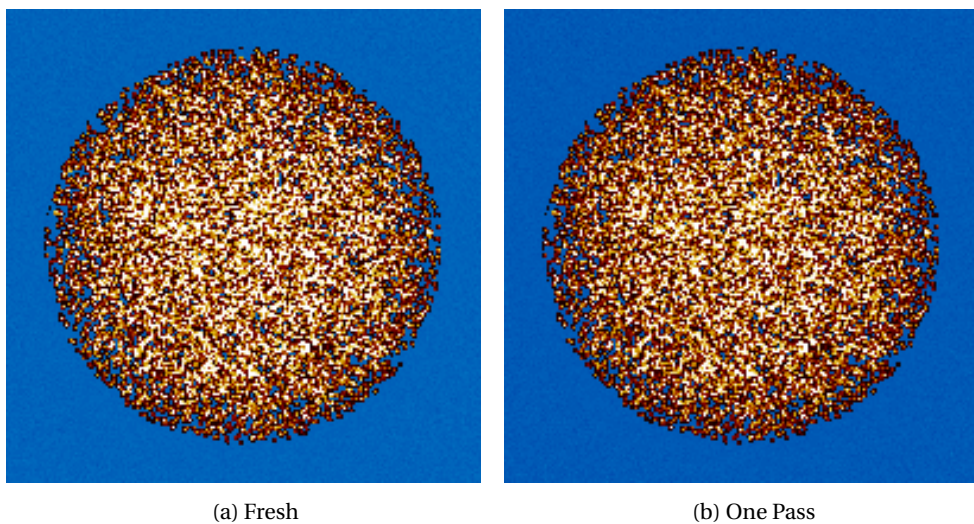


Figure 4.1: Mesh Figures For Single Pebble Burnup

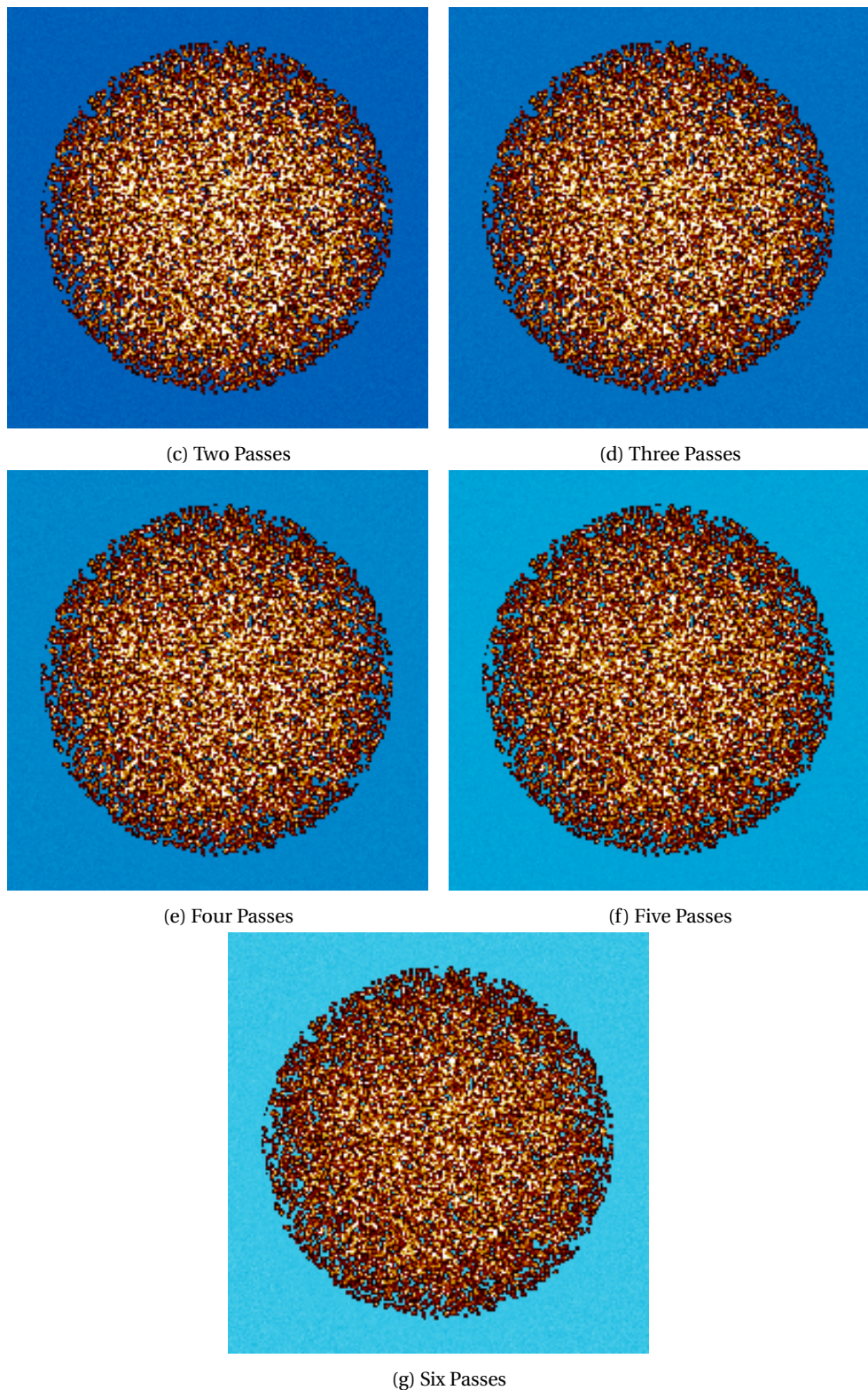
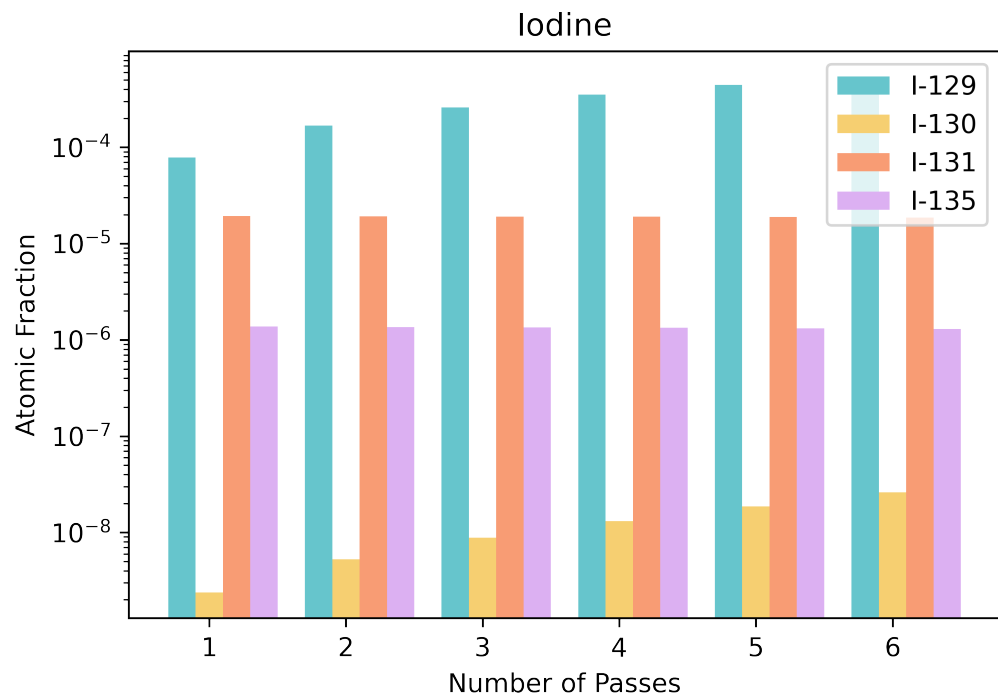


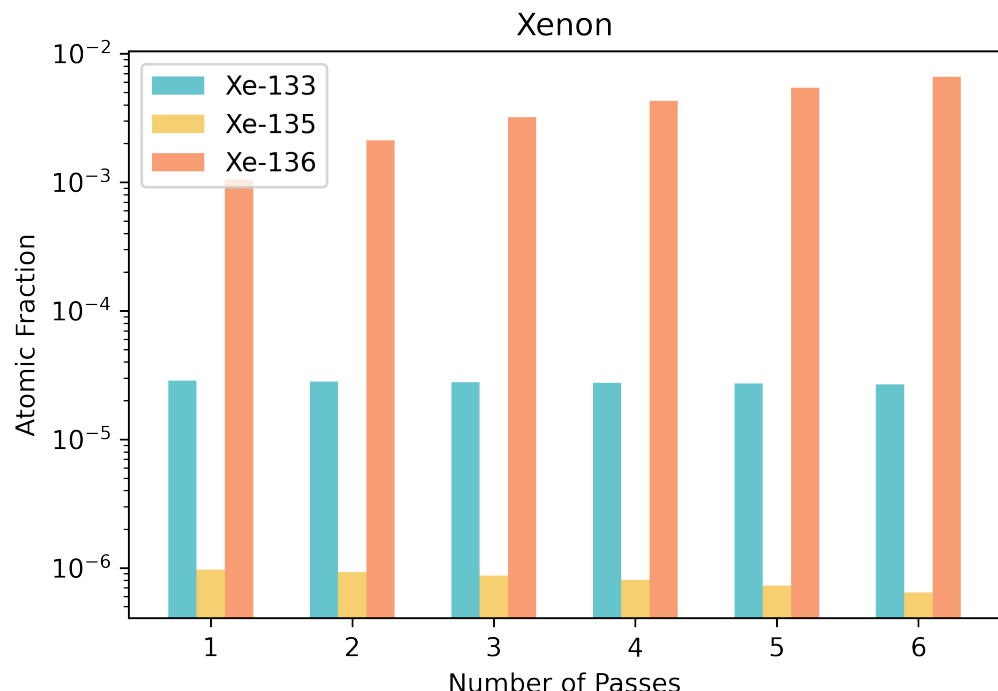
Figure 4.1: Mesh Figures For Single Pebble Burnup(cont.)

Figure 4.1 depicts the evolution of the fission rate (hot color map) and thermal flux (cold color map) over the

seven stages. The maximum cutoff for thermal flux is 0.625 eV in these figures. Over successive depletion steps, the fission rate decreases, and thermal flux increases.

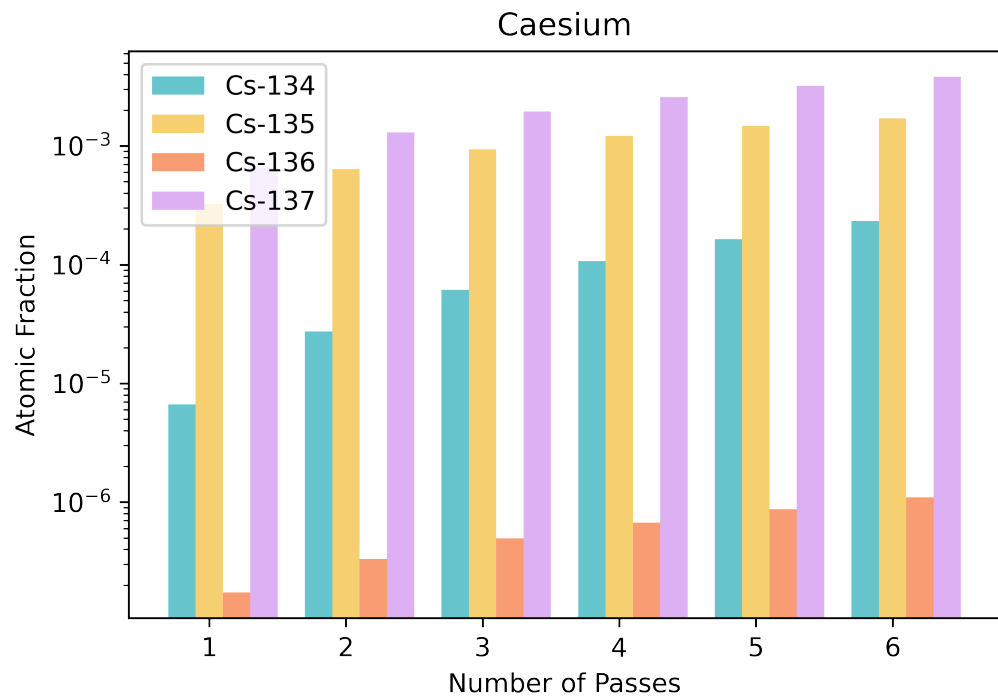


(a) Iodine

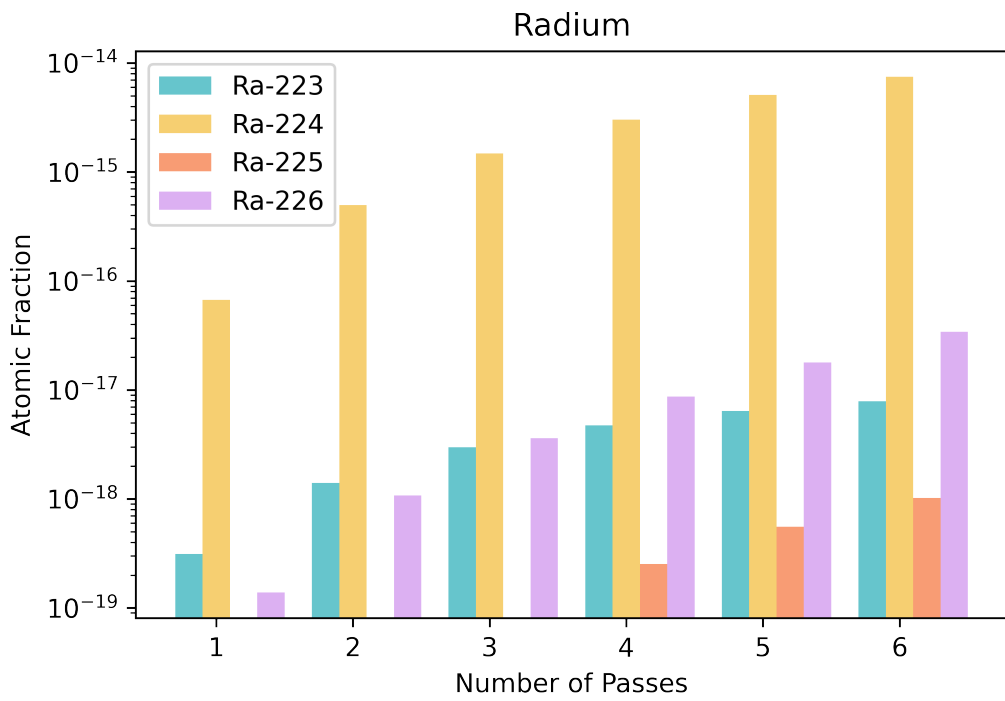


(b) Xenon

Figure 4.2: Evolution of Certain Isotopic Concentrations in Pebbles over Six Six-Month Passes (cont.)

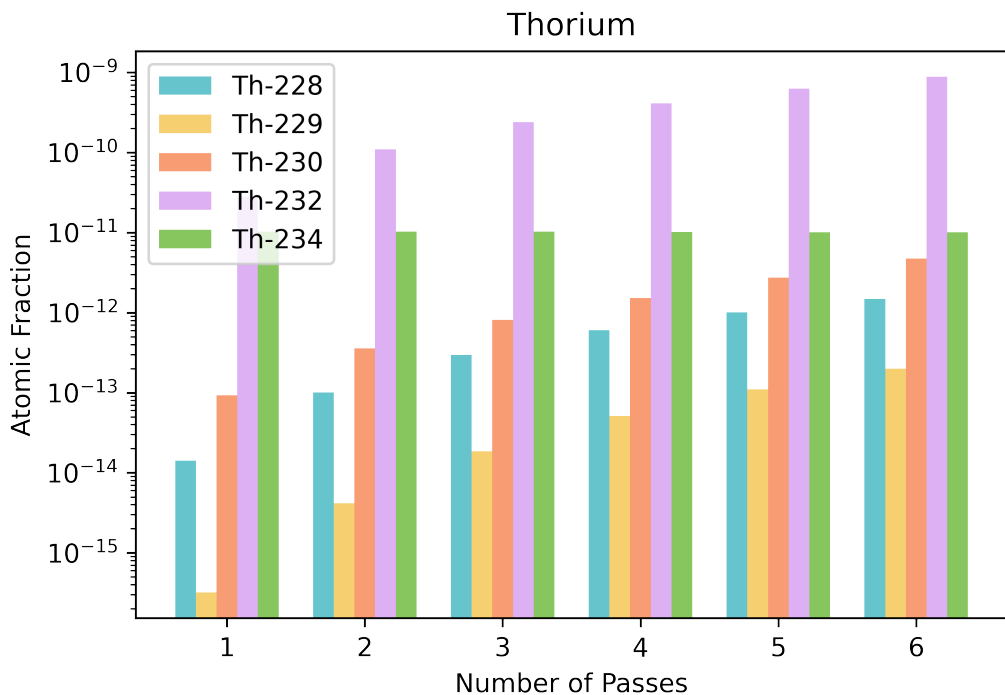


(c) Caesium

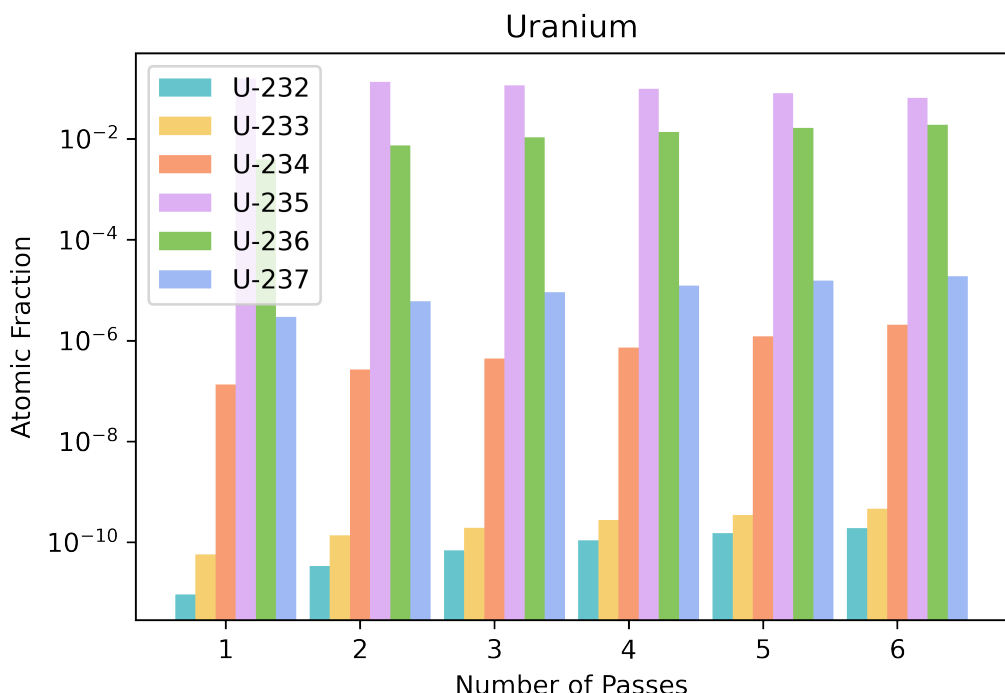


(d) Radium

Figure 4.2: Evolution of Certain Isotopic Concentrations in Pebbles over Six Six-Month Passes (cont.)

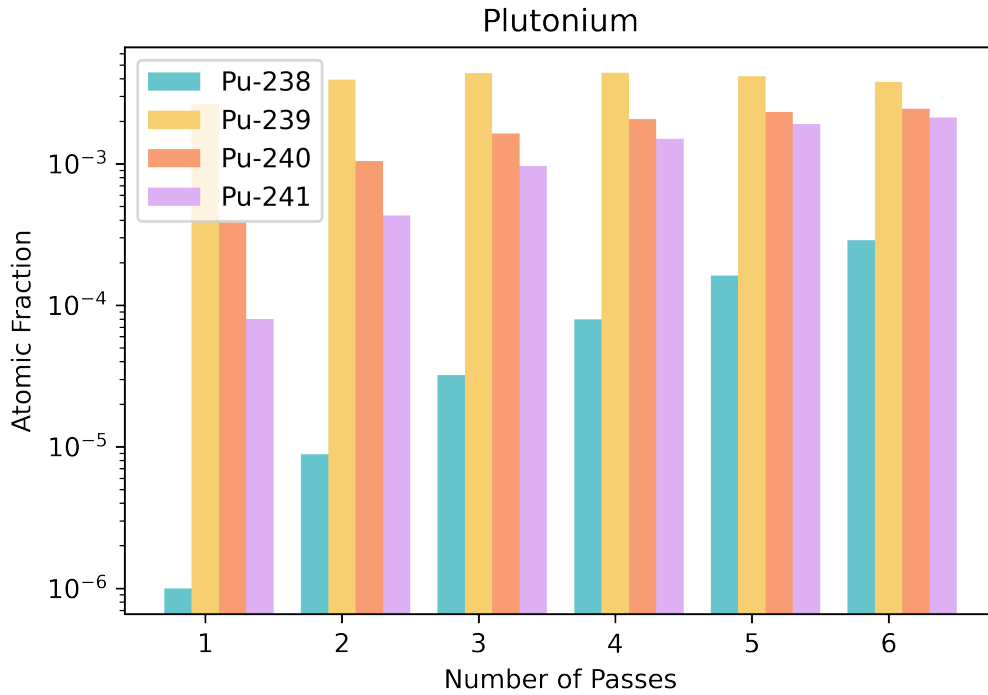


(e) thorium



(f) Uranium

Figure 4.2: Evolution of Certain Isotopic Concentrations in Pebbles over Six Six-Month Passes (cont.)



(g) Plutonium

Figure 4.2: Evolution of Certain Isotopic Concentrations in Pebbles over Six Six-Month Passes (cont.)

The full isotopic inventory tracked in the Sangamon20 reactor models extends far beyond those supplied in Figure 4.2. For a full list, see ***ref zenodo comps*** for the compositions alone, or ***ref phlox zenodo*** for a complete input file and associated output. Figure 4.2 omits any stable isotope, and focuses on those of interest in safety analysis.

The only the xenon content rivals the inventory of uranium. All isotopes of uranium steadily increase over time with the exception of ^{235}U , ending at 0.0647 by atomic fraction in the sixth pass. ^{232}U , initially the smallest fraction of uranium sees the most dramatic increase over time, increasing by two orders of magnitude between the first (9.28×10^{-12}) and sixth (1.9×10^{-10}) cycle. While the atomic fraction doesn't reach an equilibrium, the rate at which it increases each cycle is steady - increasing by 4.02×10^{-11} , 4.2×10^{-11} , and 3.9×10^{-11} from the third to fourth, fourth to fifth, and fifth to sixth pass, respectively. Plutonium content is also fairly high, with ^{239}Pu peaking at 0.00439. However, unlike many other isotopes, which peak in the sixth cycle, ^{239}Pu crests in the third and fourth passes, decreasing from 0.00439 in the fourth pass to 0.00380 in the sixth. Pu-238, meanwhile, is the least abundant, but does experience the most dramatic increase over time (especially between the first and second passes).

^{133}Xe seems to be steady around its initial concentration of 2.86×10^{-5} atomic fraction, decreasing only to

2.68×10^{-5} by the sixth pass. ^{135}Xe decreases a bit more dramatically, going from an initial 9.70×10^{-7} after its first six months, to 6.46×10^{-7} after thirty-six months. ^{136}Xe is both the greatest contributor to xenon content in the fuel, and the only isotope reported in Figure 4.2b to increase, owing to its long half life. Each cycle increases ^{136}Xe content by 0.0011, beginning at a concentration of 0.00105 in the first cycle and ending at 0.0066 after the sixth. Isotopes of iodine form a smaller portion of fission products than xenon or caesium (still a relatively high magnitude) which is of concern due to its high mobility in water and uptake in the thyroid. ^{129}I is the most abundant isotope of iodine reported here. It increases for the entirety of the pebble's life, beginning at 7.38×10^{-5} and peaking at 0.000538 at its discharge burnup. ^{130}I and ^{135}I are both relatively stable, most likely due to their short half-lives, combined with transmutation after undergoing neutron capture. While ^{130}I is the least abundant, it increases over time. Caesium has a net concentration similar to xenon's. Unsurprisingly ^{135}Cs and ^{137}Cs , which both have half-lives longer than a pebble's stint in the reactor, are in greatest abundance, and increase over time.

Of the elements reported here, radium and thorium are in lowest abundance. ^{225}Ra only appears in trace amounts (less than or equal to 9.99×10^{-20}) for the first three passes. ^{224}Ra far outweighs the other reported isotopes of radium, with an atomic fraction of 7.46×10^{-15} after thirty-six months - two orders of magnitude higher than all other isotopes of radium combined at this depletion step. Thorium has the second-least abundant atomic fractions, with fertile ^{232}Th being the most abundant, at 8.80×10^{-10} in the sixth pass.

4.2 Full-Core Control Model

Figure 4.4 shows a cross section of the core geometry at the origin in the xy and xz planes (Sub-Figures a and c, respectively) and provides a mesh of the fission rate and thermal flux in the xy and xz planes (Sub-Figures b and d, respectively). Both of these integrate over z and y, respectively, to produce a 2D image. Analytically calculated k_{eff} was 1.04077 ± 0.00054 .



Figure 4.3: Legend for Geometry Figures

Figure 4.3 is accurate for all cross sections of reactor geometry. In homogenized simulations, the shades of green

represent the material blend forming the center of the pebble at a given burnup. For heterogenized simulations, these same shades represent the TRISO particle kernel at a particular burnup.

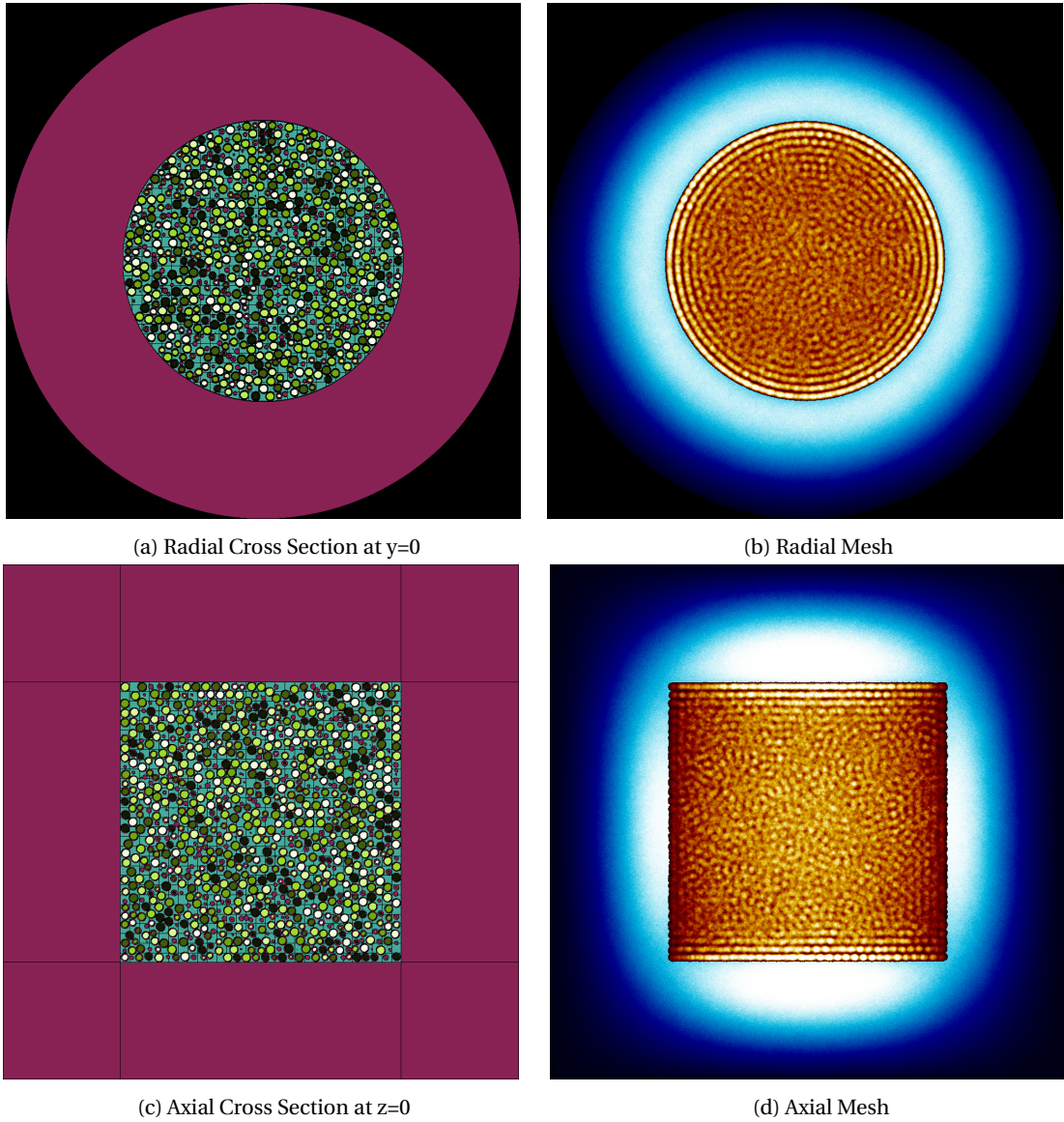


Figure 4.4: Full Core

The mesh in Figure 4.4b shows bands of concentric rings around the outer edges of the active core. These bands suggest that the outermost areas of the core are regions of high fission activity relative to the center, which is at odds with what most might expect from the neutronics behavior in a cylindrical reactor. Certainly the pebbles are physically forming rings at the outer edges, and their placement becomes more haphazard toward the center. However, the high intensities seen in this outer region in the mesh figures are unindicative of a total flux profile showing the same. Remember that Serpent 2 integrates over the z direction to produce a 2D plot of the xy plane. For

a cylinder, the distance in z each point integrates over is the same - the height of the reactor. However, points at the outermost regions are integrating in a volume composed more of pebbles - and therefore fissile material - than the center, where more space filled with coolant.

In Figure 4.4d we can see a similar banding effect on the top and bottom edge of the core region, but not on the sides. No hot-spots on the edges because Figure 4.4d is in the xz plane, and integrates over y. However, for a cylinder, the distance integrated over is not the same at all points. At the centerline, the distance is simply the diameter. However, as you move towards the edge, the distance integrated over approaches zero.

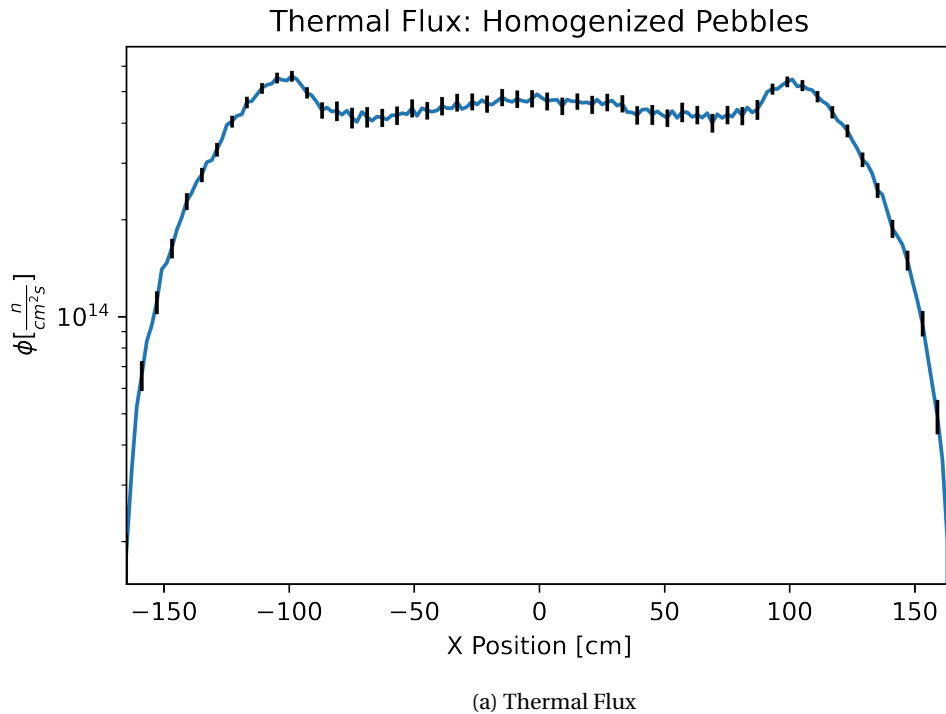


Figure 4.5: Radial Thermal and Fast Flux Profiles

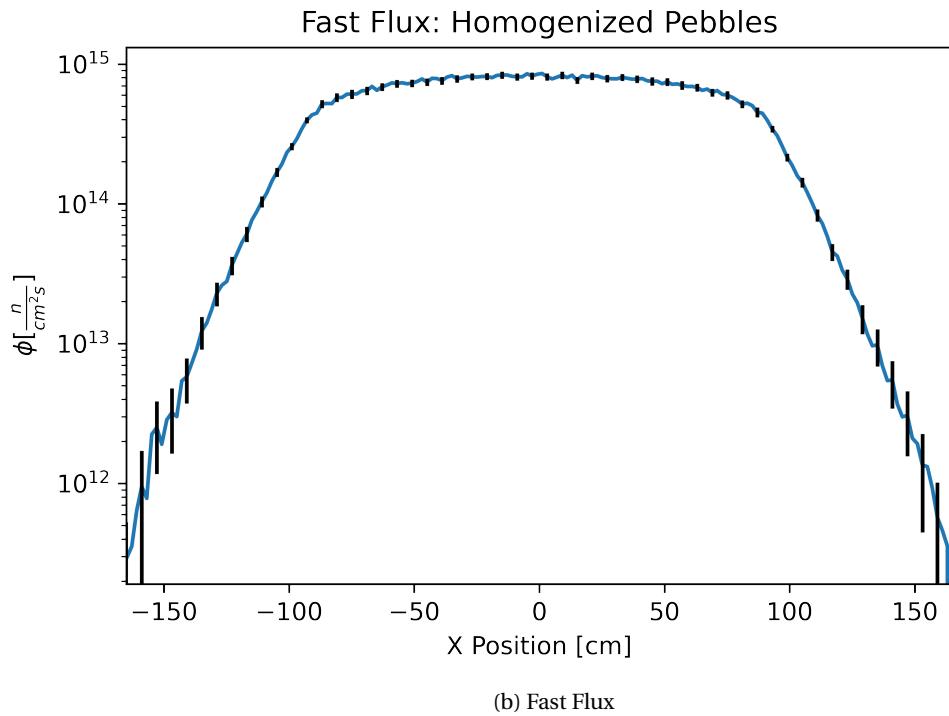


Figure 4.5: Radial Thermal and Fast Flux Profiles (cont.)

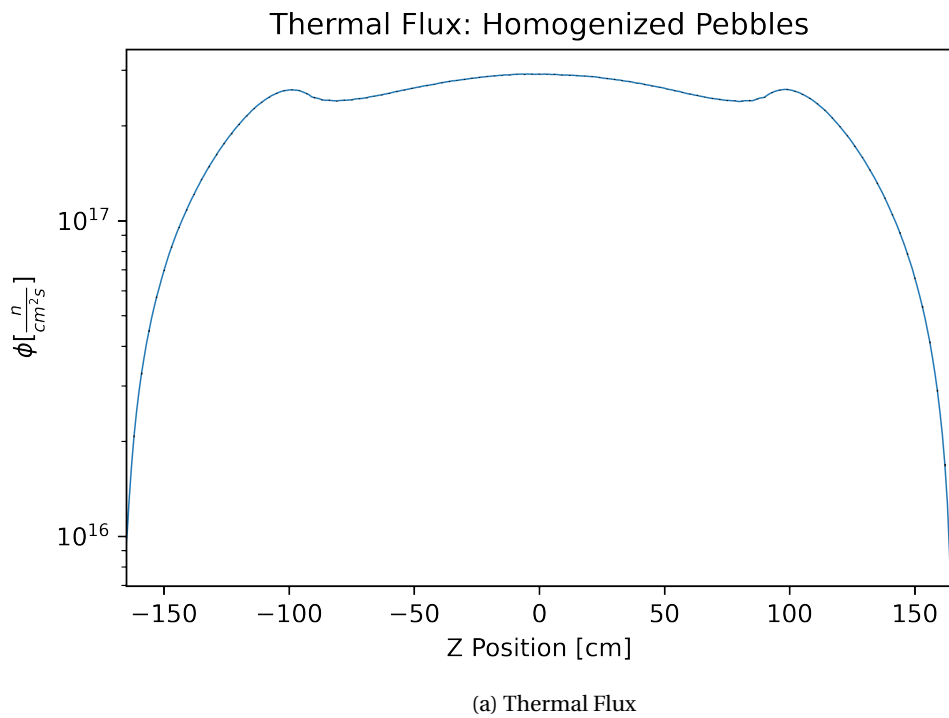


Figure 4.6: Axial Thermal and Fast Flux Profiles

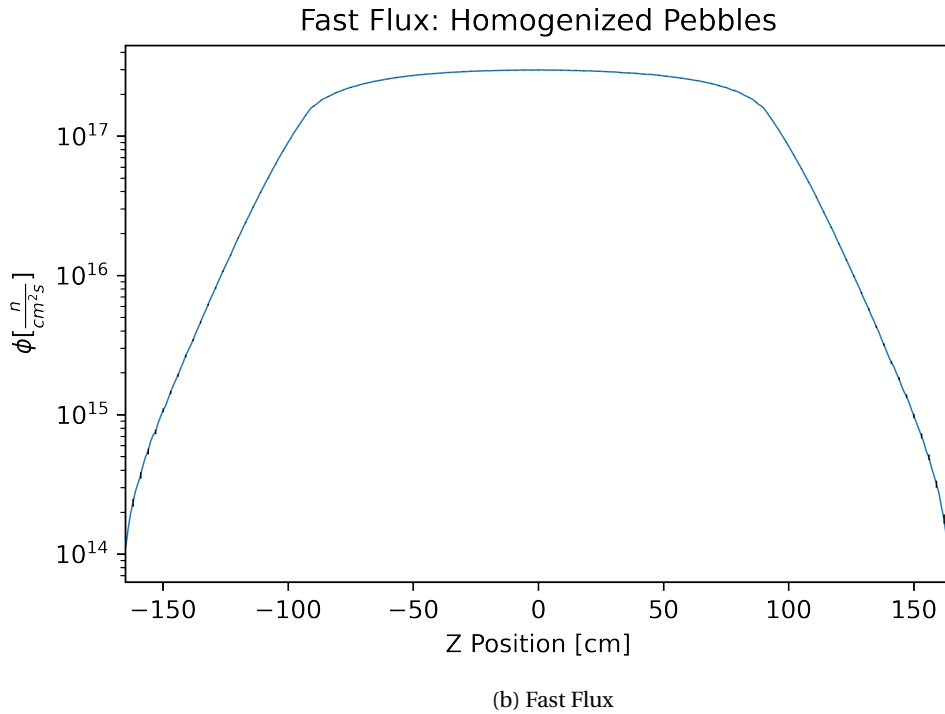


Figure 4.6: Axial Thermal and Fast Flux Profiles (cont.)

***I know that there should be continuity at 0 between the axial and radial flux profiles, and there currently is a difference of 3 orders of magnitude. I believe this is because of differing bin sizes between the detector that tracked the axial fluxes, and the detector that tracked the fluxes at the xy plane. Basically, in the axial detector, each bin had a defined length in z, 0.1 cm or what-have-you. However, these bins had no x or y limitations, and covered all x and y at that point (the bins are shaped like a stack of pancakes or such). For the radial detector, I had to create the detector bins such that they formed a uniform grid over the xy plane, centered on the origin (which is the physical center of the reactor). These bins were finite in x and y, but not in the z direction, so they covered all z that fell within the limits of the bin (these bins are like a long rectangular prism). While this uniform grid prevents the radial flux profile from warping, which is what happens if you attempt to make a detector along only one axis (the bins end up being unequal sizes), the fact that the axial detector bins differ from the radial detector bins means they don't match each other.

tl;dr: should I divide the neutron flux by bin volume so the axial and radial profiles match in magnitude (hopefully)***

Figures 4.5 and 4.6 provide the fast and thermal flux profiles in Sangamon20. The former are the radial fluxes, along the x-axis, and the latter are the center line profiles. Both axially and radially, the thermal flux sees a 'bump', which peaks approximately 10 cm into the reflector, at 100 cm. These are the highest peaks in the thermal flux, with

the second highest thermal flux being at the center line. For the fast flux profile we see a flattened peak in the active core (-90.0 cm to 90 cm) and 10 cm into the reflector. Fast flux rapidly decreases in the reflector as fast neutrons down scatter in the graphite.

Both Figures 4.5 and 4.6 show that while the radial banding seen in the fission rate mesh profiles are of high intensity, the flux peaks are elsewhere.

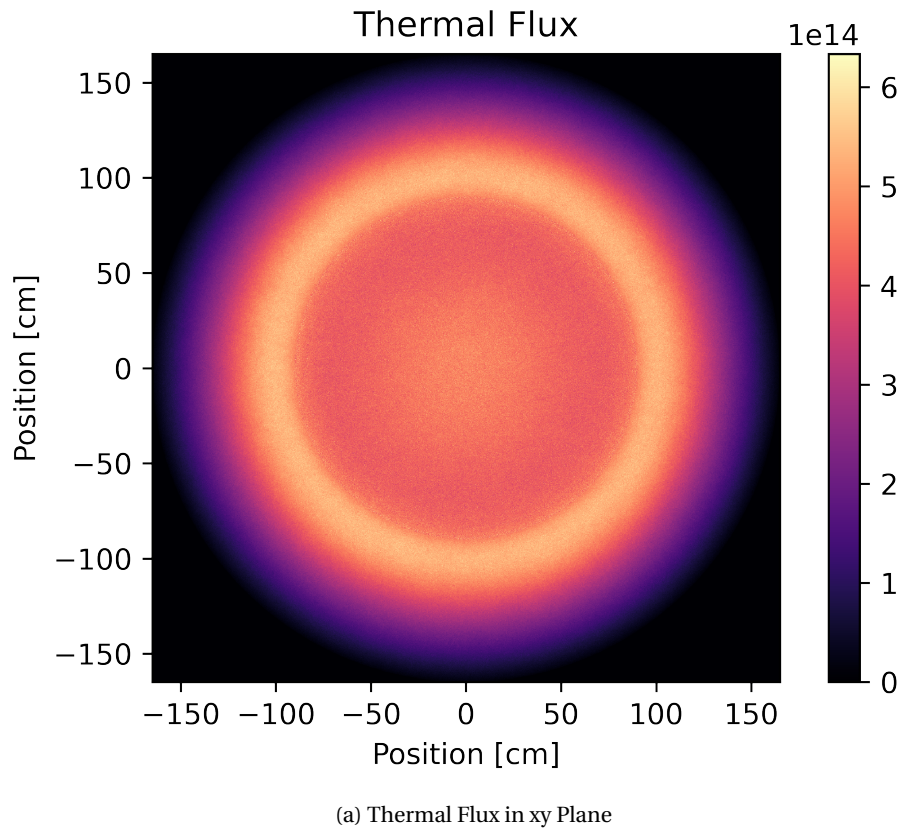
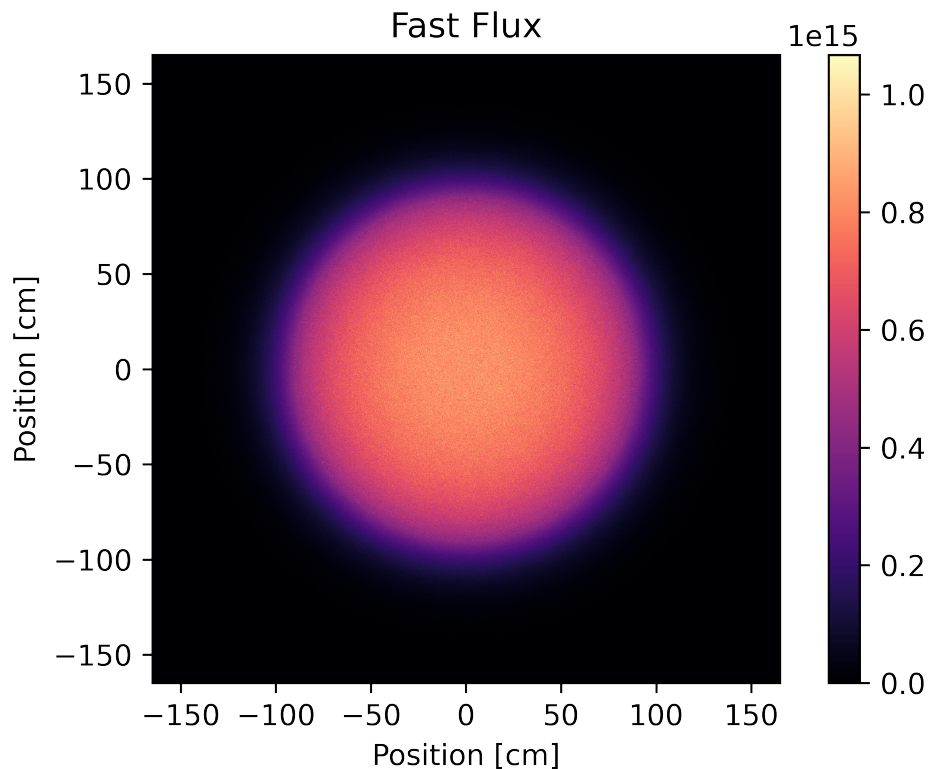


Figure 4.7: Thermal and Fast Flux Profiles



(b) Fast Flux in xy Plane

Figure 4.7: Thermal and Fast Flux Profiles (cont.)

***I kinda want to make these big to see detail (especially since I discuss some of the finer details in the image). Maybe I could show a smaller version here, and then add a larger version in the appendix, where it doesn't matter if my mesh plot takes up its own page. ***

Figure 4.7 provides the total flux over the xy plane at $z = 0$. A slight banding pattern on the active core's edge exists, but with less intensity of the fission rate banding. Once again, Figure 4.7 shows that while the banding morphology may be present in the flux profile (and do cause a slight increase relative to the region immediately surrounding it) it does not cause concentric spikes in the flux profiles.

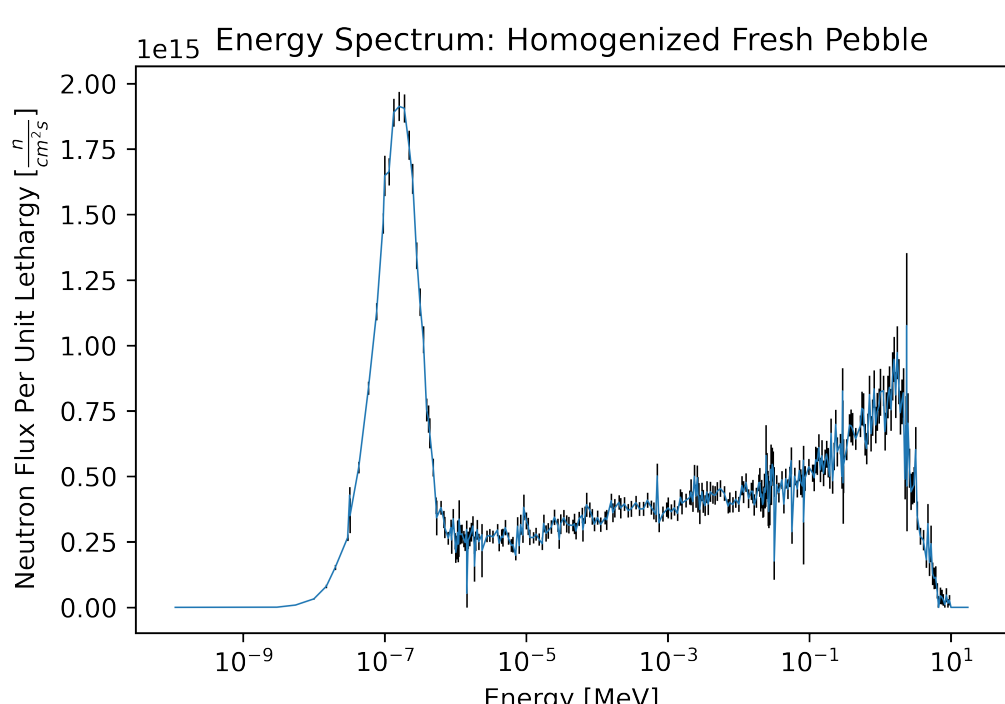
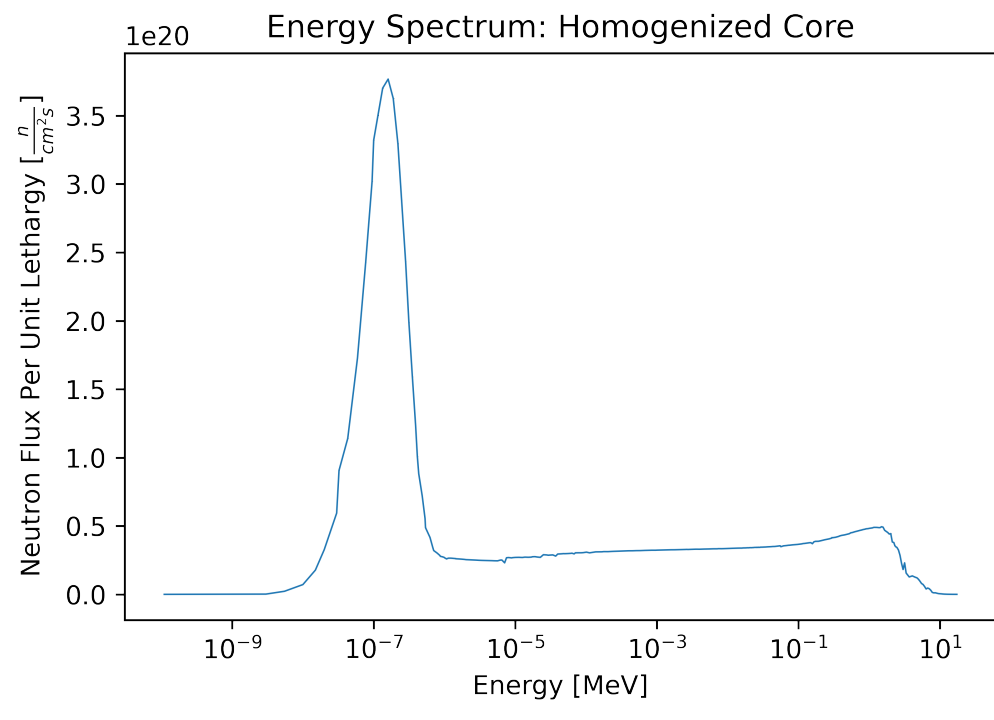
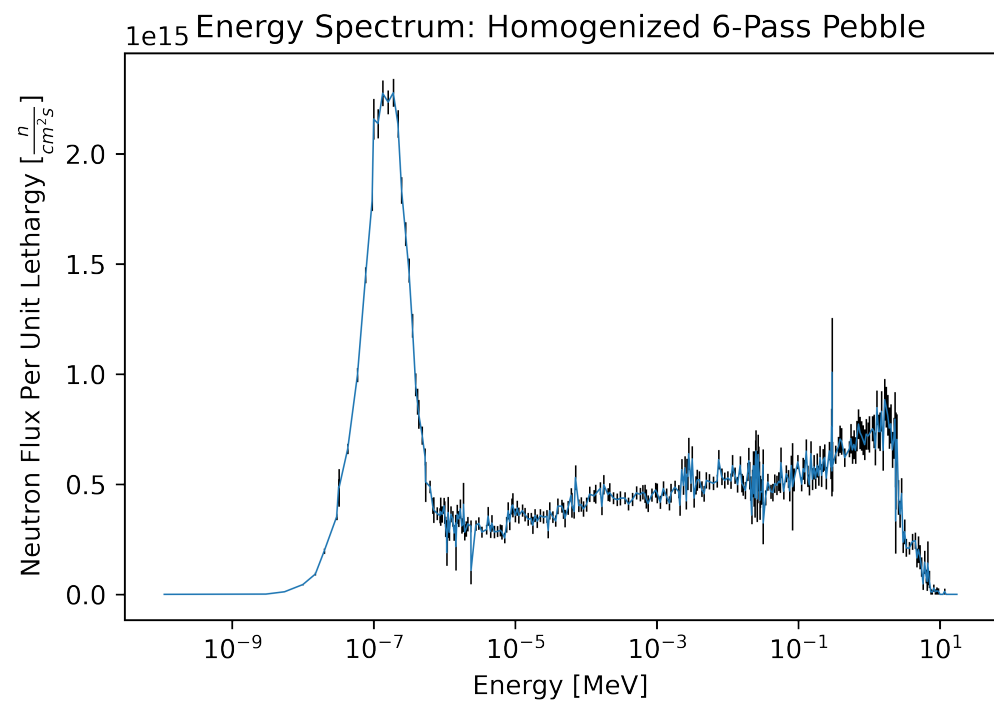
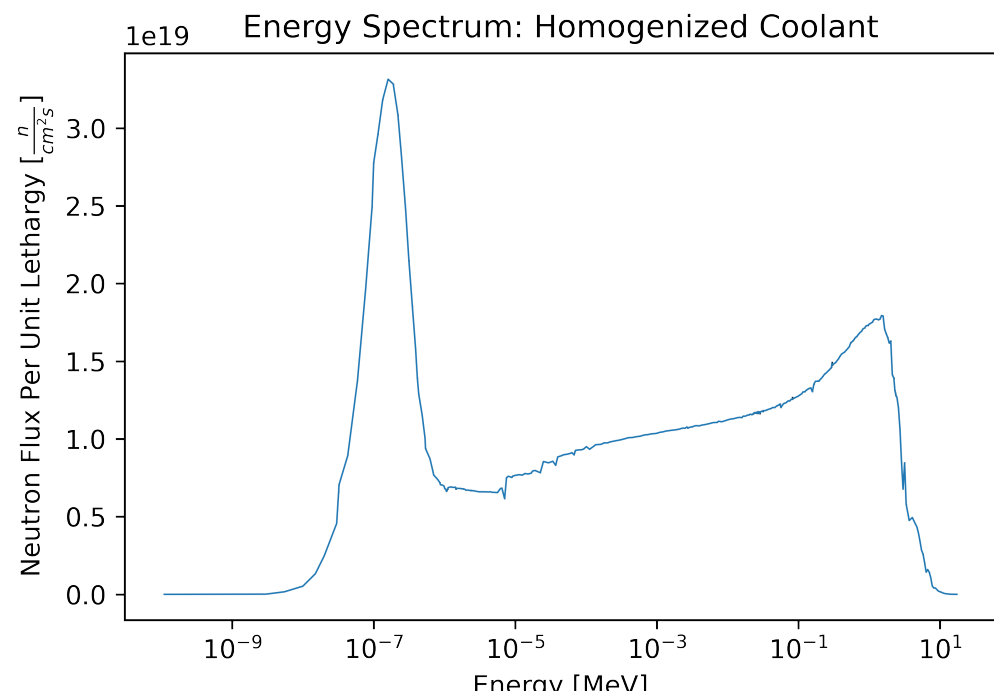


Figure 4.8: Lethargy Adjusted Neutron Flux Energy Spectra



(c) Six-Pass Pebble Spectrum



(d) Coolant Spectrum

Figure 4.8: Lethargy Adjusted Neutron Flux Energy Spectra (cont.)

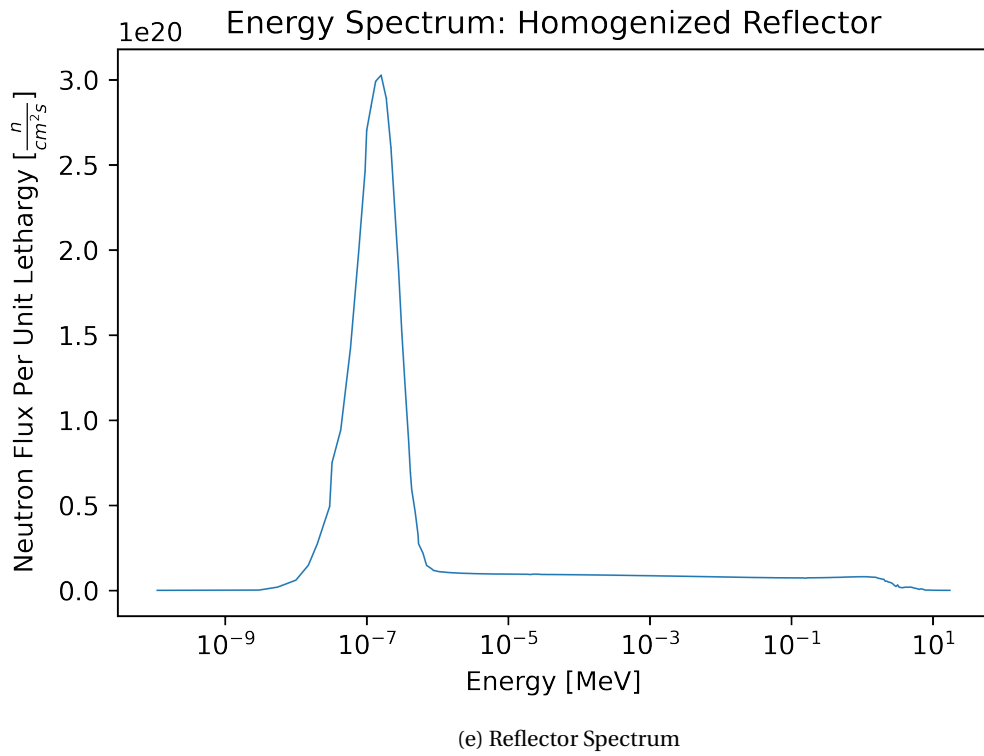


Figure 4.8: Lethargy Adjusted Neutron Flux Energy Spectra (cont.)

Above, Figure 4.13 gives the energy spectra in the reflector, coolant, overall core, and a randomly selected fresh and sixth-pass pebble. The results are per unit lethargy and use the Tripoli 315-group energy structure to set energy bin boundaries.

The thermal peak of the whole-core and reflector both occur around 10×10^{-7} MeV, which is also the energy of neutrons most-responsible for fission. The thermalization of neutrons in the reflector dominates the spectrum in Figure 4.8a, indicated by the high magnitude of the thermal peak in the reflector and core and their similar shape.

The spectra for a randomly selected fresh and sixth-pass pebble are subject to the highest uncertainty of all the provided spectra in Figure 4.13, as a single pebble is a relatively small bin. However, if coupled with the coolant spectra, Figure 4.8d, they provide a clearer look at the flux energy spectrum in the active core region. We can see that, while the thermal energy of the fresh and six-pass pebbles are similar in shape and magnitude, the higher energy range differs considerably.

4.3 Effect of Homogenizing

The results discussed previously use the assumption of a pebble that has the TRISO particles homogenized and blended with the rest of the pebble matrix in the region containing fuel. However, homogenization can cause under-predictions of k-eff as much as 5-6% [29]. And so, this test uses an otherwise identical model with explicit TRISO particles to investigate the effect of homogenization. As a reminder, the isotopic compositions come from the same burnup simulation. As such, the isotopic compositions between the homogenized and heterogenized simulations are identical.

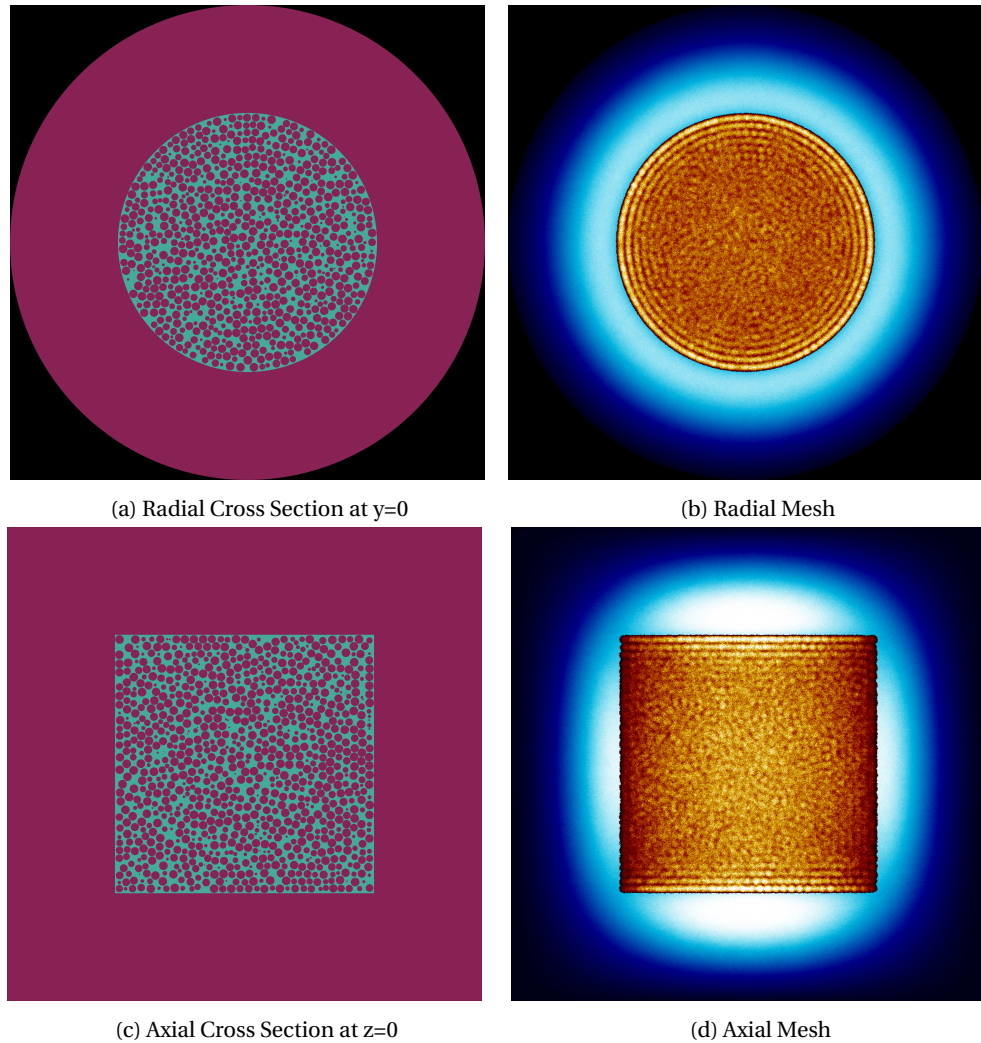


Figure 4.9: Full Core Using Heterogenized Pebbles

In agreement with [29], the heterogenized version reported a k-eff of 1.087 ± 0.00032 , compared with the homogenized's 1.041 ± 0.00054 , a difference of 4.23%.

Overall, the mesh result for the fission rate is much the same - the banding patterns are still present, if slightly

less defined. While Figure 4.9 best serves as a qualitative visualization aid, Figures 4.10, 4.11, and 4.12 support this in a more quantitative manner.

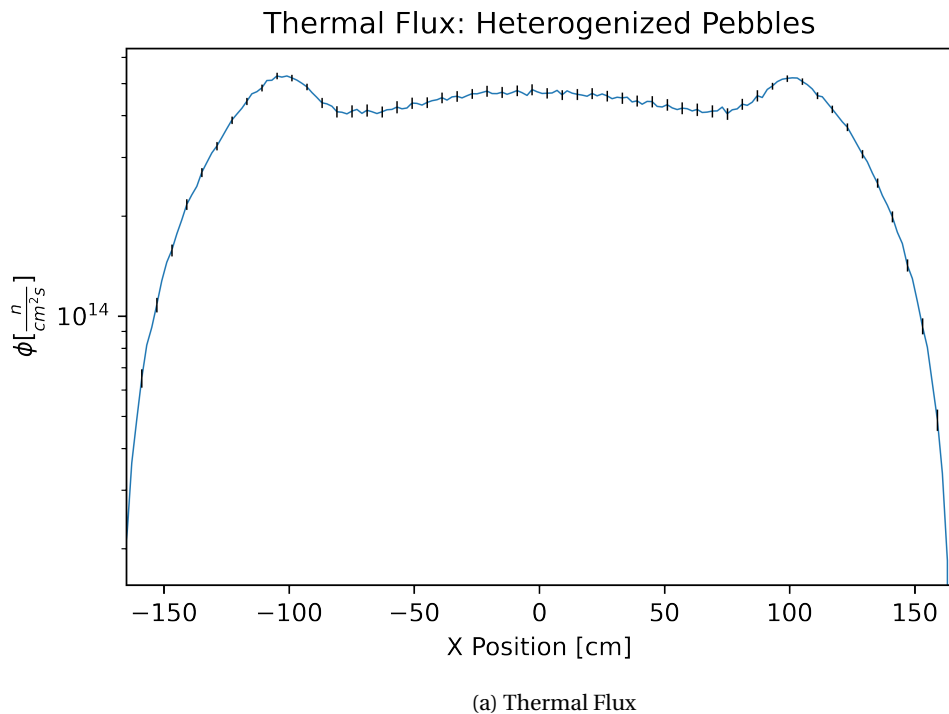


Figure 4.10: Radial Thermal and Fast Flux Profiles: Heterogenized Pebbles

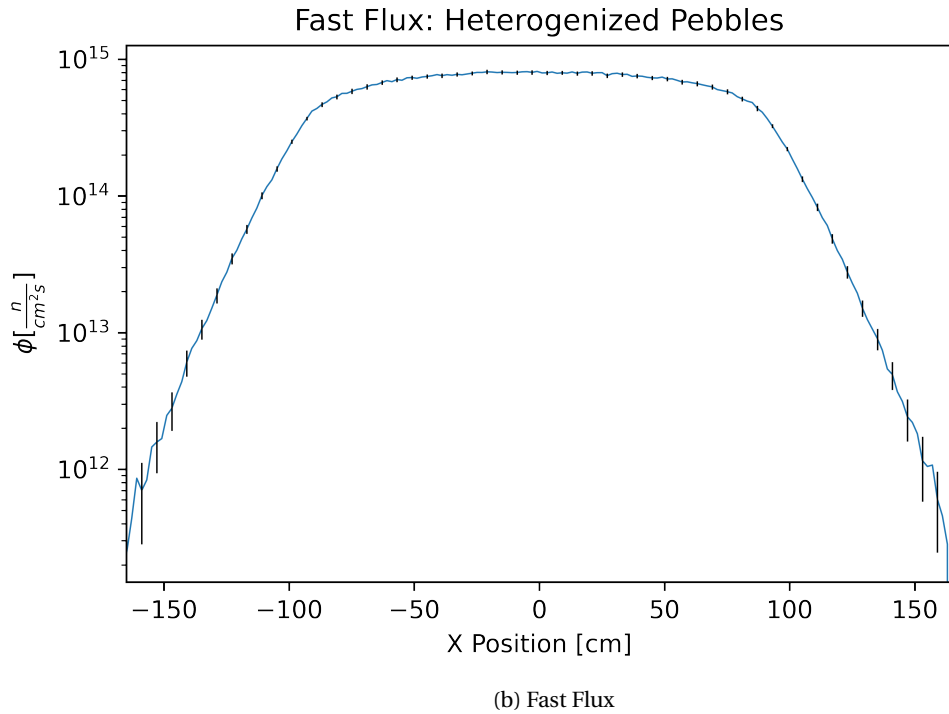


Figure 4.10: Radial Thermal and Fast Flux Profiles: Heterogenized Pebbles (cont.)

Compared with the homogenized Sangamon20, the heterogenized core reports a slightly lower neutron current at the outer edge of the reflector, at $5.718 \times 10^{11} \pm 1.735 \times 10^{-9}$, an absolute difference of approximately 2.00×10^{09} . The heterogenized model otherwise shows a similar flux profile to the homogenized model, and experiences a similar level of uncertainty in the outer edges of the reflector for the fast flux profiles, likely due to the significant thermalization of neutrons by that point in the reflector.

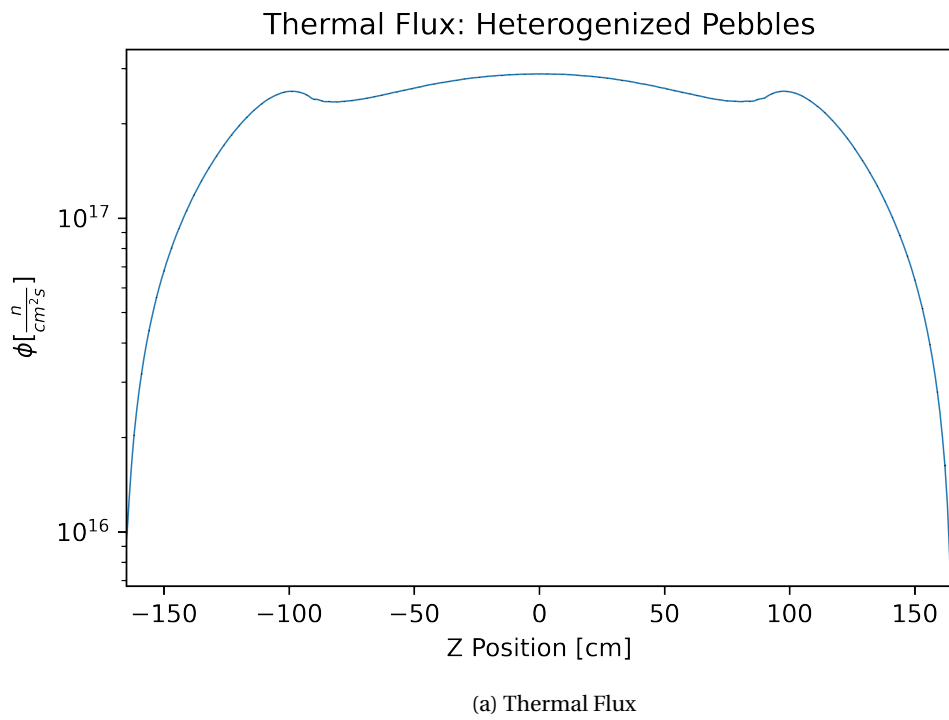


Figure 4.11: Axial Thermal and Fast Flux Profiles: Heterogenized Pebbles

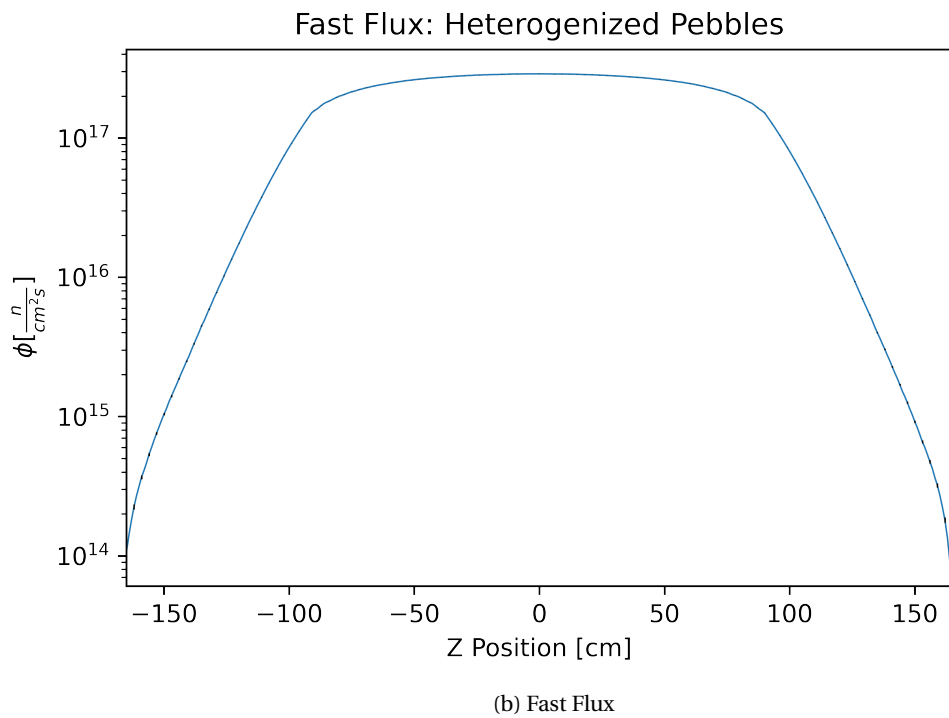
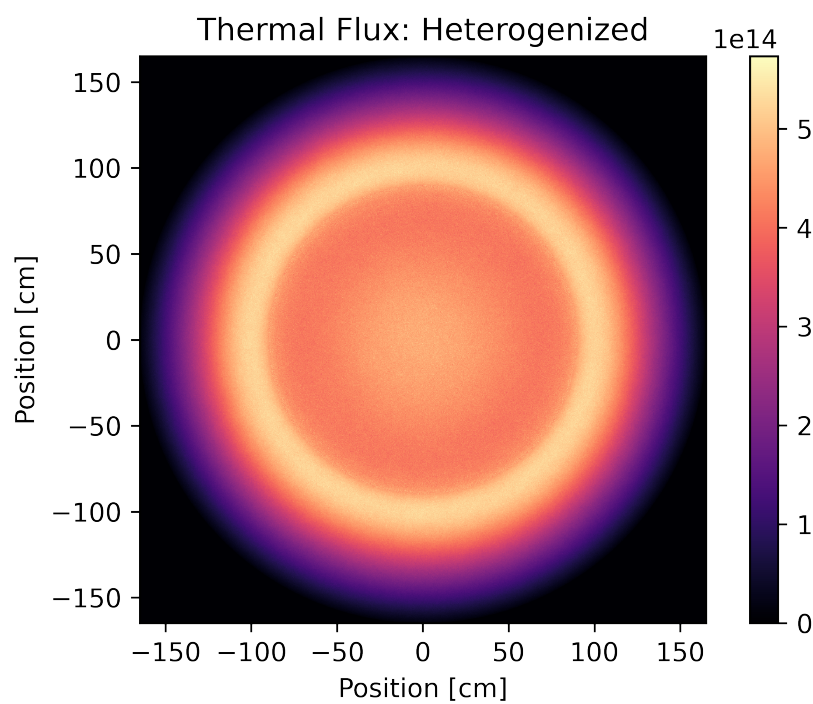
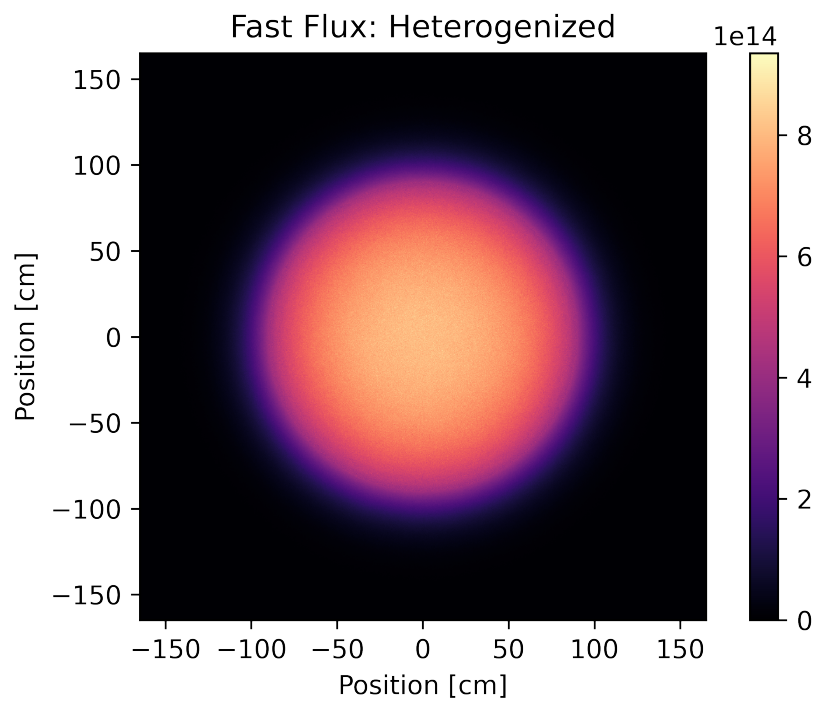


Figure 4.11: Axial Thermal and Fast Flux Profiles: Heterogenized Pebbles



(a) Thermal Flux in xy Plane: Heterogenized Pebbles



(b) Fast Flux in xy Plane: Heterogenized Pebbles

Figure 4.12: Thermal and Fast Flux Profiles

Compared with Figure 4.7, the edge pebble bands are much less distinct. This is because the homogenized pebbles have the fissile material spread over the entirety of the 2.5 cm radius fueled center. The heterogenized pebbles, meanwhile, may have the same number of fissile atoms, but the concentrate the regions capable of fission in the TRISO kernel. The rest of the pebble consists of its graphite matrix.

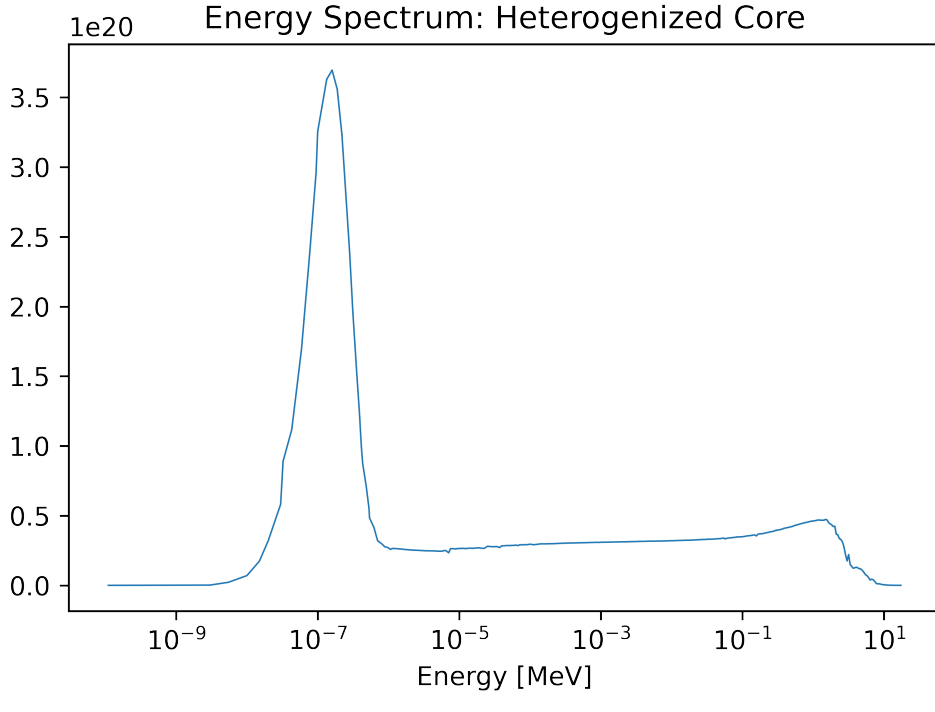
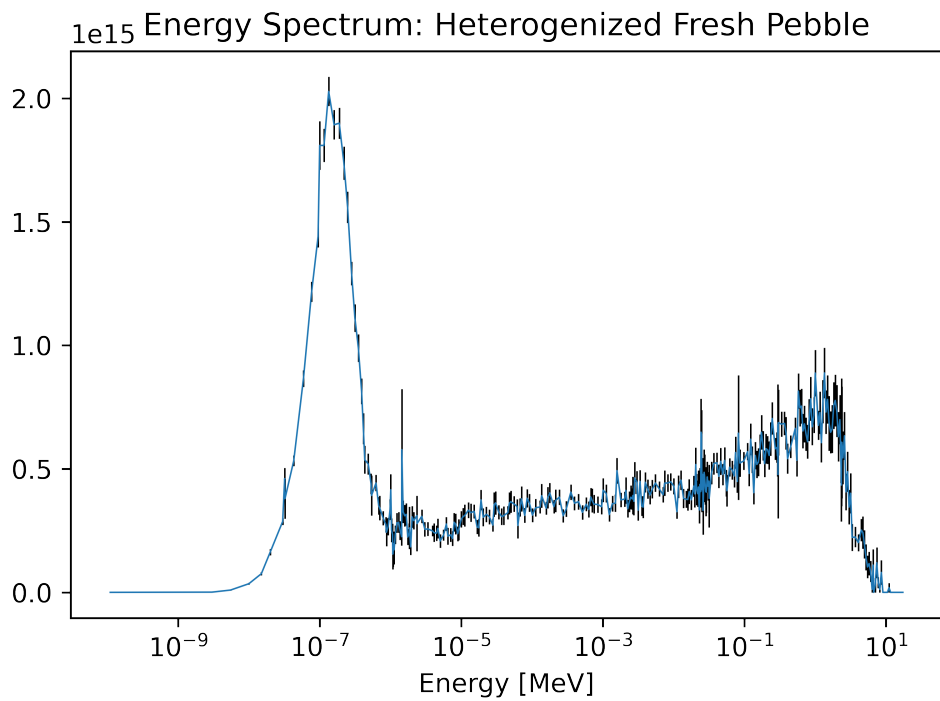
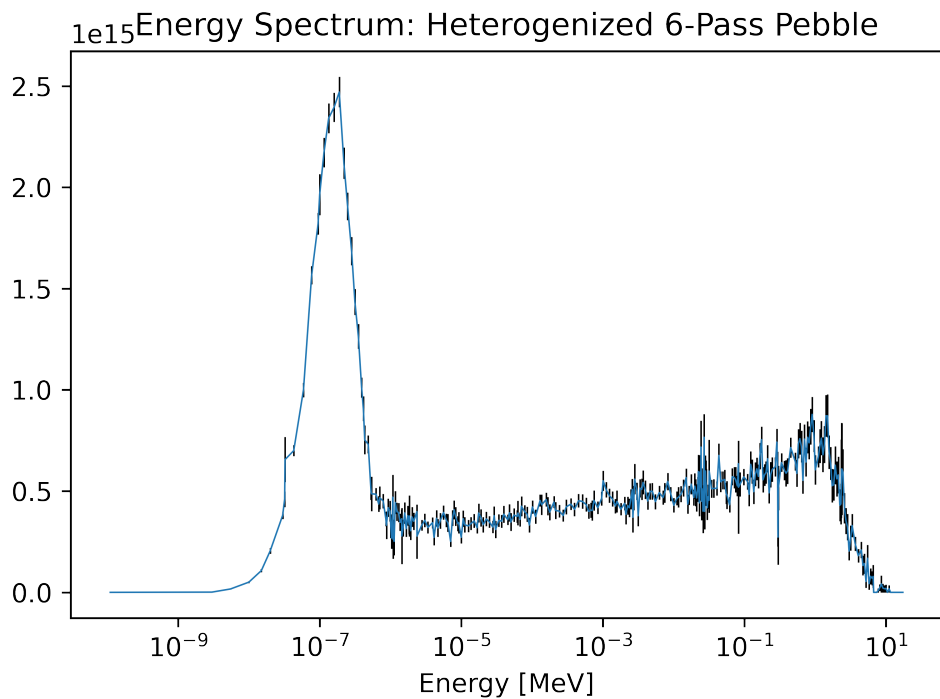


Figure 4.13: Lethargy Adjusted Neutron Flux Energy Spectra: Core Using Heterogenized Pebbles

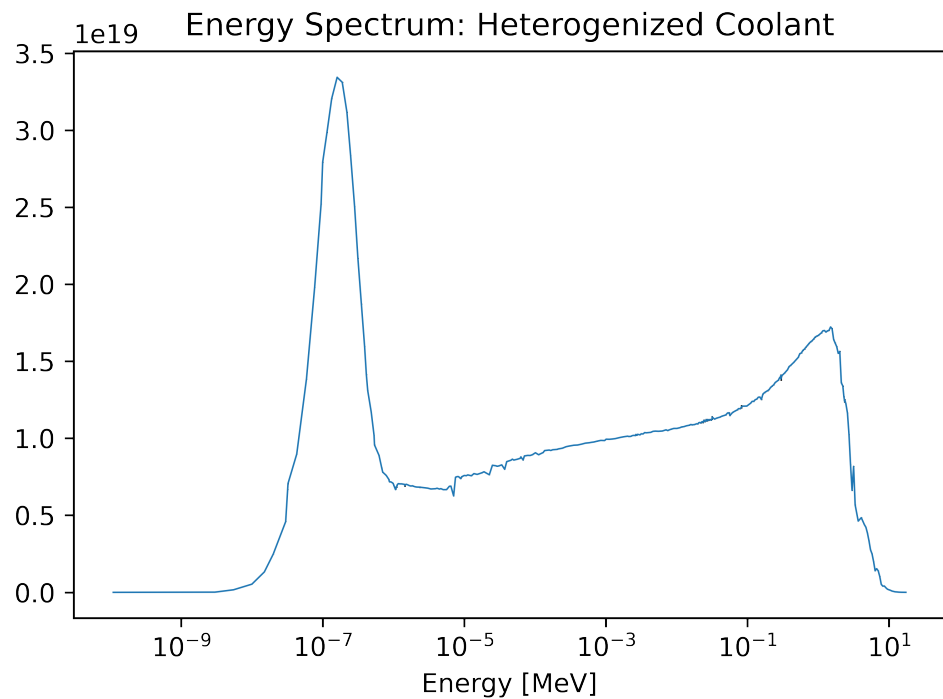


(b) Fresh Pebble Spectrum

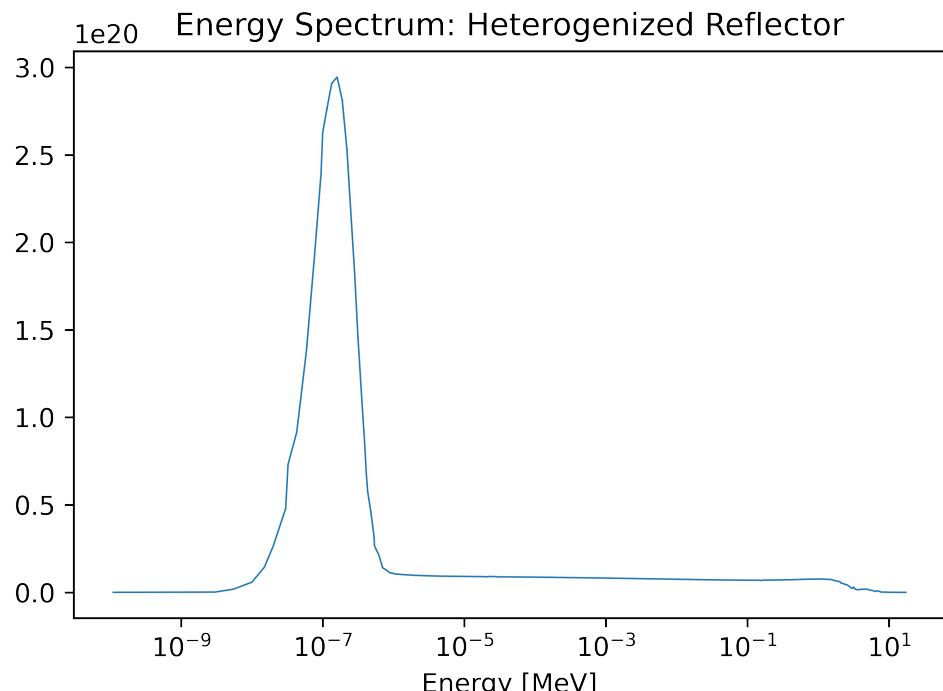


(c) Six-Pass Pebble Spectrum

Figure 4.13: Lethargy Adjusted Neutron Flux Energy Spectra: Core Using Heterogenized Pebbles (cont.)



(d) Coolant Spectrum



(e) Reflector Spectrum

Figure 4.13: Lethargy Adjusted Neutron Flux Energy Spectra: Core Using Heterogenized Pebbles (cont.)

The heterogenized spectra, much like the flux profiles, are of a similar morphology. In order to better examine the differences between the homogenized and heterogenized versions, Figures 4.14 and 4.15 plot the simple relative difference for all spectra, and the radial fast and thermal profiles. The relative difference calculation used the following:

$$\Delta i = \frac{i_{hom} - i_{het}}{i_{het}} \quad (4.1)$$

where

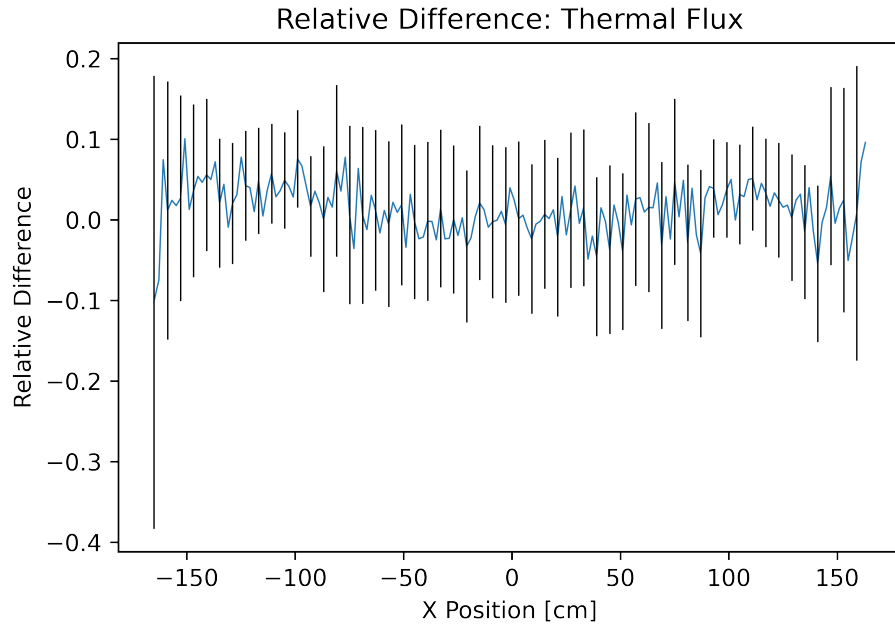
Δi = relative difference for parameter i between homogenized and heterogenized model

i_{hom} = homogenized parameter i

i_{het} = heterogenized parameter i

(4.2)

And error calculation followed simple error propagation rules.



(a) Thermal Flux

Figure 4.14: Relative Difference in Radial Thermal and Fast Flux Profiles Between Cores Using Homogenized and Heterogenized Pebbles

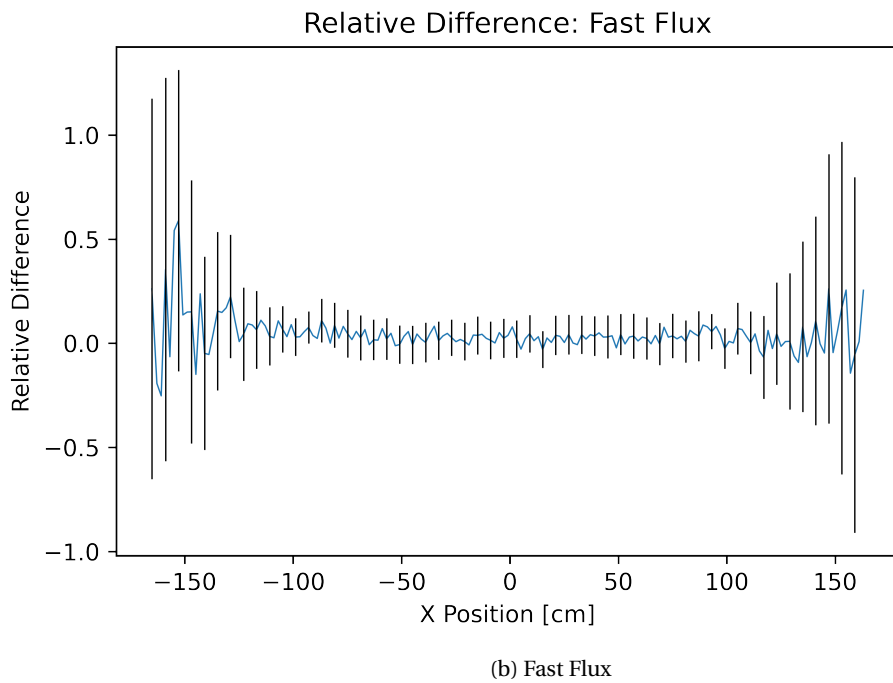
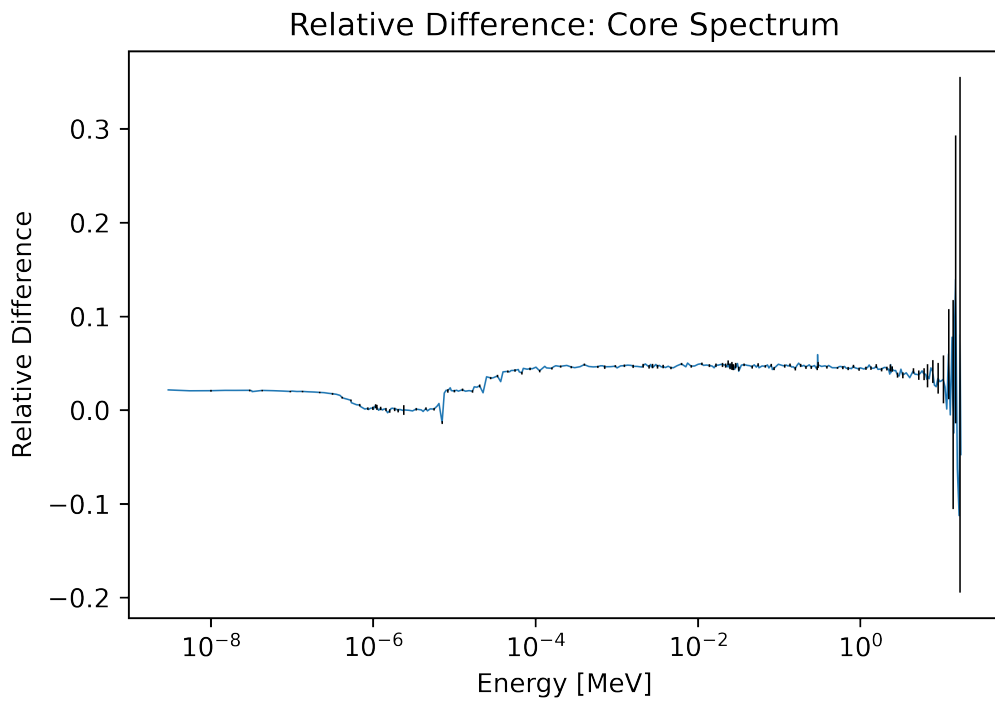
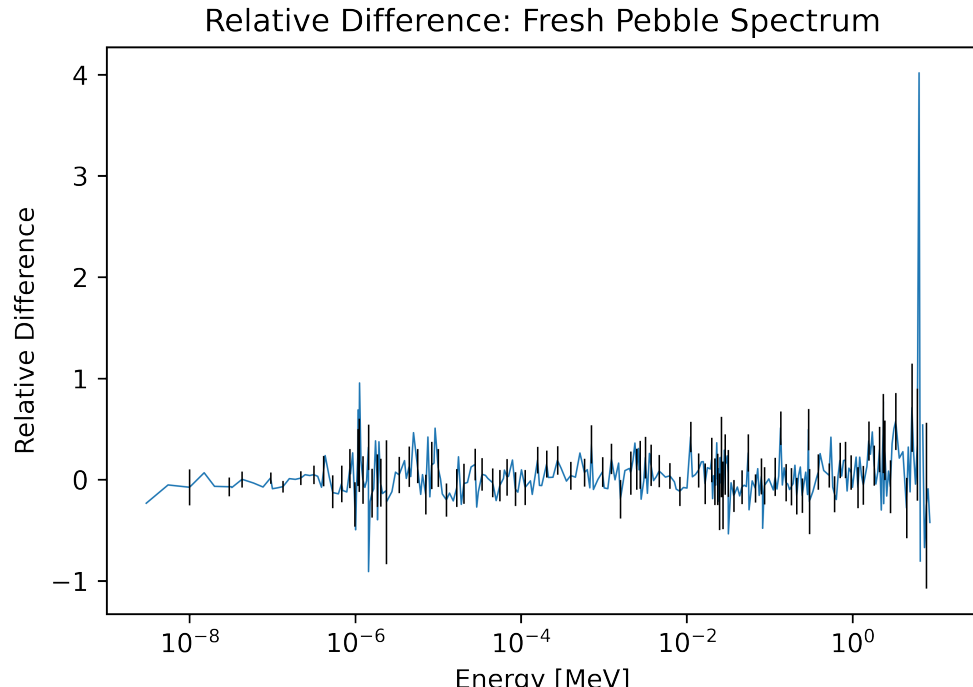


Figure 4.14: Relative Difference in Radial Thermal and Fast Flux Profiles Between Cores Using Homogenized and Heterogenized Pebbles (cont.)

For both the thermal and flux profiles, error only worsens on the outermost edges. Overall, Figures 4.14a and 4.14b suggest that the homogenized simulation is slightly over-predicting the magnitude of the flux; however, given the size of the error, these differences do not exist with certainty.

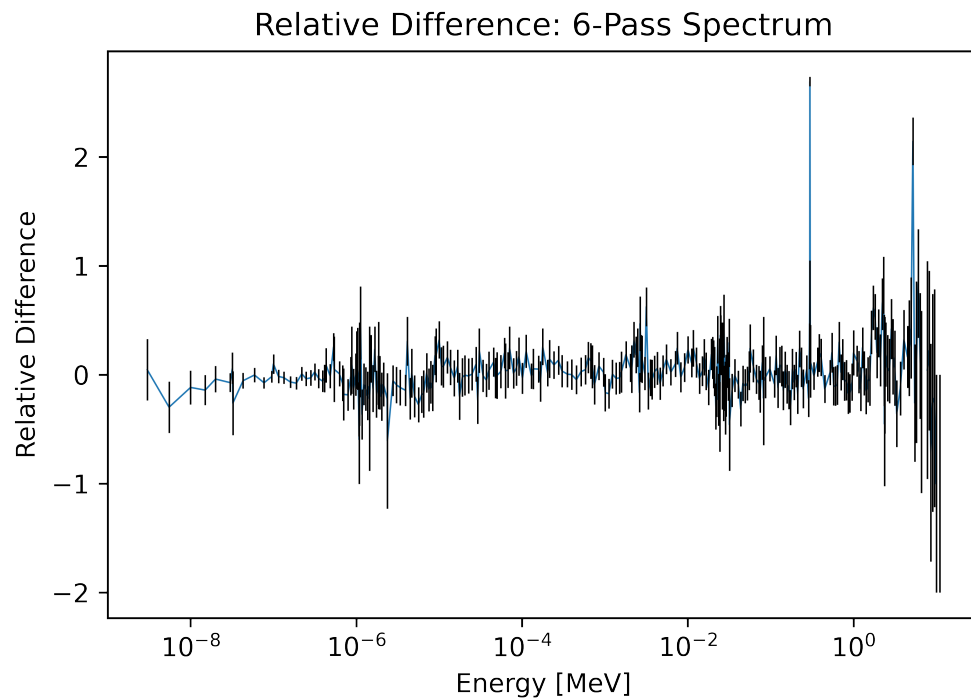


(a) Core

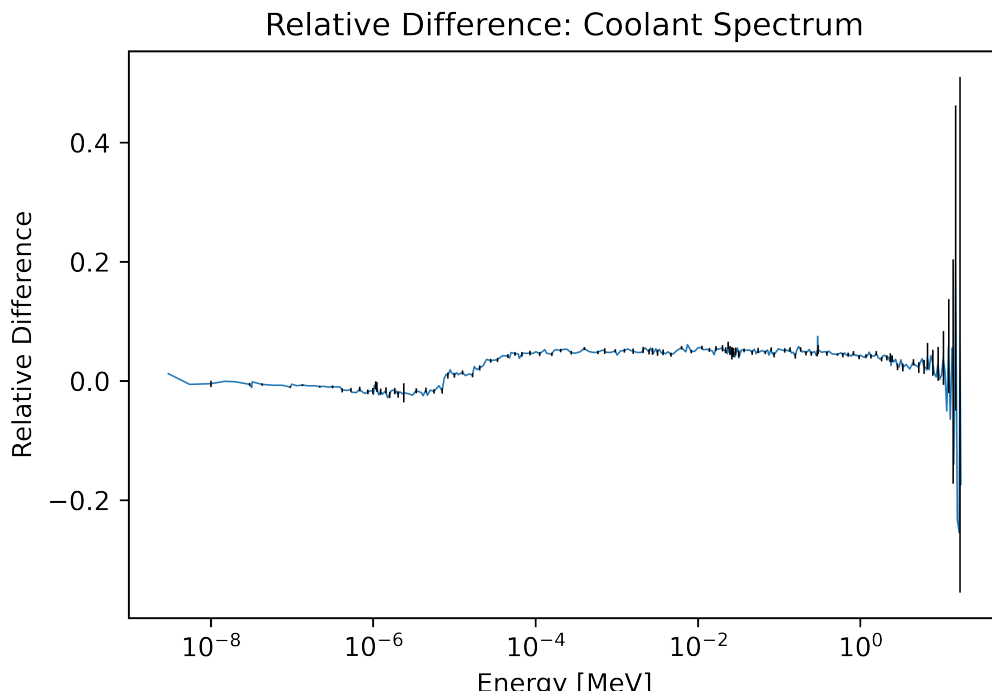


(b) Fresh Pebble

Figure 4.15: Relative Difference in Lethargy Adjusted Neutron Flux Energy Spectra Between Cores using Homogenized and Heterogenized Pebbles



(c) Six-Pass Pebble



(d) Coolant

Figure 4.15: Relative Difference in Lethargy Adjusted Neutron Flux Energy Spectra Between Cores using Homogenized and Heterogenized Pebbles (cont.)

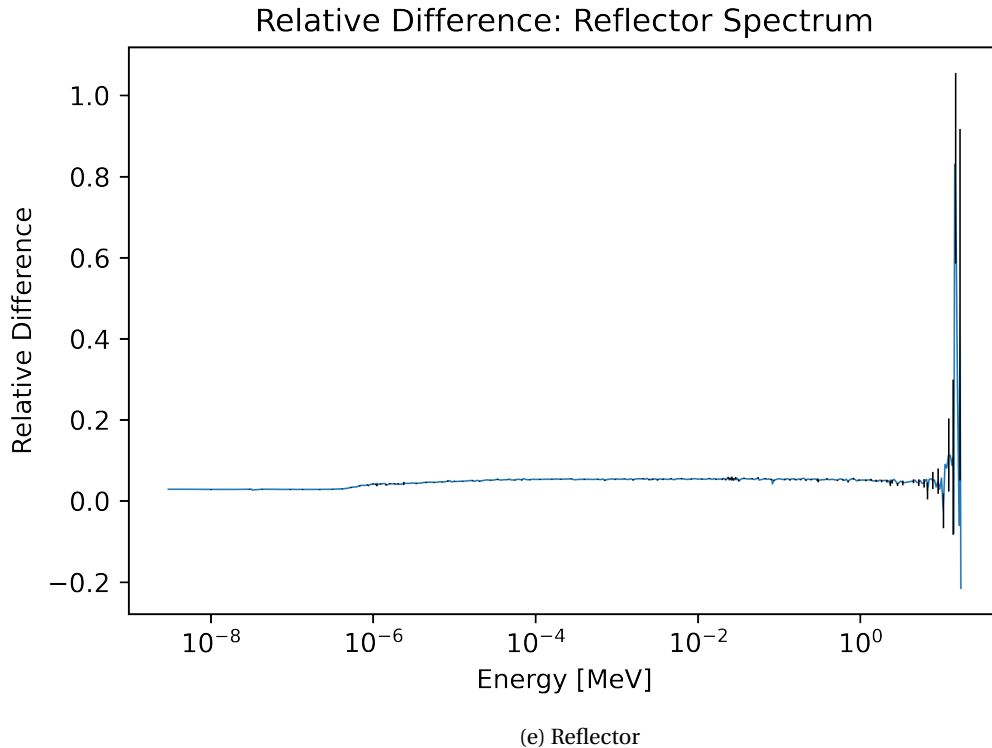


Figure 4.15: Relative Difference in Lethargy Adjusted Neutron Flux Energy Spectra Between Cores using Homogenized and Heterogenized Pebbles (cont.)

Overall, the homogenized model is over-predicting the thermal peak compared with heterogenized in the core spectra by 5%. Around 10×10^{-6} MeV, just after the thermal peak, the two spectra agree before diverging again, this time with a slightly greater disagreement. Unlike Figure 4.14, error alone leaves the relative differences seen in Figure 4.15 unaccounted for (with the exception of the highest neutron energy ranges). ***should I leave these, and include an image that gives a close up of the areas of interest, so the huge error at the tail end doesn't keep the reader from seeing detail?***

The coolant spectra differed after the thermal peak in a magnitude and shape matching the differences in core spectra. Unlike the core, however, the coolant has much closer agreement at lower energy levels, including at the thermal peak. The reflector shows a slight over estimation for the homogeneous spectra, which is consistent for all but the highest energy levels.

It is in the pebble spectra that we see the most dramatic disagreement. Around the thermal peak, in both Figures 4.15b and 4.15c, the relative difference spikes; though the error is still substantial in this region compared with the peaks in the relative difference. Between 10×10^{-7} and 5×10^{-2} , the differences are minimal and likely accounted for by noise or error. Between 10×10^{-2} and 10×10^{-1} , the difference has a slight blip, which may be indicative of a

fission product with a resonance around this region **I don't think I said that quite right***.

The most dramatic peaks occur in the sixth-pass pebble at 0.2995 MeV, at which point the homogenized reactor is over-predicting the lethargy-adjusted neutron flux by a factor of 2.69. Both the fresh and sixth-pass spectra have another peak at higher energy levels - fresh peaks at 6.3763 MeV, while the sixth-pass spectra has its second peak at 5.2205 MeV. One possibility is that the ^{235}U in the pebble is more likely to undergo fission in a homogenized pebble, which disperses the ^{235}U atoms in what is almost pure graphite.

4.4 Sensitivity Tests

Two additional studies look at the effects of assuming a one-sixth core symmetry, and the effects of changing the fuel composition in each pebble, effectively shuffling the pebbles without re-generating their location. All tests use the homogenized pebble assumption as a base.

4.4.1 Effects of Symmetry Assumption

Overall, the effects of using a one-sixth core symmetry were minimal.

Run	k_{eff}	$k_{eff} \% \Delta$	$J^+ [\frac{n}{cm^2 s}]$	$J^+ \% \Delta$
Run 1	1.03990 ± 0.00055	0.0836%	$5.921 \times 10^{11} \pm 1.717 \times 10^3$	0.637%
Run 2	1.03979 ± 0.00050	0.0942%	$5.884 \times 10^{11} \pm 1.636 \times 10^3$	0.000%
Run 3	1.04150 ± 0.00054	0.0701%	$5.908 \times 10^{11} \pm 1.468 \times 10^3$	0.402%
Run 4	1.03927 ± 0.00057	0.144%	$5.910 \times 10^{11} \pm 1.713 \times 10^3$	0.436%
Run 5	1.04154 ± 0.00054	0.0740%	$5.884 \times 10^{11} \pm 1.752 \times 10^3$	0.000%
Run 6	1.04047 ± 0.00050	0.0288%	$5.888 \times 10^{11} \pm 1.672 \times 10^3$	0.067%

Table 4.1: Sensitivity Run Summary

Figure 5.22 provides cross-sections of the geometry, and fission rate/thermal flux meshes for the one-sixth core symmetry test. The fission rate mesh naturally exhibits a six-part repeating pattern, and still shows the banding patterns on the outer edges.

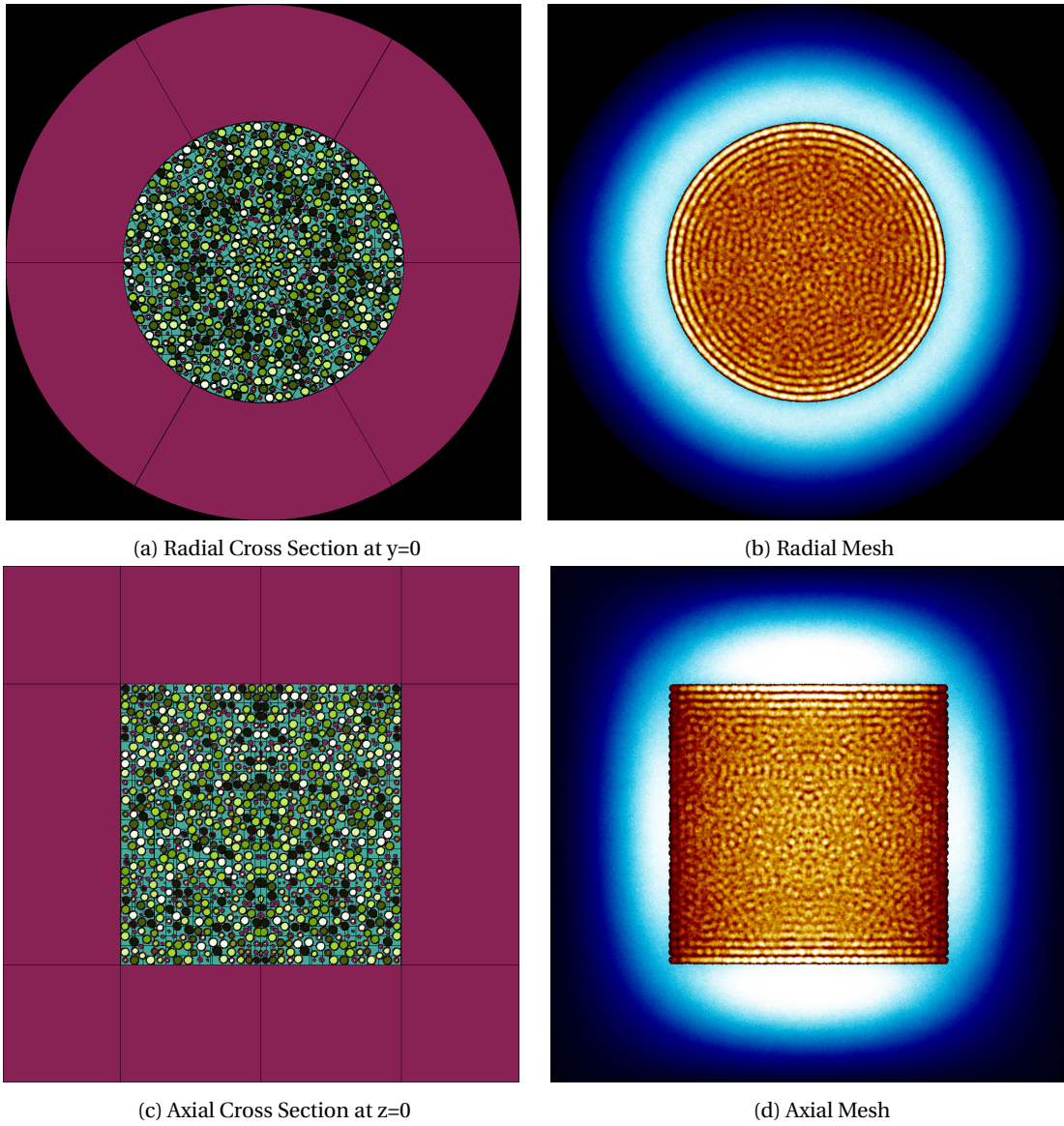


Figure 4.16: Sensitivity Analysis: $0^\circ - 60^\circ$

*** alright, I tried to convey my observation as best I could, but I have a suspicion it isn't nearly as clear on paper as it is in my head. Any suggestions are welcome, and if it seems like it would be better to leave this section out, I can*** One point of interest is the degree to which the region from 0 to 60 degrees matches the same region in the control fission rate mesh. An image subtraction program generated Figure 4.17 by subtracting the radial meshes for the control (Figure 4.4b) and first symmetry test (Figure 4.16b).

Within the region between 0 and 60 degrees, the two meshes are almost identical, pixel for pixel. While this might be unsurprising in the center of this region, the perfect match towards the edges of it are less so. As a reminder, the symmetry tests all use a one-sixth symmetry, and a periodic boundary condition, i.e., if a neutron leaves the

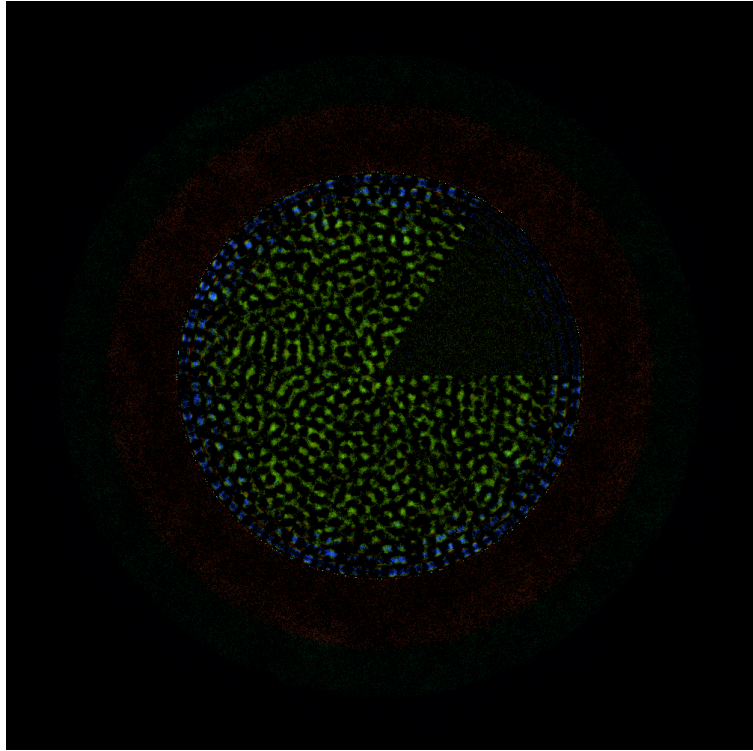


Figure 4.17: An Image Generated by Subtracting 4.16b from 4.4b.

slice on one side, it re-enters the slice on the other. In effect, the edges of the 0 to 60 degree slice in the symmetry test are seeing entirely different materials, compared with the control. The edges in 4.17 are not a gradient, but rather a hard line, which may suggest that with proper mixing nearest-neighbor pebbles have a weak effect on core parameters calculated via integration over large portions of the core ***there's 100% a shorter term for this i'm not thinking of***. However, note that Sangamon20 uses only fuel pebbles, and this observation may be false in a reactor design using, for example, adsorber pebbles.

4.4.2 Effects of Pebble Shuffling

The final test on the effects of changes to core modeling is another test of consistency between similar HTGR designs with a different pebble configurations. Rather than re-generate the pebble locations several times, the 'shuffling' test simply reassigns each pebble with a different fuel composition (creating a new input file). For example, the pebbles that were once fresh are now first-pass, the first pass pebbles are now second-pass, and so on. This shuffling happened several times, and the results of this test are in Table 4.2.

Run	k_{eff}	$k_{eff} \%\Delta$	$J^+ [\frac{n}{cm^2 s}]$	$J^+ \%\Delta$
Run 1	1.03994 ± 0.00054	0.0797%	$5.897 \times 10^{11} \pm 1.710 \times 10^{03}$	0.626%
Run 2	1.03999 ± 0.00055	0.0749%	$5.902 \times 10^{11} \pm 1.595 \times 10^{03}$	0.210%
Run 3	1.04002 ± 0.00053	0.0721%	$5.896 \times 10^{11} \pm 1.675 \times 10^{03}$	0.295%
Run 4	1.04103 ± 0.00057	0.0249%	$5.884 \times 10^{11} \pm 1.845 \times 10^{03}$	0.192%
Run 5	1.03960 ± 0.00053	0.112%	$5.904 \times 10^{11} \pm 1.665 \times 10^{03}$	0.013%
Run 6	1.04014 ± 0.00057	0.0605%	$5.898 \times 10^{11} \pm 1.524 \times 10^{03}$	0.329%

Table 4.2: Shuffling Run Summary

Overall, much like the symmetry test, re-mixing the pebbles had little effect on overall results. Likely, provided the pebbles are sufficiently mixed, and no 'pockets' of like pebbles exist, designs that are otherwise identical should provide similar results.

Chapter 5

Conclusion

This chapter provides a synopsis of results and discussion, alongside recommendations of future work.

5.1 Summary and Discussion

Previous work in HTGR pebble-bed modeling noted that the specific lattice arrangement used had little effect [10], [8], [29]. The pebble-shuffling and symmetry tests support this observation in regards to a random arrangement of the pebbles.

The symmetry test showed that for minimal banding - areas of like pebbles creating streaks and rings once reflected - the difference between a full core model and one using symmetry to simplify is less than 0.65% in the outward neutron current, and less than 0.15% for k_{eff} . Additionally otherwise-identical models with a well-mixed core and different dispersal of pebbles differ less than 0.63% in the outward current at the outer reflector edge, and less than 0.12% in k_{eff} . For reactor designs beyond Sangamon20, this suggests that one does not need to re-create the same reactor over and over with slightly different pebble arrangements in order to accurately characterize a core.

The heterogenized tests highlight the need for an accurate representation of TRISO particles. While the overall differences between the fast and thermal flux profiles are minimal, the homogenized pebbles will under-predict k-eff by more than 4.0%, while over-predicting the magnitude of the neutron energy lethargy-adjusted flux core spectrum by as much as 5.0%. The most dramatic changes to spectra are within the pebbles themselves, where high-energy neutron peaks are over-estimated in the fresh and sixth-pass pebbles by a factor of 2-4. Additionally, the total outward neutron current, used to gauge the effectiveness of the reflector, differed by only 0.349%. This is likely because the reflector is thick enough to minimize fast neutron leakage, which prevents the fast flux changes (see Figure 4.14b in the active core from affecting the outer regions of the reflector. The thermal flux isn't changed to a degree unexplained by error (see Figure 4.14a, so the thermal neutron current is also similar.

For isotopic inventories, most isotopes either increased or decreased at a uniform rate with each pass through the core. However, some isotopes, such as ^{239}Pu , reach a peak concentration in MOL, and subsequently decline.

When choosing a once-through-then-out (OTTO) or mult-pass fuel cycle, one must decide which isotopes it is most important to minimize.

5.2 Future Work

The symmetry test showed that, with random mixing, simplifying the simulation by approximating the whole-core with only a slice of it had minimal effects for a one-sixth symmetry. However, the 'banding' and petal-like pebble patterns this symmetry creates highlights a potential issue, however unlikely. What if the random pebble dispersal happens to lump a number of the same or similar burnup pebbles together? How would this affect a whole core model, or one using symmetry? Future work could explore the effects of pebble 'lumping', such as the size of pebble-lump needed before it causes a noticeable effect.

Additionally, this design used an infinite lattice of like pebbles in the depletion model to arrive at an equilibrium composition. It is possible to improve the accuracy of the equilibrium composition. By tracking compositions over time in the actual core, as opposed to an infinite lattice, or splitting the core into axial layers to track the pebble isotopic inventory as a function of the number of passes and current height in the core.

The current core is not thermodynamically optimal, and future work could adjust the height-diameter ratio, provided it follows 3.3. As the current design is slight supercritical, there should be room to shift to a slightly less critical shape that is more thermally beneficial. If a slight excess reactivity exists at this point, one could explore adding in an additional "half-pass" - i.e., half of the sixth-pass pebbles go for a seventh pass, and the other half replaced with fresh pebbles. Alternatively, one could explore the addition of neutron-absorber pebbles to handle excess reactivity.

Finally, the pebble dispersal method used here does not account for gravity, which would make the pebbles settle closer together. Without using a core that has a diameter which is an integer multiple of the pebble diameter, it is not possible to get a perfect close-pack arrangement (shaking a vessel will help achieve closer packing, but this is not possible here). One could simulate the effects of gravity by dispersing the pebbles over a volume with a slightly shorter height, instead of the full height. However, it is note that at a packing fraction of around 0.58, the model is already approaching the theoretical maximum packing fraction, so the difference this would make may be minimal.

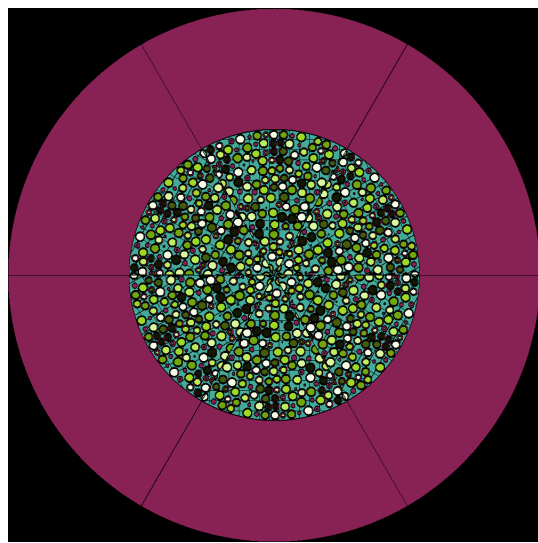
Appendix

*** Bits surrounded by *** are notes for the reviewer, so you can ctrl-f to search for them. I also included a section of general comments/concerns at the very end ***

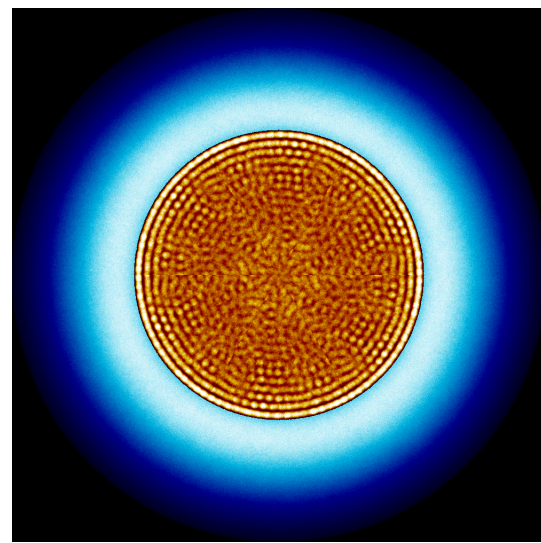
*** I think this section, or at least, the description at the end, could stand to be longer, but I didn't want to be repetitive or get too bogged down in color theory.***

5.3 Appendix A: Symmetry Test

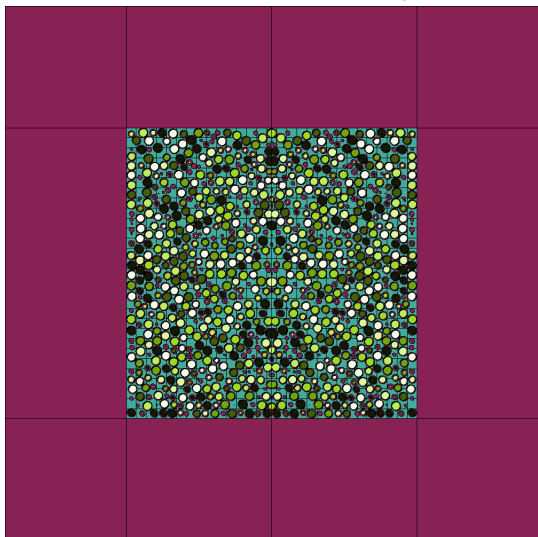
Appendix A contains the geometry cross sections, fission rate/thermal flux meshes, and image difference results from the other symmetry tests.



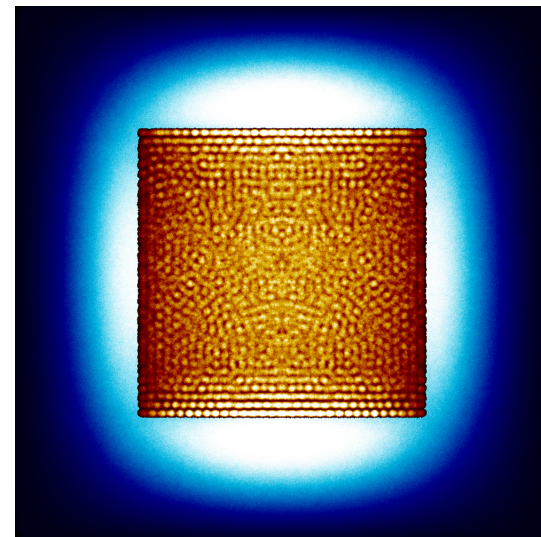
(a) Radial Cross Section at $y=0$



(b) Radial Mesh



(c) Axial Cross Section at $z=0$



(d) Axial Mesh

Figure 5.1: Sensitivity Analysis: $60^\circ - 120^\circ$

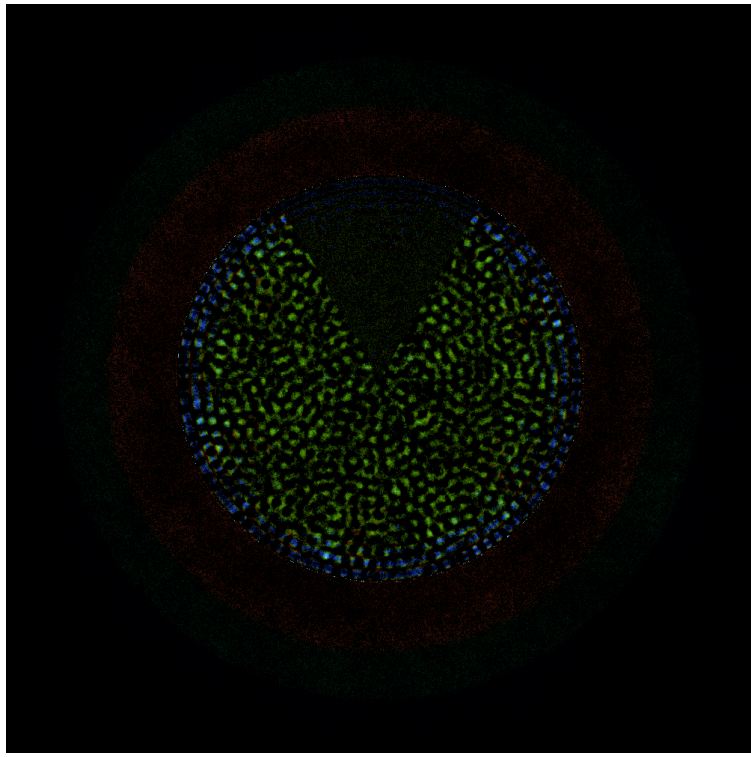
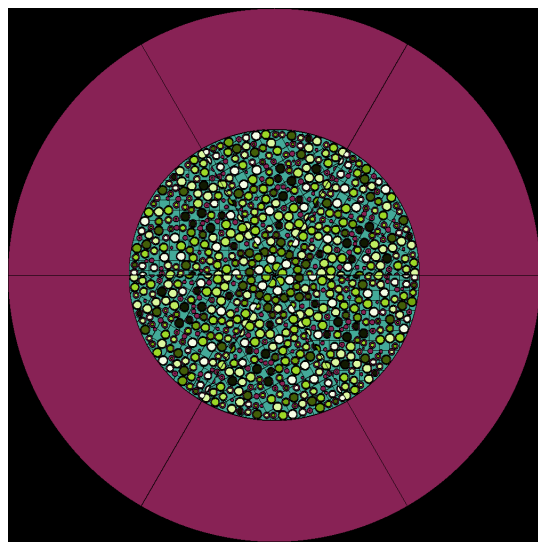
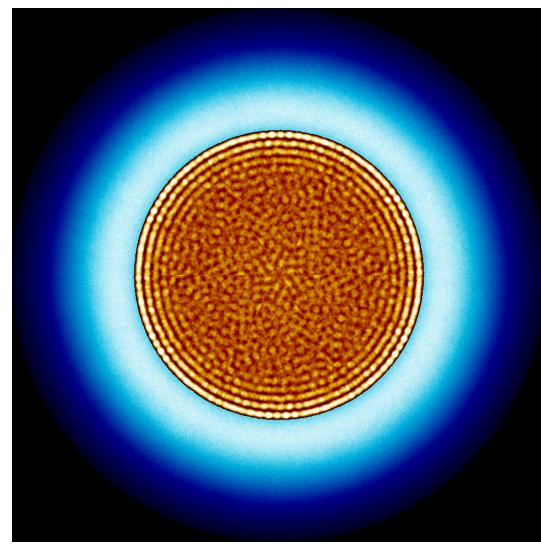


Figure 5.2: An Image Generated by Subtracting 5.1b from 4.4b.

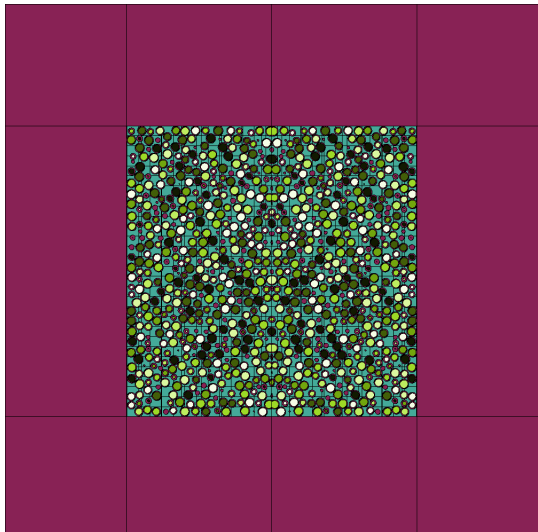
Figure ?? provides fission rate and thermal flux visualization meshes for the symmetry test using the 60 - 120 degree slice. Figure 5.2 is the result of using image-difference between the control's full-core radial mesh and the symmetry test's mesh.



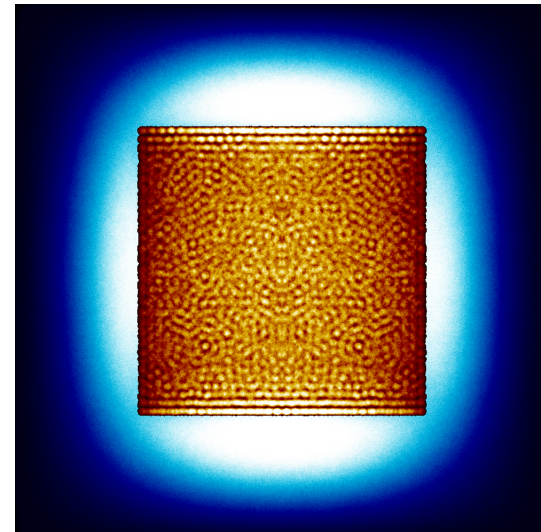
(a) Radial Cross Section at $y=0$



(b) Radial Mesh



(c) Axial Cross Section at $z=0$



(d) Axial Mesh

Figure 5.3: Sensitivity Analysis: $120^\circ - 180^\circ$

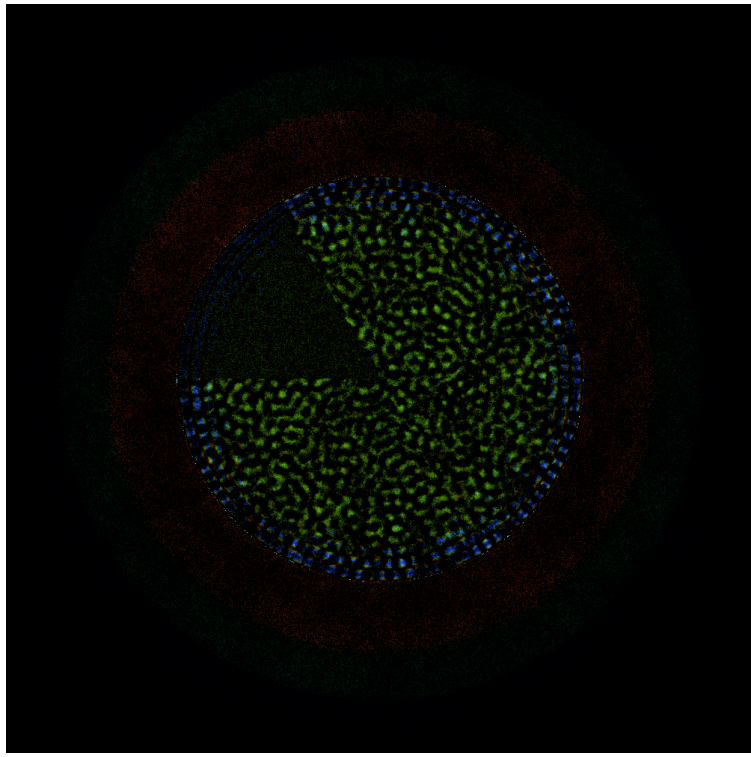
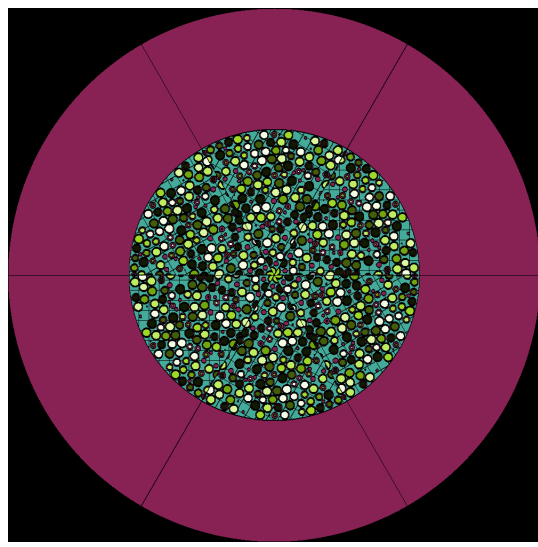
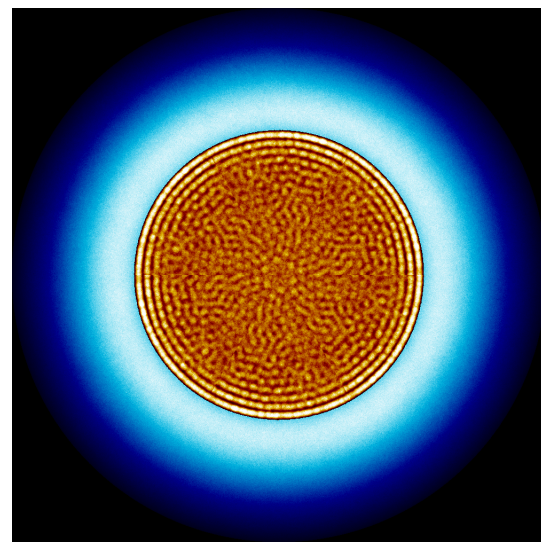


Figure 5.4: An Image Generated by Subtracting 5.3b from 4.4b.

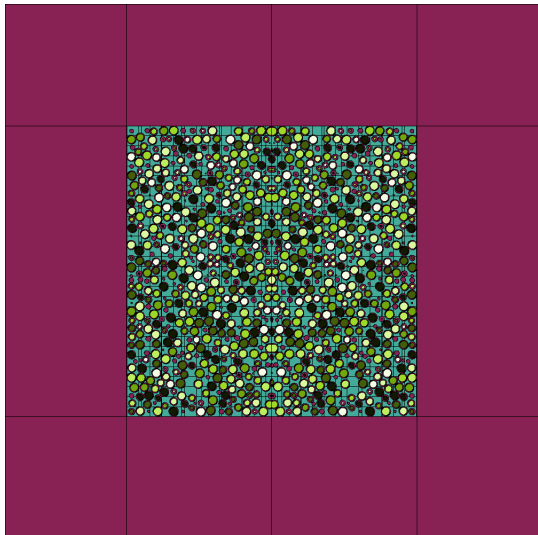
Figure 5.3 provides fission rate and thermal flux visualization meshes for the symmetry test using the 120 - 180 degree slice. Figure 5.4 is the result of using image-difference between the control's full-core radial mesh and the symmetry test's mesh.



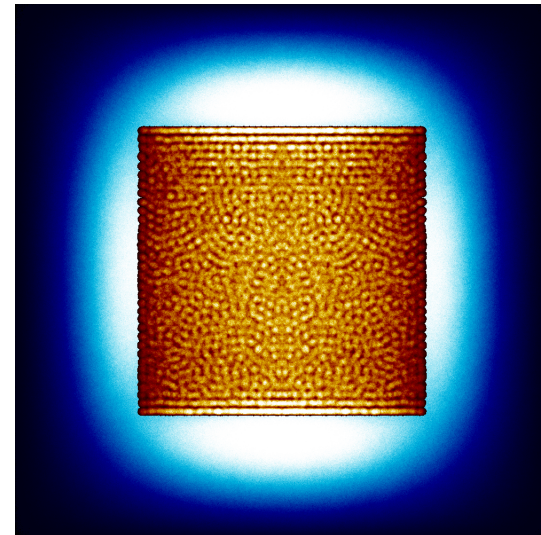
(a) Radial Cross Section at $y=0$



(b) Radial Mesh



(c) Axial Cross Section at $z=0$



(d) Axial Mesh

Figure 5.5: Sensitivity Analysis: $180^\circ - 240^\circ$

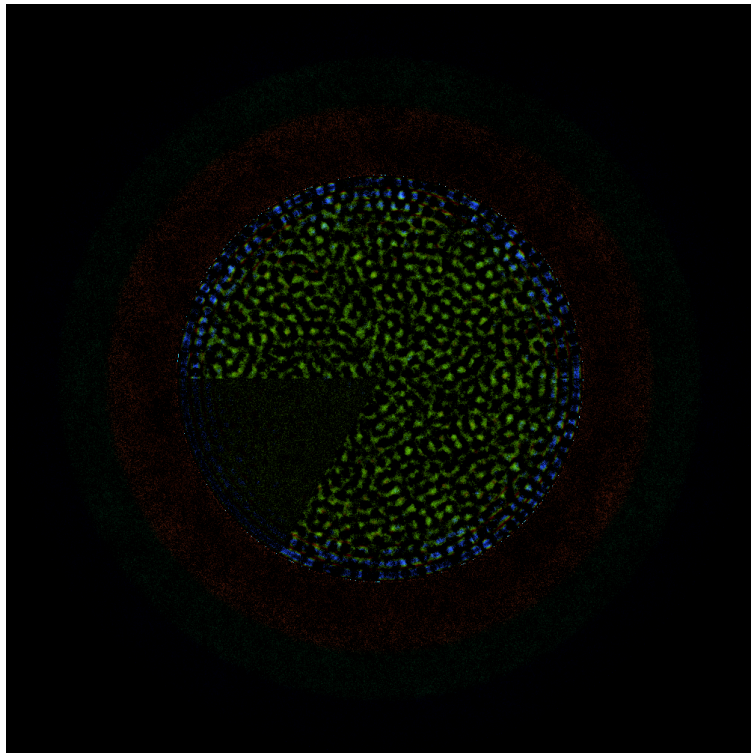
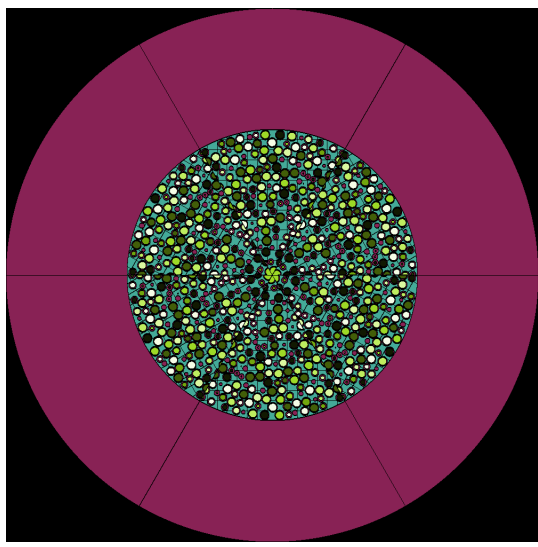
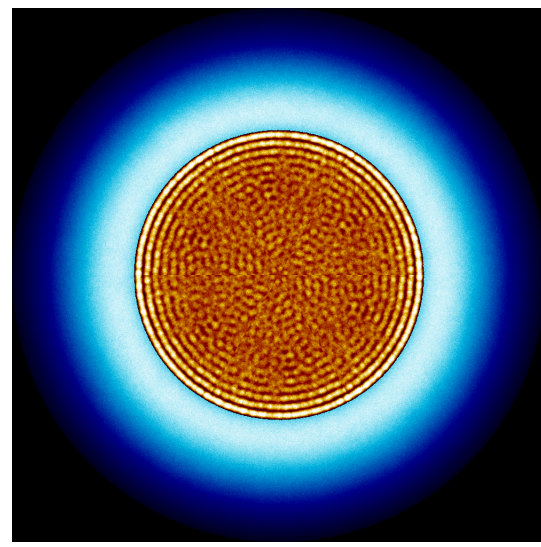


Figure 5.6: An Image Generated by Subtracting 5.5b from 4.4b.

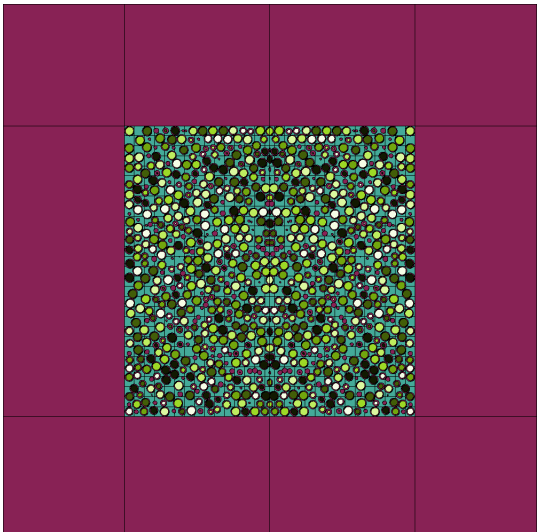
Figure 5.5 provides fission rate and thermal flux visualization meshes for the symmetry test using the 180 - 240 degree slice. Figure 5.6 is the result of using image-difference between the control's full-core radial mesh and the symmetry test's mesh.



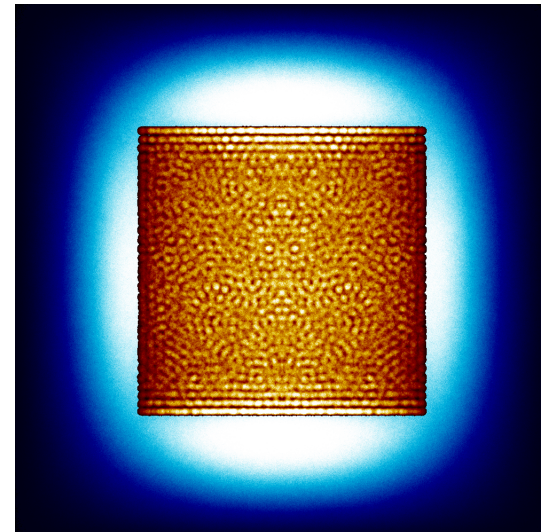
(a) Radial Cross Section at $y=0$



(b) Radial Mesh



(c) Axial Cross Section at $z=0$



(d) Axial Mesh

Figure 5.7: Sensitivity Analysis: $240^\circ - 300^\circ$

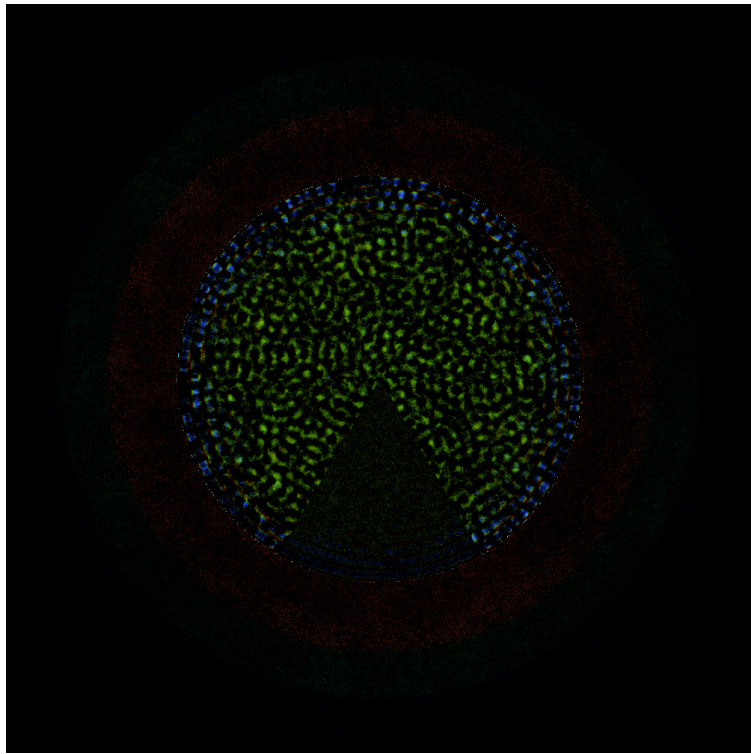
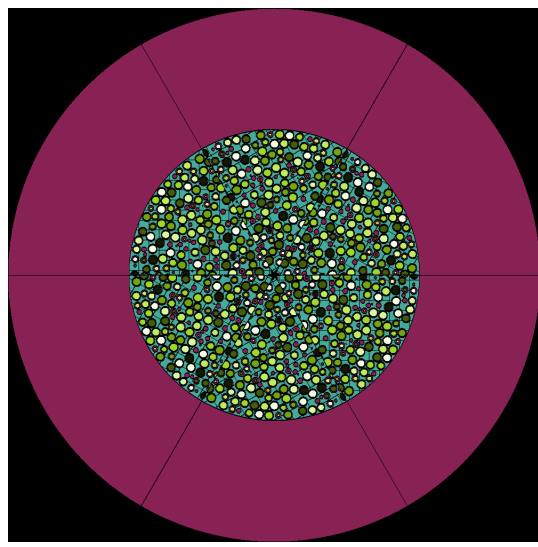
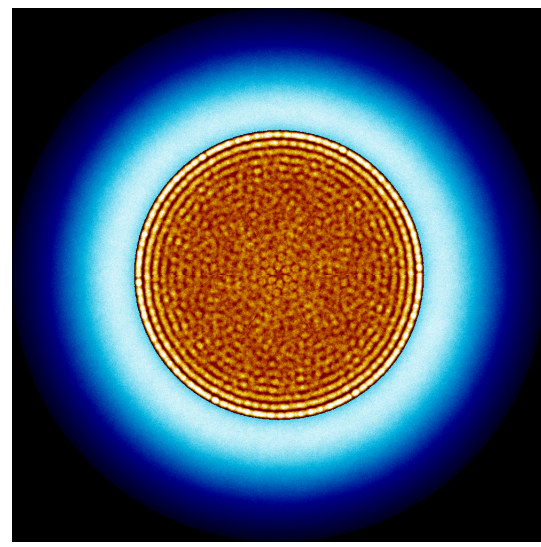


Figure 5.8: An Image Generated by Subtracting 5.7b from 4.4b.

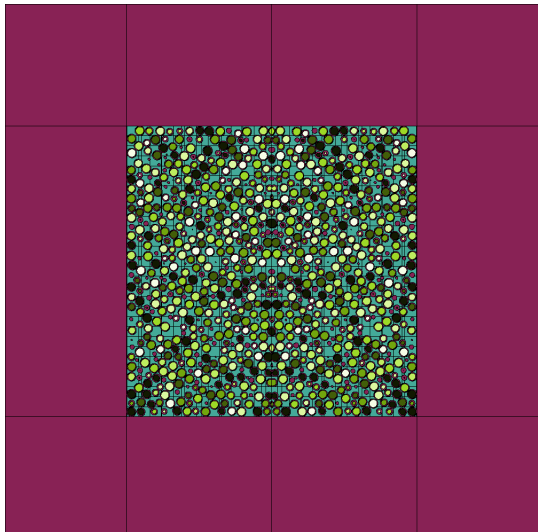
Figure 5.7 provides fission rate and thermal flux visualization meshes for the symmetry test using the 240 - 300 degree slice. Figure 5.8 is the result of using image-difference between the control's full-core radial mesh and the symmetry test's mesh.



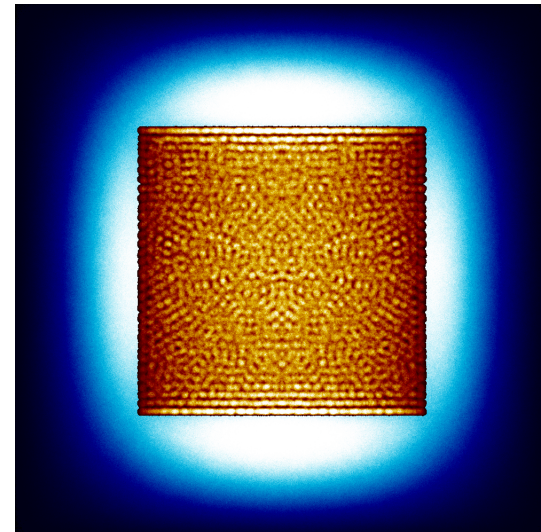
(a) Radial Cross Section at $y=0$



(b) Radial Mesh



(c) Axial Cross Section at $z=0$



(d) Axial Mesh

Figure 5.9: Sensitivity Analysis: $300^\circ - 360^\circ$

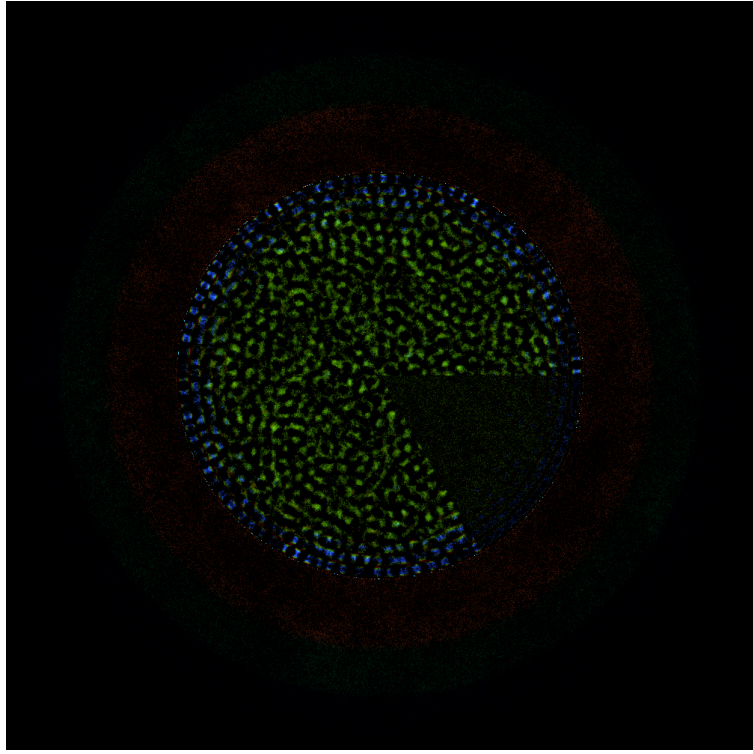


Figure 5.10: An Image Generated by Subtracting 5.9b from 4.4b.

Figure 5.9 provides fission rate and thermal flux visualization meshes for the symmetry test using the 300 - 360 degree slice. Figure 5.10 is the result of using image-difference between the control's full-core radial mesh and the symmetry test's mesh.

To help explain the color difference plots, it may be helpful to go into further depth on RGB (red, green, blue) based colors and how the individual values correspond to colors when mixed.

In the RGB color format, values for red, green, and blue can range from 0 to 255. The higher the value for a color, the more of it is present in the resulting color. If the values for red, green, and blue are the same, then the resulting color is a shade of grey. If all values are set to their maximum, 255, then the result is pure white. If all values are 0, then the result is pure black. In general, colors with low RGB values are darker than ones with greater RGB values.

To understand why the differences in the active core are in green, it is useful to further describe basic color theory and complementary colors. The fission rate meshes are shown in a hot color map, which ranges in color from an almost-white shade of yellow, to very dark browns. In between these maximum and minimum shades are varying shades of yellow, orange, and brown. To create a shade of yellow in RGB format, one uses a large amount of red and green. To create the sort of almost-white yellow, one simply takes the base yellow, with large amounts of red and green, and increases the blue value (which, as described before, will transition the color to a lighter shade as all three RGB values approach the maximum of 255). To move from yellow to an orangey-brown, one shifts the green

value down. Lowering red and green while keeping blue at a low value produces the darkest shades of brown seen in the color map.

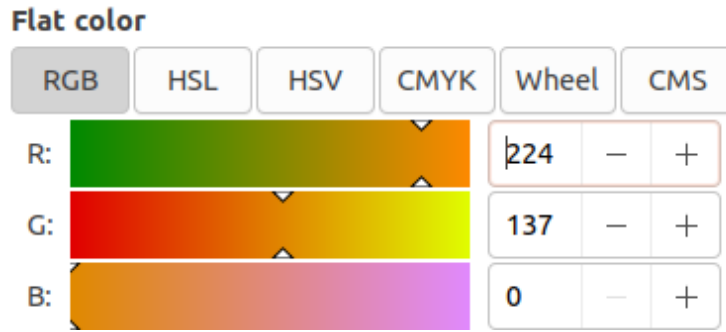


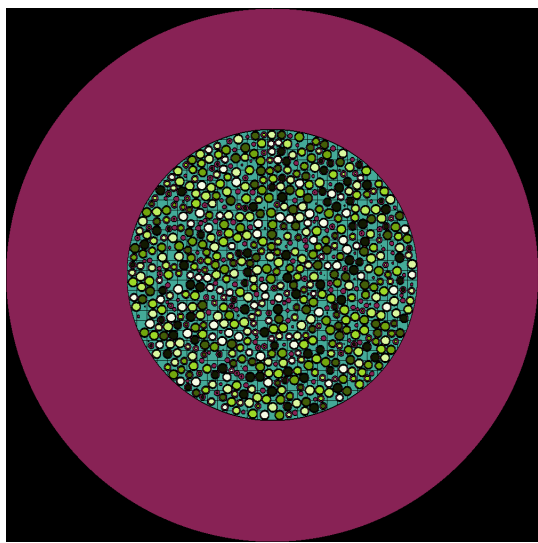
Figure 5.11: An example of RGB values. If the value for red and blue are held constant, shifting the value for green up or down shifts the resulting color along the color gradient to the left of the green value, which ranges from red to yellow. The arrows on the green gradient indicate what the current color is. As one can see, moving the slider to the right - increasing the value of green - will make the color more yellow, while moving it to the left, or decreasing the green level, will shift it towards orange and red.

Figure 5.11 gives an example of selecting a color using RGB values. Image difference works by subtracting the RGB values from each other - for example, subtracting (200, 150, 50) from (100, 200, 75) results in (100, 50, 25). Absolute values are used because negative values don't exist in RGB colors. So, when two colors which have contrasting values of green, and similar values of red and blue, the result is, of course, a shade of green.

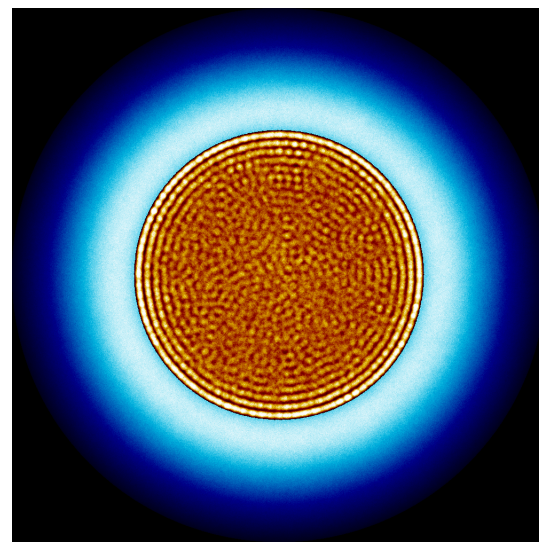
In each of the image differences, the section used to approximate the entire core (for example, the section from 60 to 120 degrees in Figure 5.2). Is very dark, which indicates that this region has little to no difference from the full-core control mesh.

5.4 Appendix B: Shuffle Test

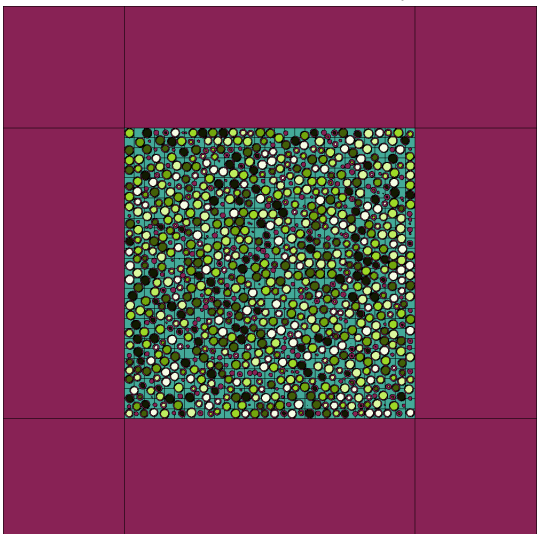
Appendix B contains the geometry cross sections, fission rate/thermal flux meshes, and image difference results from the shuffling tests.



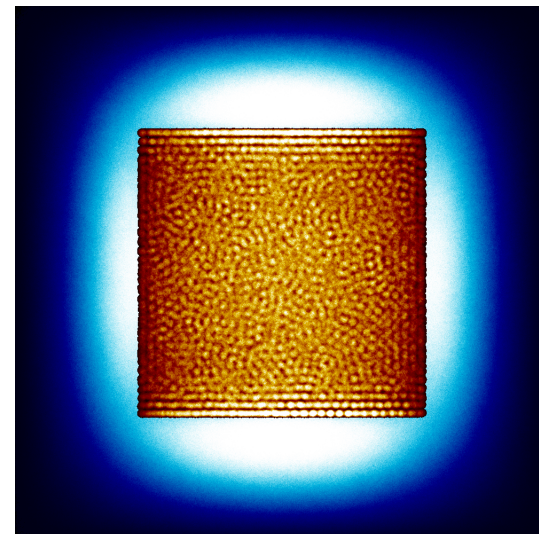
(a) Radial Cross Section at $y=0$



(b) Radial Mesh



(c) Axial Cross Section at $z=0$



(d) Axial Mesh

Figure 5.12: Shuffle Analysis: Run 1

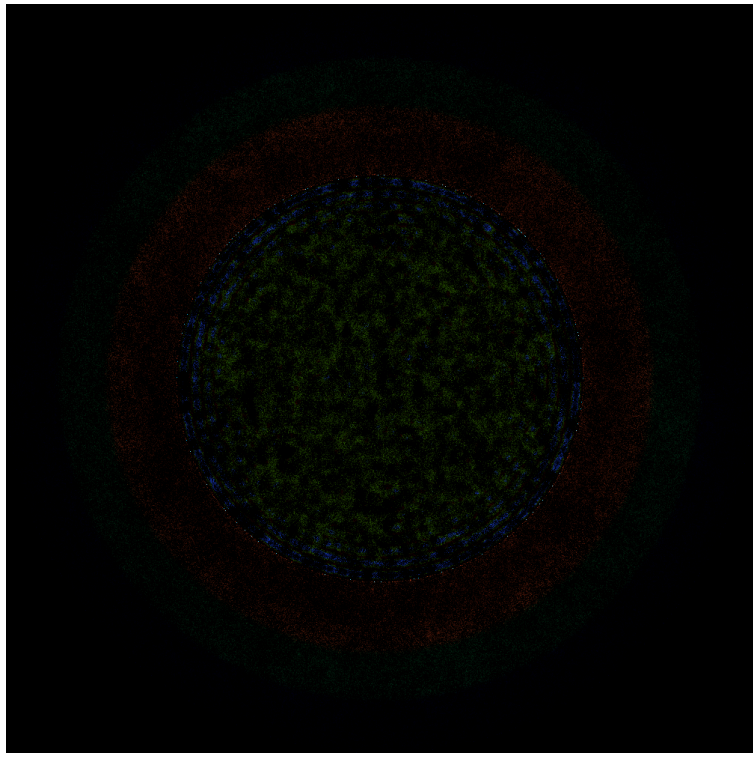
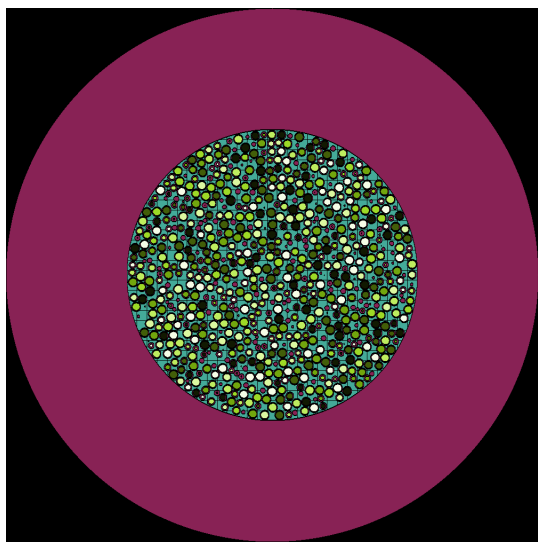
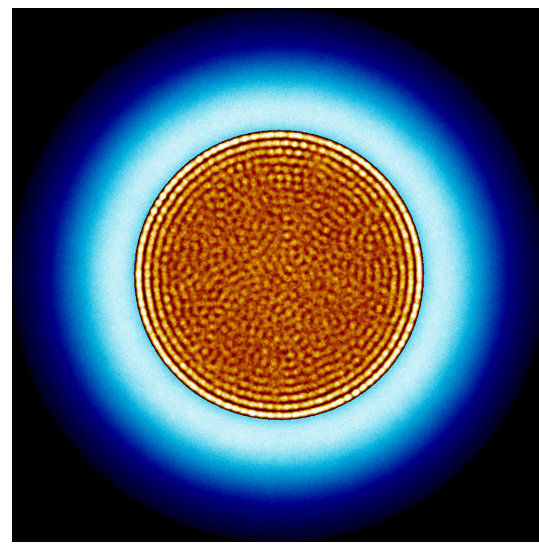


Figure 5.13: An Image Generated by Subtracting ?? from 4.4b.

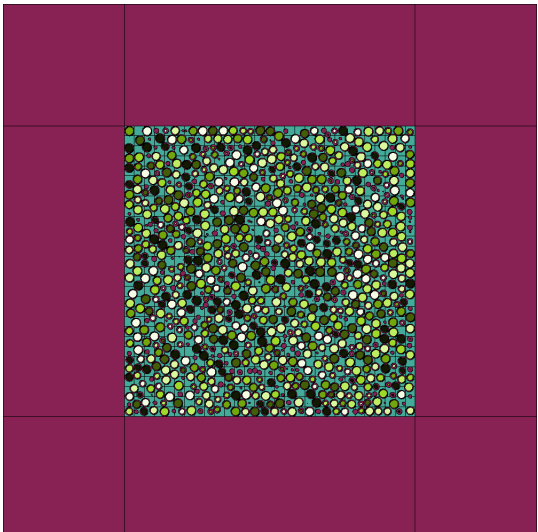
Figure 5.12 provides the thermal flux and fission rate meshes and geometric cross sections axially and radially. Figure 5.13 is the result of the image difference between the full core control mesh and Figure 5.12b.



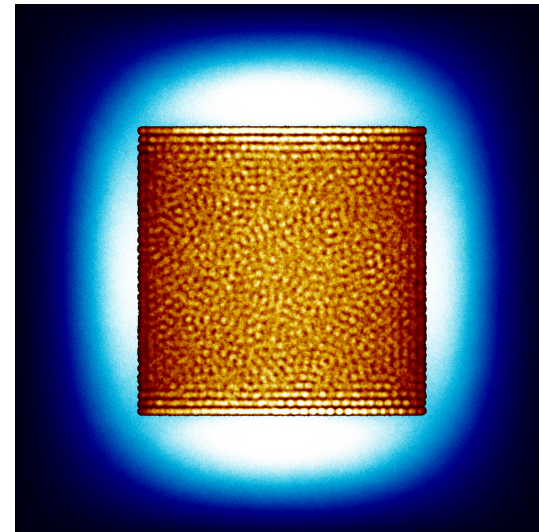
(a) Radial Cross Section at $y=0$



(b) Radial Mesh



(c) Axial Cross Section at $z=0$



(d) Axial Mesh

Figure 5.14: Shuffle Analysis: Run 2

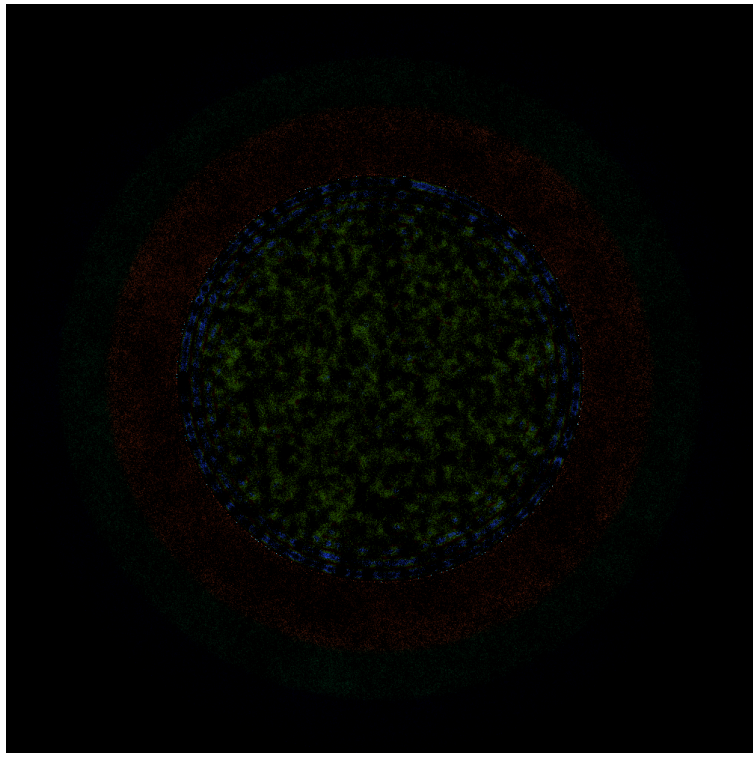
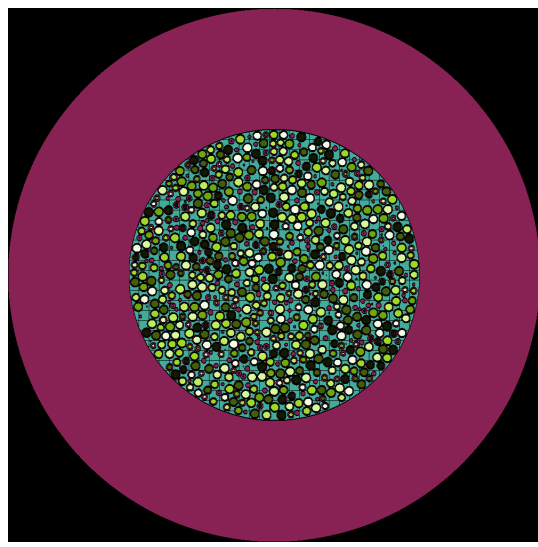
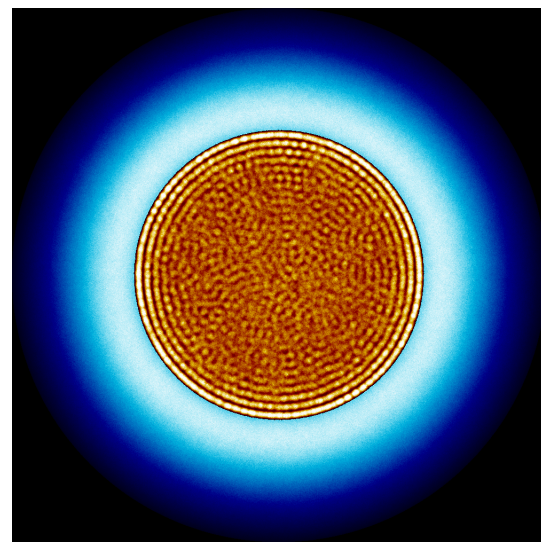


Figure 5.15: An Image Generated by Subtracting ?? from 4.4b.

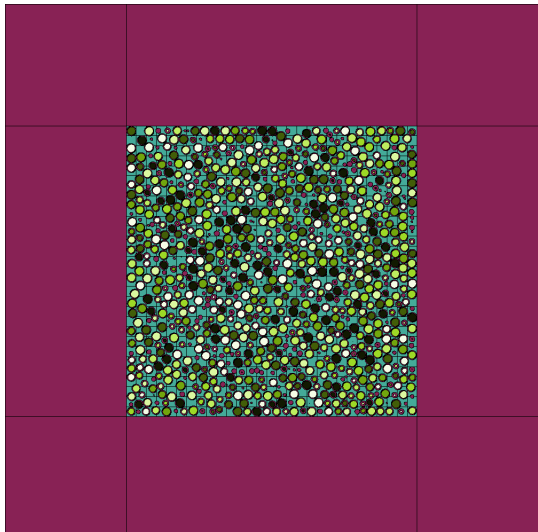
Figure 5.14 provides the thermal flux and fission rate meshes and geometric cross sections axially and radially. Figure 5.15 is the result of the image difference between the full core control mesh and Figure 5.14b.



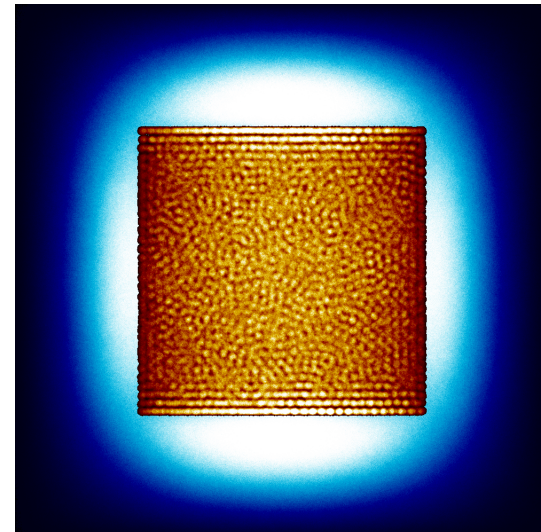
(a) Radial Cross Section at $y=0$



(b) Radial Mesh



(c) Axial Cross Section at $z=0$



(d) Axial Mesh

Figure 5.16: Shuffle Analysis: Run 3

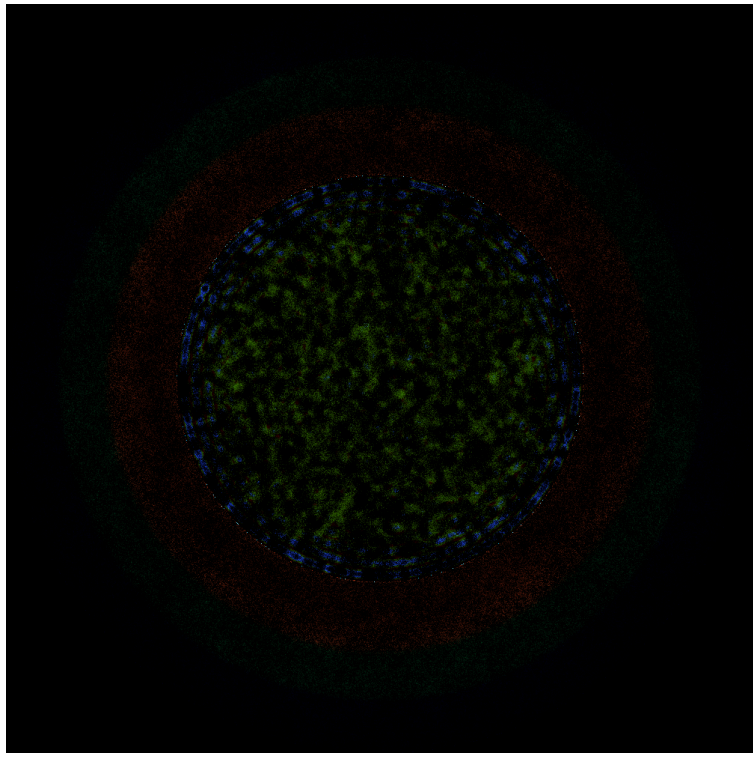
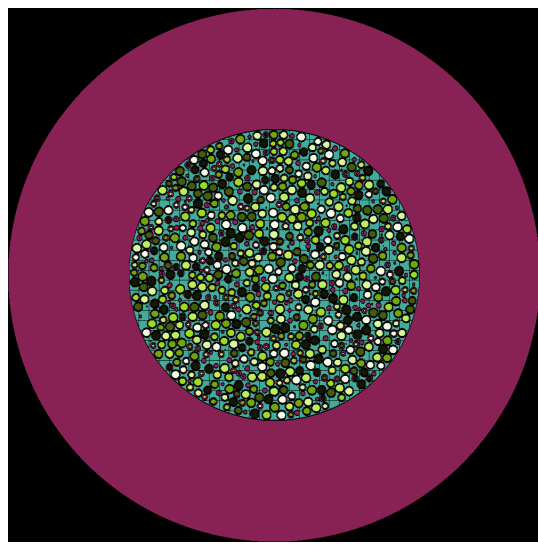
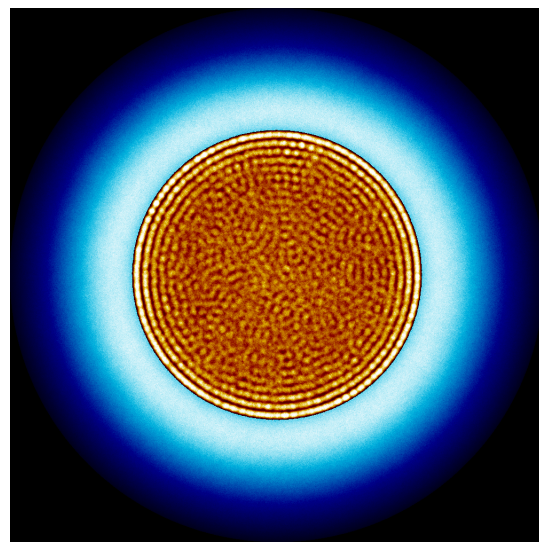


Figure 5.17: An Image Generated by Subtracting ?? from 4.4b.

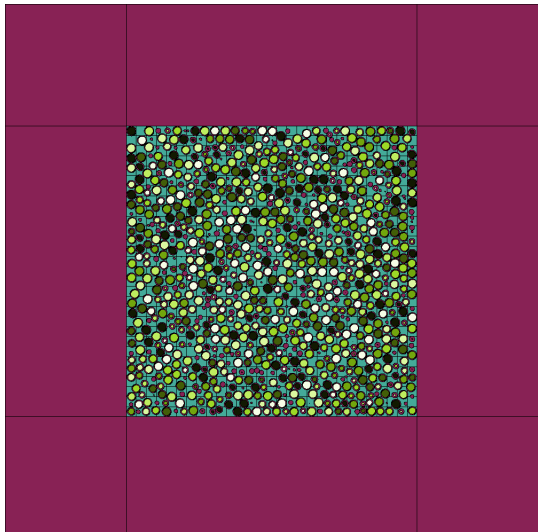
Figure 5.16 provides the thermal flux and fission rate meshes and geometric cross sections axially and radially. Figure 5.17 is the result of the image difference between the full core control mesh and Figure 5.16b.



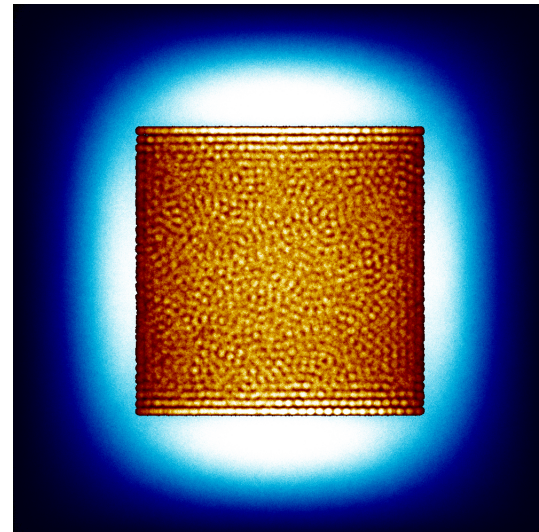
(a) Radial Cross Section at $y=0$



(b) Radial Mesh



(c) Axial Cross Section at $z=0$



(d) Axial Mesh

Figure 5.18: Shuffle Analysis: Run 4

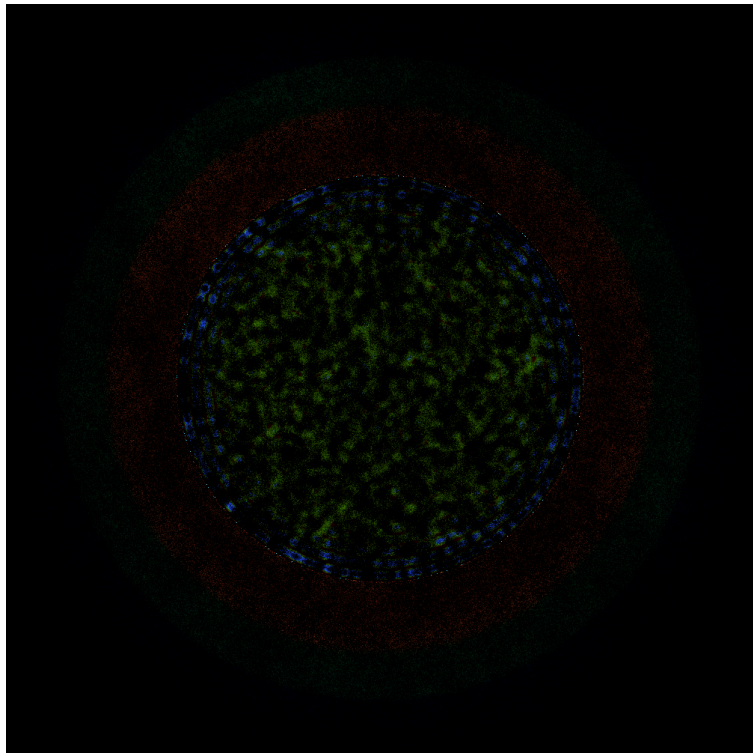
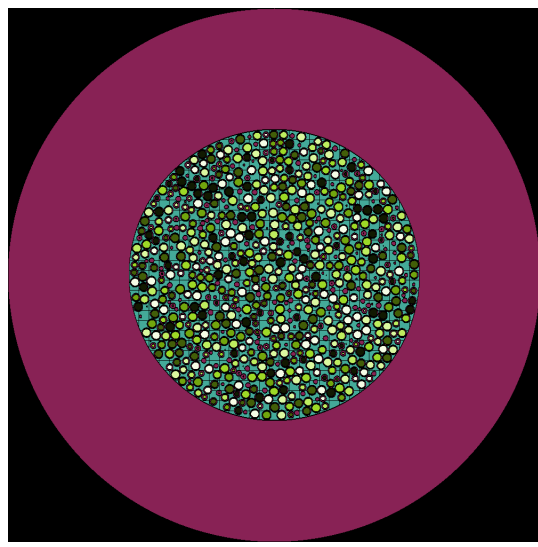
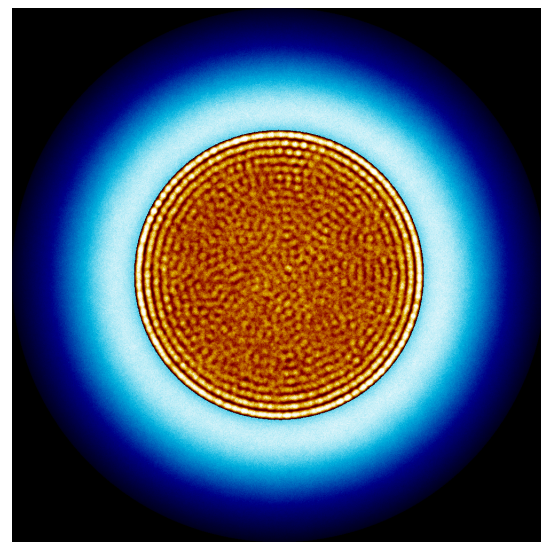


Figure 5.19: An Image Generated by Subtracting ?? from 4.4b.

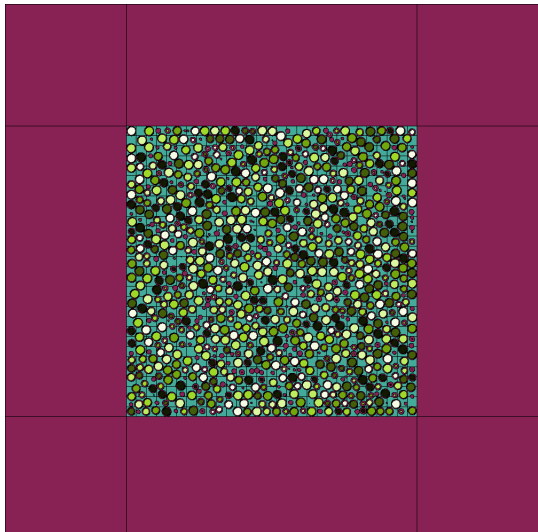
Figure 5.18 provides the thermal flux and fission rate meshes and geometric cross sections axially and radially. Figure 5.19 is the result of the image difference between the full core control mesh and Figure 5.18b.



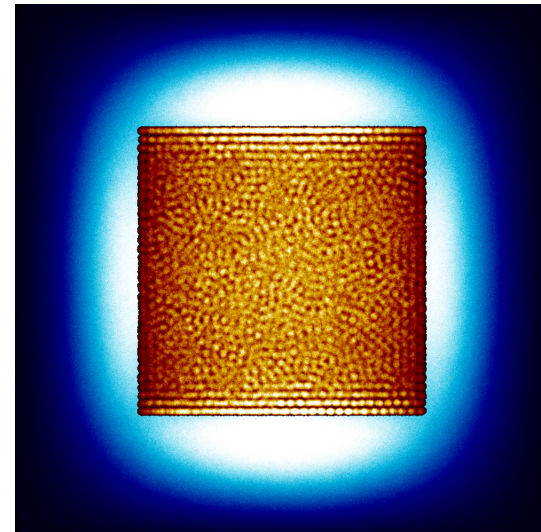
(a) Radial Cross Section at $y=0$



(b) Radial Mesh



(c) Axial Cross Section at $z=0$



(d) Axial Mesh

Figure 5.20: Shuffle Analysis: Run 5

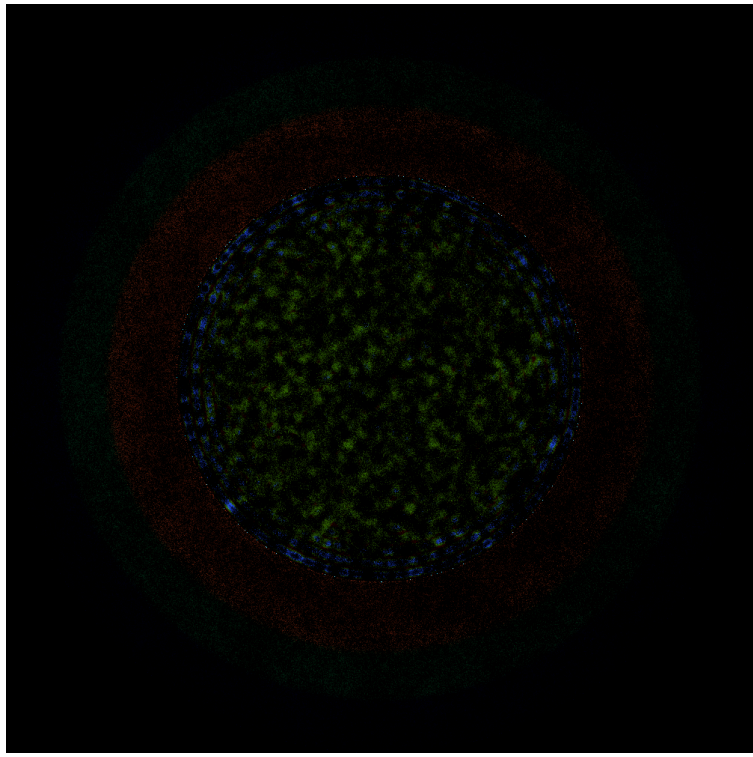
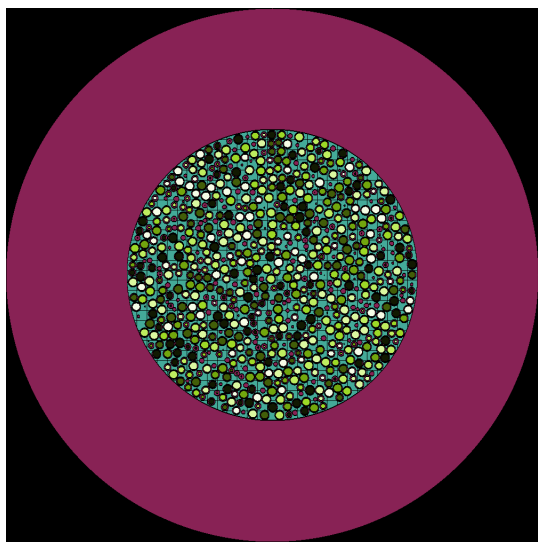
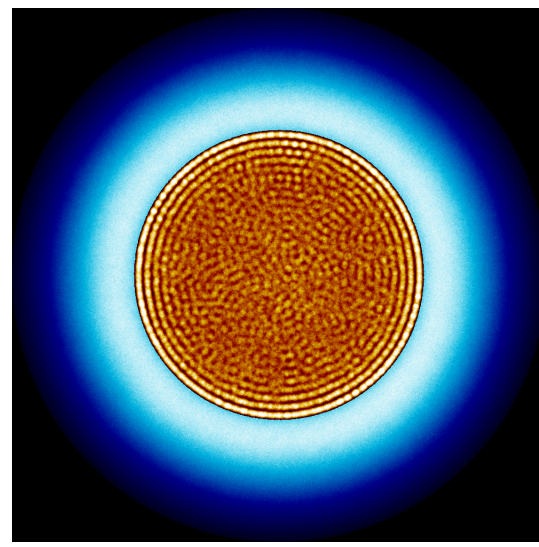


Figure 5.21: An Image Generated by Subtracting ?? from 4.4b.

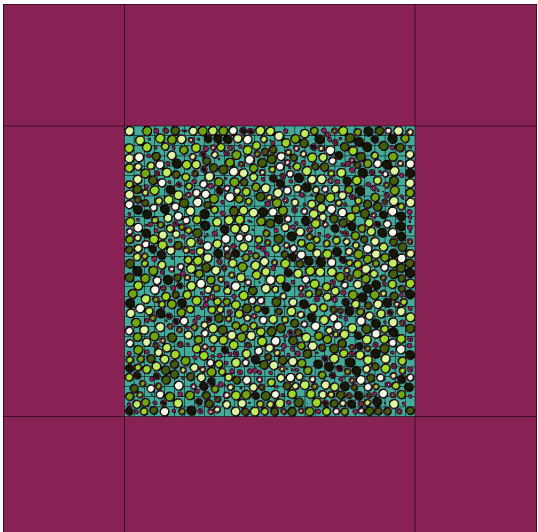
Figure 5.20 provides the thermal flux and fission rate meshes and geometric cross sections axially and radially. Figure 5.21 is the result of the image difference between the full core control mesh and Figure 5.20b.



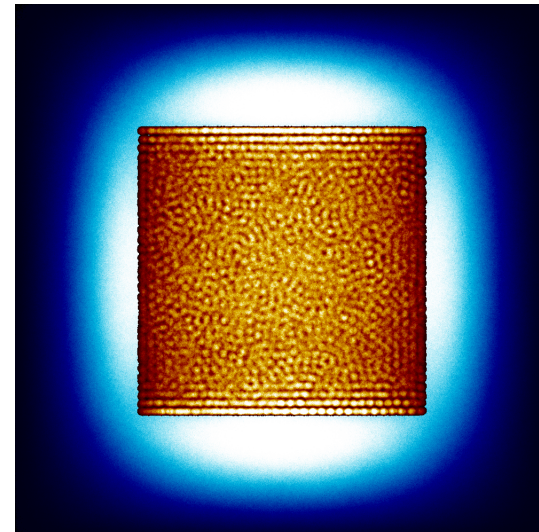
(a) Radial Cross Section at $y=0$



(b) Radial Mesh



(c) Axial Cross Section at $z=0$



(d) Axial Mesh

Figure 5.22: Shuffle Analysis: Run 6

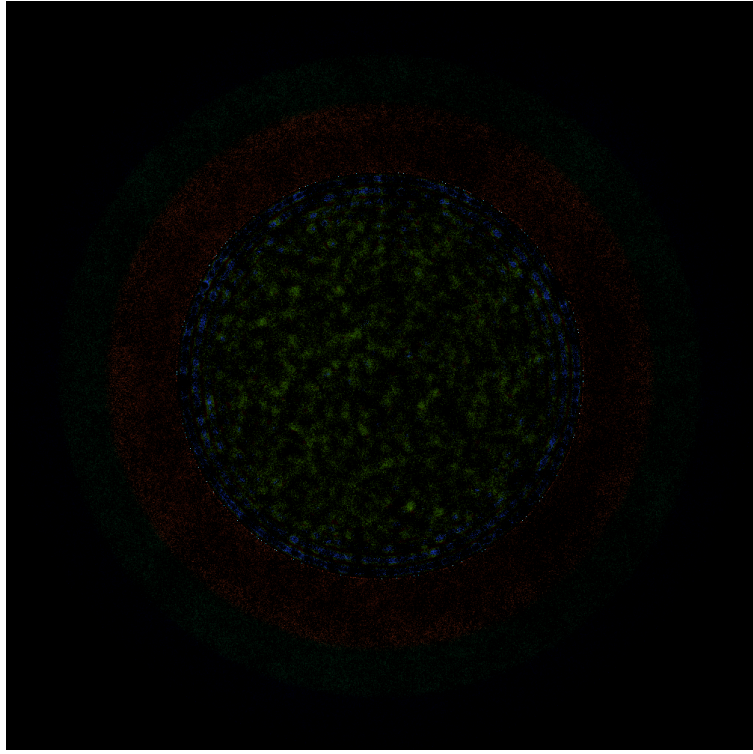


Figure 5.23: An Image Generated by Subtracting ?? from 4.4b.

Figure 5.1 provides the thermal flux and fission rate meshes and geometric cross sections axially and radially. Figure 5.23 is the result of the image difference between the full core control mesh and Figure 5.22b.

Comparing the image difference results of Appendix B, the shuffling test, to Appendix A, the symmetry test, shows that there is a smaller difference caused by the shuffling tests overall. The small differences in this particular test would most likely indicate that the core is well-mixed, i.e., that each bin in the vertical direction, along the z axis, has each of the 7 fuel compositions represented equally. In theory, if certain regions were highlighted in bright green, it would indicate regions that are poorly mixed.

*** questions, comments, and concerns:

I want to expand the end section for appendix b, but i'm not sure how to put want I want to say.

The fission rate meshes are integrated over z, which is why the result is a radial image in x and y. For the shuffling tests, if the image difference result shows little difference, it means the pebbles in that area are (vertically) well-mixed (the pebble comps are present in equal amounts). Otherwise, shuffling the fuel compositions, say, making the fresh pebbles 6-pass pebbles, would cause a large shift. In this same way, a region highlighted with bright green (theoretically) suggests a region that is not well-mixed - i.e., one pebble composition is likely dominating. There are a few areas where differences are shown, but I wonder if this may be accounted for by the fact that shuffling pebble comps puts a different pebble burnup in the peak power region alone.

Given that none of the image difference results in Appendix B have bright green, it's hard for me to double check this and make sure. I suppose I could force a poorly mixed region by selecting pebbles with coordinates with same/similar z values and modify them?

Other than the above, I don't like that the captions beneath are the same, but I don't know how to truly make them meaningfully different.***

References

- [1] H. Reutler and G. H. Lohnert, "Advantages of going modular in HTRs," vol. 78, no. 2, pp. 129–136. [Online]. Available: <http://www.sciencedirect.com/science/article/pii/002954938490298X>
- [2] M. T. Simnad, "The early history of high-temperature helium gas-cooled nuclear power reactors," vol. 16, no. 1, pp. 25–32. [Online]. Available: <https://www.sciencedirect.com/science/article/pii/036054429190084Y>
- [3] J. M. Beck and L. F. Pincock, "High temperature gas-cooled reactors lessons learned applicable to the next generation nuclear plant," p. 78.
- [4] "Results of experiments at the AVR reactor," vol. 121, no. 2, pp. 143–153, publisher: North-Holland. [Online]. Available: <https://www.sciencedirect.com.proxy2.library.illinois.edu/science/article/pii/002954939090099J>
- [5] Serpent - a monte carlo reactor physics burnup calculation code. [Online]. Available: <http://montecarlo.vtt.fi/>
- [6] J. Leppänen. Serpent – a continuous-energy monte CarloReactor physics burnup calculation code. [Online]. Available: http://montecarlo.vtt.fi/download/Serpent_manual.pdf
- [7] I. MURATA, A. TAKAHASHI, T. MORI, and M. NAKAGAWA, "New sampling method in continuous energy monte carlo calculation for pebble bed reactors," vol. 34, no. 8, pp. 734–744, publisher: Taylor & Francis _eprint: <https://doi.org/10.1080/18811248.1997.9733737>. [Online]. Available: <https://doi.org/10.1080/18811248.1997.9733737>
- [8] Z. Karriem, C. Stoker, and F. Reitsma, "MCNP modelling of HTGR pebble-type fuel," in *Advanced Monte Carlo for Radiation Physics, Particle Transport Simulation and Applications*, A. Kling, F. J. C. Barão, M. Nakagawa, L. Távora, and P. Vaz, Eds. Springer, pp. 841–846.
- [9] A. T. Cisneros, "Pebble bed reactors design optimization methods and their application to the pebble bed fluoride salt cooled high temperature reactor (PB-FHR)." [Online]. Available: <http://gradworks.umi.com/36/16/3616613.html>
- [10] M. Türkmen and Çolak, "Effect of pebble packing on neutron spectrum and the isotopic composition of HTGR fuel," vol. 46, pp. 29–36. [Online]. Available: <https://www.sciencedirect.com/science/article/pii/S0306454912000953>
- [11] C. J. Hamilton, N. D. Holder, V. H. Pierce, and M. W. Robertson, "HTGR spent fuel composition and fuel element block flow." [Online]. Available: <https://www.osti.gov/biblio/7157851>
- [12] P. J. Venter, M. N. Mitchell, and F. Fortier, "PBMR REACTOR DESIGN AND DEVELOPMENT," p. 15.
- [13] H.-C. Kim, S. Y. Kim, J. K. Kim, and J. M. Noh, "Monte carlo benchmark calculations for 400mwth PBMR core," p. 5.
- [14] F. Albornoz and S. Korochinsky, "MCNP modelling of the PBMR equilibrium core," p. 11.
- [15] "Criticality and burnup analyses of a PBMR-400 full core using monte carlo calculation method," vol. 38, no. 2, pp. 298–301, publisher: Pergamon. [Online]. Available: <http://www.sciencedirect.com/science/article/pii/S0306454910003828>

- [16] F. Reitsma, W. R. Joubert, A. M. Ougouag, and H. D. Gougar, "INVESTIGATION OF THE POWER PEAKING IN THE PBMR PEBBLE- BED REACTOR," p. 13.
- [17] Areva modular reactor selected for NGNP development - world nuclear news. [Online]. Available: https://www.world-nuclear-news.org/NN-Areva_modular_reactor_selected_for_NGNP_development-1502124.html
- [18] INL. Basis for NGNP reactor design down-selection. [Online]. Available: <https://inldigitallibrary.inl.gov/sites/sti/sti/5223031.pdf>
- [19] T.K.Kim, W.S. Yang, T.A. Taiwo, and H.S. Khalil, "Whole-core depletion studies in support of fuel specification for the next generation nuclear plant (NGNP) core." [Online]. Available: <https://publications.anl.gov/anlpubs/2004/11/51497.pdf>
- [20] B. Harlan, "X-energy xe-100 reactor initial NRC meeting," xe-100 Reactor initial NRC meeting. [Online]. Available: <https://adamswebsearch2.nrc.gov/webSearch2/main.jsp?AccessionNumber=ML18253A109>
- [21] N. Agnihotri and E. Mulder. An intrinsically safe generation IV reactor. [Online]. Available: <http://digitaleditions.nuclearplantjournal.com/SO17/24/>
- [22] H.-C. Kim, S.-Y. Kim, C.-H. Shin, J.-K. Kim, and J.-M. Noh, "Monte carlo benchmark calculations for HTR-10 initial core," pp. 5–6, publisher: Korean Nuclear Society. [Online]. Available: <https://www.koreascience.or.kr/article/CFKO200533239312837.page>
- [23] D. She, F. Xie, F. Li, S. Liu, and K. Wang, "EXPLICIT MODELLING OF DOUBLE-HETEROGENEOUS PEBBLE-BED REACTORS WITH THE RMC CODE," p. 12.
- [24] S. Liu, Z. Li, K. Wang, Q. Cheng, and D. She, "Random geometry capability in RMC code for explicit analysis of polytype particle/pebble and applications to HTR-10 benchmark," vol. 111, pp. 41–49. [Online]. Available: <https://www.sciencedirect.com/science/article/pii/S0306454917302724>
- [25] G. van Rossum and F. L. Drake, "Python reference manual," p. 196.
- [26] C. R. Harris, K. J. Millman, S. J. van der Walt, R. Gommers, P. Virtanen, D. Cournapeau, E. Wieser, J. Taylor, S. Berg, N. J. Smith, R. Kern, M. Picus, S. Hoyer, M. H. van Kerkwijk, M. Brett, A. Haldane, J. F. del Río, M. Wiebe, P. Peterson, P. Gérard-Marchant, K. Sheppard, T. Reddy, W. Weckesser, H. Abbasi, C. Gohlke, and T. E. Oliphant, "Array programming with NumPy," vol. 585, no. 7825, pp. 357–362, bandiera_abtest: a Cc_license_type: cc_by Cg_type: Nature Research Journals Number: 7825 Primary_atype: Reviews Publisher: Nature Publishing Group Subject_term: Computational neuroscience;Computational science;Computer science;Software;Solar physics Subject_term_id: computational-neuroscience;computational-science;computer-science;software;solar-physics. [Online]. Available: <https://www.nature.com/articles/s41586-020-2649-2>
- [27] A. Scopatz, P. K. Romano, P. P. H. Wilson, and K. D. Huff, "PyNE: Python for nuclear engineering," in *Transactions of the American Nuclear Society*, ser. Reactor Physics: General—I, vol. 107. American Nuclear Society, pp. 985–987. [Online]. Available: <http://epubs.ans.org/?a=14978>
- [28] S. S. Tulluri, "Analysis of random packing of uniform spheres using the monte carlo simulation method," p. 107.
- [29] F. B. Brown, W. R. Martin, W. Ji, J. L. Conlin, and J. C. Lee, "STOCHASTIC GEOMETRY AND HTGR MODELING WITH MCNP5," p. 13.
- [30] Amir Afzali, "High temperature, gas-cooled pebble bed reactor licensing modernization project demonstration," u.S. Department of Energy (DOE) Office of Nuclear Energy Under DOE Idaho Operations Office Contract DE-AC07-0SID14517. [Online]. Available: <https://www.nrc.gov/docs/ML1822/ML18228A779.pdf>
- [31] W. Moe, "Licensing modernization project for advanced reactor technologies: FY 2018 project status report."
- [32] F. Ho, R. Vollmar, and R. Turner. Graphite design handbook. [Online]. Available: <https://www.osti.gov/servlets/purl/714896/>

- [33] M. El-Genk and T. Schriener, Post-operation radiological source term and dose rate estimates for the scalable liquid metal-cooled small modular reactor | elsevier enhanced reader. [Online]. Available: <https://reader.elsevier.com/reader/sd/pii/S0306454918300550?token=72A5D70FC4A85A4EF41A5E9256B0B120D6DBE8E80266F7BFD35BB528A887F463F8647F134921742AAE435B0A9D635F61>
- [34] Accuratus. Silicon carbide SiC material properties. [Online]. Available: <https://www.accuratus.com/silicar.html>
- [35] W. Johnson and G. Engle, "Properties of unirradiated fuel element graphites h-451 and TS-1240," pp. GA-A-13 752, 7 283 150. [Online]. Available: <http://www.osti.gov/servlets/purl/7283150-NEjJgM/>
- [36] M. B. Richards, "Reaction of nuclear-grade graphite with low concentrations of steam in the helium coolant of an MHTGR," vol. 15, no. 9, pp. 729–739. [Online]. Available: <http://www.sciencedirect.com/science/article/pii/036054429090112F>
- [37] S. G. Nagley, C. M. Barnes, D. L. Husser, M. L. Nowlin, and W. C. Richardson, "Fabrication of uranium oxycarbide kernels for HTR fuel," p. 10.
- [38] "Accident analysis for nuclear power plants with modular high temperature gas cooled reactors," OCLC: 637106283.
- [39] M. Rainer, "Fission product transport and source terms in HTRs: Experience from AVR pebble bed reactor," vol. 2008.
- [40] E. Eaves, "Can north america's advanced nuclear reactor companies help save the planet?" vol. 73, no. 1, p. 27. [Online]. Available: <http://search.ebscohost.com/login.aspx?direct=true&db=ulh&AN=120392537>
- [41] M. Englert, F. Friess, and M. V. Ramana, "Accident scenarios involving pebble bed high temperature reactors," vol. 25, no. 1, pp. 42–55. [Online]. Available: <https://www.tandfonline.com/doi/full/10.1080/08929882.2017.1275320>
- [42] Y. Brits, F. Botha, H. van Antwerpen, and H.-W. Chi, "A control approach investigation of the xe-100 plant to perform load following within the operational range of 100 – 25 – 100%," vol. 329, pp. 12–19. [Online]. Available: <http://www.sciencedirect.com/science/article/pii/S0029549317305630>
- [43] ESPI Metals. Graphite-pyrolytic grade. [Online]. Available: <https://www.espimetals.com/index.php/technical-data/74-graphite-pyrolytic-grade>
- [44] M. V. Ramana, "The checkered operational history of high-temperature gas-cooled reactors," vol. 72, no. 3, pp. 171–179. [Online]. Available: <https://doi.org/10.1080/00963402.2016.1170395>
- [45] Z. Zhang and Y. Sun, "Economic potential of modular reactor nuclear power plants based on the chinese HTR-PM project," vol. 237, no. 23, pp. 2265–2274. [Online]. Available: <http://www.sciencedirect.com/science/article/pii/S002954930700283X>
- [46] G. W. Helmreich, J. D. Hunn, J. W. McMurray, R. D. Hunt, B. C. Jolly, M. P. Trammell, D. R. Brown, B. J. Blamer, T. J. Reif, and H. T. Kim, "Year one summary of x-energy pebble fuel development at ORNL." [Online]. Available: <https://www.osti.gov/biblio/1376502>
- [47] M. Hussain, F. Reitsma, M. Subki, and H. Kiuchi, "Advances in small modular reactor technology developments." [Online]. Available: <http://aris.iaea.org>
- [48] B. Harlan, "ANS xe 100 overview 2017." [Online]. Available: http://local.ans.org/dc/wp-content/uploads/2014/01/ANS_Xe-100-Overview_04052017.pdf
- [49] H. G. Hereward, H. R. Paneth, G. C. Laurence, and B. W. Sargent, "Measurement of the diffusion length of thermal neutrons in graphite," vol. 25a, no. 1, pp. 15–25, publisher: NRC Research Press. [Online]. Available: <https://www.nrcresearchpress.com/doi/abs/10.1139/cjr47a-002>
- [50] E. Mulder, "Reactor physics overview of the xe-100 GEN IV reactor," NPREG 596 Graduate Seminar.

- [51] R. Nanstad and W. L. Server. Milestone report-08-2011-assessment of thermal annealing-FINAL.pdf. [Online]. Available: <https://www.energy.gov/sites/prod/files/Milestone%20Report-08-2011-Assessment%20of%20Thermal%20Annealing-FINAL.pdf>
- [52] O. K. Chopra and A. S. Rao, "Degradation of LWR core internal materials due to neutron irradiation." [Online]. Available: <https://www.nrc.gov/docs/ML1027/ML102790482.pdf>
- [53] T. Dudley, O. Tsaoi, and E. Mulder, "THE REACTOR CORE NEUTRONIC MODEL FOR THE PBMR PLANT TRAINING SIMULATOR," p. 13.
- [54] E. J. Mulder, "Pebble bed reactor with equalised core power distribution inherently safe and simple." [Online]. Available: <https://juser.fz-juelich.de/record/820874/>
- [55] NASA's Goddard Institute for Space Studies, "Global surface temperature." [Online]. Available: <https://climate.nasa.gov/vital-signs/global-temperature>
- [56] Pebble bed modular reactor SOC ltd. [Online]. Available: <http://www.pbmr.co.za/index2.asp?Content=129>
- [57] L. Lommers and G. Honma, "NGNP high temperature materials white paper." [Online]. Available: <https://www.osti.gov/biblio/1055953-ngnp-high-temperature-materials-white-paper>
- [58] Cole Gentry. generate random particle or pebble bed files for HTGR calc - discussion forum for serpent users. [Online]. Available: <https://ttuki.vtt.fi/serpent/viewtopic.php?f=3&t=2267&p=6161&hilit=growth+and+shake#p6161>